



Nonlinear Micromorphic Continuum Mechanics and Finite Strain Elastoplasticity

by Richard A. Regueiro

ARL-CR-0659

November 2010

prepared by

**University of Colorado at Boulder
1111 Engineering Dr.
Boulder, CO 80309**

W911NF-07-D-0001

NOTICES

Disclaimers

The findings in this report are not to be construed as an official Department of the Army position unless so designated by other authorized documents.

Citation of manufacturer's or trade names does not constitute an official endorsement or approval of the use thereof.

Destroy this report when it is no longer needed. Do not return it to the originator.

Army Research Laboratory

Aberdeen Proving Ground, MD 21005

ARL-CR-0659**November 2010**

Nonlinear Micromorphic Continuum Mechanics and Finite Strain Elastoplasticity

Richard A. Regueiro
University of Colorado at Boulder

prepared by

University of Colorado at Boulder
1111 Engineering Dr.
Boulder, CO 80309

REPORT DOCUMENTATION PAGE				Form Approved OMB No. 0704-0188	
<p>Public reporting burden for this collection of information is estimated to average 1 hour per response, including the time for reviewing instructions, searching existing data sources, gathering and maintaining the data needed, and completing and reviewing the collection information. Send comments regarding this burden estimate or any other aspect of this collection of information, including suggestions for reducing the burden, to Department of Defense, Washington Headquarters Services, Directorate for Information Operations and Reports (0704-0188), 1215 Jefferson Davis Highway, Suite 1204, Arlington, VA 22202-4302. Respondents should be aware that notwithstanding any other provision of law, no person shall be subject to any penalty for failing to comply with a collection of information if it does not display a currently valid OMB control number.</p> <p>PLEASE DO NOT RETURN YOUR FORM TO THE ABOVE ADDRESS.</p>					
1. REPORT DATE (DD-MM-YYYY)		2. REPORT TYPE		3. DATES COVERED (From - To)	
November 2010		Final		1 June 2008 to 1 May 2010	
4. TITLE AND SUBTITLE Nonlinear Micromorphic Continuum Mechanics and Finite Strain Elastoplasticity				5a. CONTRACT NUMBER	
				5b. GRANT NUMBER	
				5c. PROGRAM ELEMENT NUMBER	
6. AUTHOR(S) Richard A. Regueiro				5d. PROJECT NUMBER	
				5e. TASK NUMBER	
				5f. WORK UNIT NUMBER	
7. PERFORMING ORGANIZATION NAME(S) AND ADDRESS(ES) University of Colorado at Boulder 1111 Engineering Dr. Boulder, CO 80309				8. PERFORMING ORGANIZATION REPORT NUMBER ARL-CR-0659	
9. SPONSORING/MONITORING AGENCY NAME(S) AND ADDRESS(ES) U.S. Army Research Office P.O. Box 12211 Research Triangle Park, NC 27709				10. SPONSOR/MONITOR'S ACRONYM(S) ARO	
				11. SPONSOR/MONITOR'S REPORT NUMBER(S)	
12. DISTRIBUTION/AVAILABILITY STATEMENT Approved for public release; distribution unlimited.					
13. SUPPLEMENTARY NOTES					
14. ABSTRACT The report presents the detailed formulation of nonlinear micromorphic continuum kinematics and balance equations (balance of mass; microinertia; linear, angular, and first moment of momentum; energy; and the Clausius-Duhem inequality). The theory is extended to elastoplasticity assuming a multiplicative decomposition of the deformation gradient and microdeformation tensor. A general three-level (macro, micro, and microgradient) micromorphic finite strain elastoplasticity theory results, with simpler forms presented for linear isotropic elasticity, J2 flow associative plasticity, and nonassociative Drucker-Prager pressure-sensitive plasticity. Assuming small elastic deformations for the class of materials of interest, bound particulate materials (ceramics, metal matrix composites, energetic materials, infrastructure materials, and geologic materials), the constitutive equations formulated in the intermediate configuration are mapped to the current configuration, and a new elastic Truesdell objective higher order stress rate is defined. A semi-implicit time integration scheme is presented for the Drucker-Prager model mapped to the current configuration. A strategy to couple the micromorphic continuum finite element implementation to a direct numerical simulation of the grain-scale response of a bound particulate material is outlined that will lead to a concurrent multiscale computational method for simulating dynamic failure in bound particulate materials.					
15. SUBJECT TERMS nonlinear micromorphic continuum mechanics; finite strain elastoplasticity; concurrent multiscale computational, method; bound particulate materials					
16. SECURITY CLASSIFICATION OF:			17. LIMITATION OF ABSTRACT UU	18. NUMBER OF PAGES 92	19a. NAME OF RESPONSIBLE PERSON John Clayton
a. REPORT Unclassified	b. ABSTRACT Unclassified	c. THIS PAGE Unclassified			19b. TELEPHONE NUMBER (Include area code) (410) 278-7981

Contents

Acknowledgments	v
1. Introduction	1
1.1 Description of Problem	1
1.2 Proposed Approach	4
1.3 Focus of Report	4
1.4 Notation	5
2. Technical Discussion	6
2.1 Statement of Work (SOW) and Specific Tasks	6
2.1.1 Specific Tasks	8
2.2 Nonlinear Micromorphic Continuum Mechanics	9
2.2.1 Kinematics	9
2.2.2 Micromorphic Balance Equations and Clausius-Duhem Inequality . .	11
2.3 Finite Strain Micromorphic Elastoplasticity	22
2.3.1 Kinematics	24
2.4 Clausius-Duhem Inequality in $\bar{\mathcal{B}}$	27
2.4.1 Constitutive Equations	36
2.4.2 Linear Isotropic Elasticity and J_2 Flow Isochoric Plasticity	36
2.4.3 Drucker-Prager Pressure-Sensitive Plasticity	41
2.5 Numerical Time Integration	55
3. Upscaling from Grain-Scale to Micromorphic Elastoplasticity	62

4. Coupled Formulation	64
4.1 Kinematics	64
4.2 Partitioning of Energy	69
5. Conclusion	70
5.1 Results	70
5.2 Conclusions	70
5.3 Future Work	70
6. References	71
Appendix A	77
Appendix B	79
Appendix C	81

List of Figures

1	(a) Microstructure of alumina, composed of grains bound by a glassy phase. (b) Silicon carbide (SiC) reinforced 2080 aluminum metal matrix composite (Chawla, 2004). The four black squares are indents to identify the region. (c) Cracking in explosive HMX grains and at the grain-matrix interfaces (Baer, 2007). (d) Cracking in asphalt pavement.	2
2	Two-dimensional illustration of the concurrent computational multiscale modeling approach in the contact interface region between a bound particulate material (e.g., ceramic target) and deformable solid body (e.g., refractory metal projectile).	5
3	Map from reference \mathcal{B}_0 to current configuration \mathcal{B} accounting for relative position Ξ , ξ of microelement centroid C' , c' with respect to centroid of macroelement C , c . \mathbf{F} and χ can load and unload independently (although coupled through constitutive equations and balance equations), and thus the additional current configuration is shown.	10
4	Differential area of microelement da' within macroelement da in current configuration \mathcal{B}	22
5	Multiplicative decomposition of deformation gradient \mathbf{F} and microdeformation tensor χ into elastic and plastic parts, and the existence of an intermediate configuration $\bar{\mathcal{B}}$. Since \mathbf{F}^e , \mathbf{F}^p , χ^e , and χ^p can load and unload independently (although coupled through constitutive equations and balance equations), additional configurations are shown. The constitutive equations and balance equations presented in the report govern these deformation processes, and so generality is preserved.	26
6	Two-dimensional illustration of micromorphic continuum homogenization of grain-scale response at a FE Gauss integration point X in the overlap region. v^{RVE} implies a RVE if needed to approximate stress from a DE simulation at a particular point of integration in Ω^{avg} , for example in Christoffersen et al. (1981); Rothenburg and Selvadurai (1981).	63

Acknowledgments

This work was supported by the U.S. Army Research Laboratory (Dr. John Clayton) under the Auspices of the U.S. Army Research Office Scientific Services Program administered by Battelle (Delivery Order 0356, Contract No. W911NF-07-D-0001).

1. Introduction

1.1 Description of Problem

Dynamic failure in bound particulate materials is a combination of physical processes including grain and matrix deformation, intra-granular cracking, matrix cracking, and inter-granular-matrix/binder cracking/debonding, and is influenced by global initial boundary value problem (IBVP) conditions. Discovering how these processes occur by experimental measurements is difficult because of their dynamic nature and the influence of global boundary conditions (BCs). Typically, post-mortem microscopy observations are made of fractured/fragmented/comminuted material (Kipp et al., 1993), or real-time in-situ infrared-optical surface observations are conducted of the dynamic failure process (Guduru et al., 2001). These observation techniques, however, miss the origins of dynamic failure internally in the material. Under quasi-static loading conditions, non-destructive high spatial resolution (a few microns) synchrotron micro-computed tomography can be conducted (Fredrich et al., 2006)* to track three-dimensionally the internal grain-scale fracture process leading to macro-cracks (though these cracks can propagate unstably). Dynamic loading, however, can generate a significantly different microstructural response, usually fragmented and comminuted material (Kipp et al., 1993). Global BCs, such as lateral confinement on cylindrical compression specimens, also can influence the resulting failure mode, generating in a glass ceramic composite axial splitting and fragmentation when there is no confinement and shear fractures with confinement (Chen and Ravichandran, 1997). Thus, we resort to physics-based modeling to help uncover these origins dynamically.

Examples of bound particulate materials include, but are not limited to, the following: polycrystalline ceramics (crystalline grains with amorphous grain boundary phases, figure 1(a)), metal matrix composites (metallic grains with bulk amorphous metallic binder, figure 1(b)), particulate energetic materials (explosive crystalline grains with polymeric binder, figure 1(c)), asphalt pavement (stone/rubber aggregate with hardened binder, figure 1(d)), mortar (sand grains with cement binder), conventional quasi-brittle concrete (stone aggregate with cement binder), and sandstones (sand grains with clayey binder). Bound particulate materials contain grains (quasi-brittle or ductile) bound by binder material often called the “matrix.” The heterogeneous particulate nature of these materials governs their mechanical behavior at the grain-to-macroscales, especially in IBVPs for which localized deformation nucleates. Thus, grain-scale material model resolution is needed in regions of localized deformation nucleation (e.g., at a macro-crack tip, or at the high shear

*Such experimental techniques are not yet mature, but can provide meaningful insight into the origins of ‘static’ fracture, and thus could play an important role in the discovery of the origins of dynamic failure.

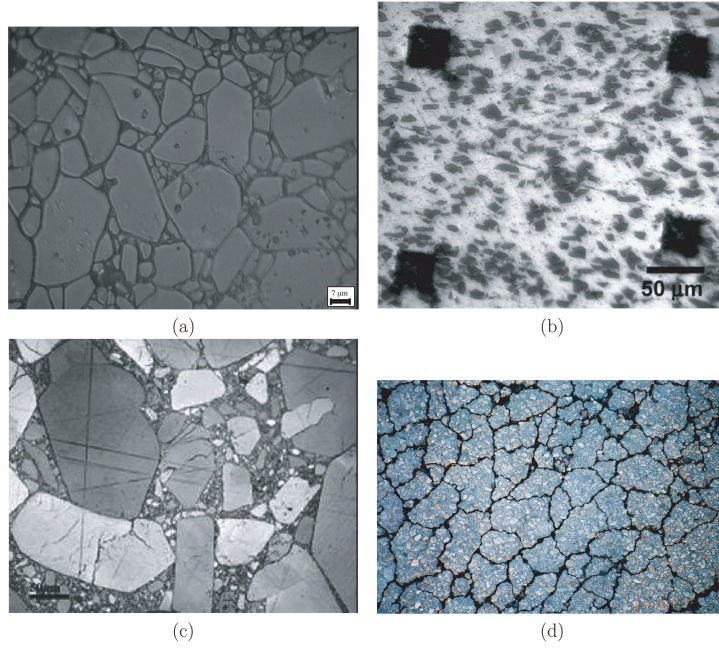


Figure 1. (a) Microstructure of alumina, composed of grains bound by a glassy phase. (b) Silicon carbide (SiC) reinforced 2080 aluminum metal matrix composite (Chawla, 2004). The four black squares are indents to identify the region. (c) Cracking in explosive HMX grains and at the grain-matrix interfaces (Baer, 2007). (d) Cracking in asphalt pavement.

strain rate interface region between a projectile and target material[†]). To predict dynamic failure for realistic IBVPs, a modeling approach needs to account *simultaneously* for the underlying grain-scale physics and macroscale continuum IBVP conditions.

Traditional single-scale continuum constitutive models have provided the basis for understanding the dynamic failure of these materials for IBVPs on the macroscale (Rajendran and Grove, 1996; Dienes et al., 2006; Johnson and Holmquist, 1999), but cannot *predict* dynamic failure because they do not account explicitly for the material’s particulate nature. Direct Numerical Simulation (DNS) directly represents the grain-scale mechanical behavior under static (Caballero et al., 2006) and dynamic loading conditions (Kraft et al., 2008; Kraft and Molinari, 2008b). Currently, DNS is the best approach to understanding fundamentally dynamic material failure, but IT is deficient in the following ways: (1) it is limited by current computing power (even massively parallel computing) to a small representative volume element (RVE) of the material and (2) it usually must assume unrealistic BCs on the RVE (e.g., periodic, or prescribed uniform traction or

[†]Both projectile and target material could be modeled with such grain-scale material model resolution at their interface region where significant fracture and comminution occurs. We start by assuming the projectile is a deformable solid continuum body without grain-scale resolution, and then extend to include such resolution in the future.

displacement). Thus, multiscale modeling techniques are needed to predict dynamic failure in bound particulate materials.

Current multiscale approaches attempt to do this, but fall short by one or more of the following limitations: (1) not providing proper BCs on the microstructural DNS region (called the “unit cell” by Feyel and Chaboche (2000), extended to account for discontinuities in Belytschko et al. (2008)); (2) homogenizing at the macroscale the underlying microstructural response in the unit cell and thus not maintaining a computational “open window” to model microstructurally dynamic failure[‡]; and (3) not making these methods adaptive, i.e., moving a computational “open window” with grain-scale model resolution over regions experiencing dynamic failure.

Feyel and Chaboche (2000) and Belytschko et al. (2008) recognized the complexities and limitations of unit cell methods as they are currently formulated, implemented, and applied. Feyel (2003) stated that, in addition to the periodicity assumption for the microstructure (impossible to model fracture), “... real structures have edges, either external or internal ones (in case of a multimaterial structure). In the present FE2 framework, nothing has been done to treat such effects. As a consequence, one cannot expect a good solution near edges. This is clearly a weak point of the approach ...” In fact, for a non-periodic heterogeneous microstructure found in bound particulate materials, we should not expect predictive results for modeling nucleation of fracture anywhere in the unit cell.

Belytschko et al. (2008) introduced discontinuities into Feyel and Chaboche’s (2000) unit cell (calling it a “perforated unit cell”) and relaxed the periodicity assumption to model fracture nucleation, while up-scaling the effects of unit cell discontinuities to the macroscale to obtain global cracks embedded in the finite element (FE) solution (using the extended FE method). BCs on the unit cell are an issue, as well as the interaction of adjacent unit cells. As noted in Belytschko et al. (2008), if regular displacement BCs (i.e., no jumps) are applied to unit cells that are fracturing, then the fracture is constrained non-physically. Belytschko et al. (2008) proposed to address this issue by solving iteratively for displacement BCs by applying a traction instead. What traction to apply is still an unknown and can be provided by the coarse-scale FE solution. Belytschko et al. (2008) stated that “... the application of boundary conditions on the unit cell and information transfer to/from the unit cell pose several difficulties ... When the unit cell localizes, prescribed linear displacements as given in the analysis are not compatible with the discontinuities ... The effects of boundaries and adjacent discontinuities are not reflected in the method.”

[‡]This is a problem especially for modeling fragmentation and comminution microstructurally.

1.2 Proposed Approach

A finite strain micromorphic plasticity model framework (Regueiro, 2010b) is applied to formulate a simple pressure-sensitive plasticity model to account for the underlying microstructural mechanical response in bound particulate materials (pressure-sensitive heterogeneous materials). Linear isotropic elasticity and nonassociative Drucker-Prager plasticity with cohesion hardening/softening are assumed for the constitutive equations (Regueiro, 2009). Micromorphic continuum mechanics is used in the sense of Eringen (1999). This was found to be one of the more general higher order continuum mechanics frameworks for accounting for underlying microstructural mechanical response. Until this work, however, the finite strain formulation based on multiplicative decomposition of the deformation gradient \mathbf{F} and microdeformation tensor χ has not been presented in the literature with sufficient account of the reduced dissipation inequality and conjugate plastic power terms to dictate the plastic evolution equation forms. We provide such details in this report.

To illustrate the application of the micromorphic plasticity model to the problem of interest, we refer figure 2, which illustrates a concurrent multiscale modeling framework for bound particulate materials (target) impacted by a deformable solid (projectile). The higher order continuum micromorphic plasticity model is used in the overlap region between a continuum FE and DNS representation of the particulate material. The additional degrees of freedom provided by the micromorphic model (microshear, micro-dilation/compaction, and microrotation) allow the overlap region to be placed closer to the region of interest, such as at a projectile-target interface. Further, from this interface region, standard continuum mechanics and constitutive models can be used.

1.3 Focus of Report

Regarding the approach described in section 1.2, this report primarily on the nonlinear micromorphic continuum mechanics and finite strain elastoplasticity constitutive model tasks. How this generalized continuum model couples via an overlapping region to the DNS region (figure 2) is described in sections 2.4 and 2.5.

The discrete element (DE) and/or FE representation of the particulate microstructure is intentionally not shown so as not to clutter the drawing of the microstructure. The grains (binder matrix not shown) of the microstructure are “meshed” using DEs and/or FEs with cohesive surface elements (CSEs). The open circles denote continuum FE nodes that have prescribed degrees of freedom (DOFs) $\hat{\mathbf{D}}$ based on the underlying grain-scale response, while the solid circles denote continuum FE nodes that have free DOFs \mathbf{D} governed by the micromorphic continuum model. We intentionally leave an “open window” (i.e., DNS) on the particulate microstructural mesh in order to model dynamic failure. If the continuum

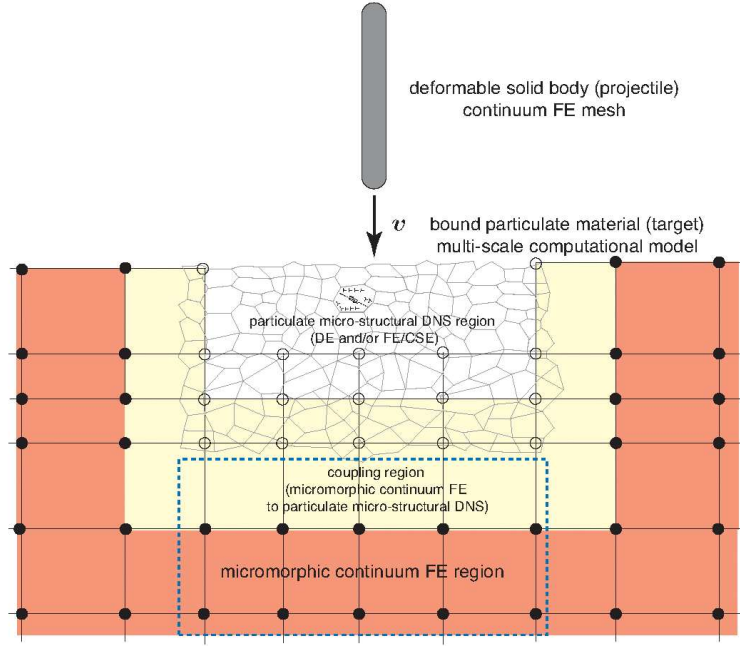


Figure 2. Two-dimensional illustration of the concurrent computational multiscale modeling approach in the contact interface region between a bound particulate material (e.g., ceramic target) and deformable solid body (e.g., refractory metal projectile).

mesh overlays the whole particulate microstructural region, as in Klein and Zimmerman (2006) for atomistic-continuum coupling, then the continuum FEs would eventually become too deformed by following the microstructural motion during fragmentation. The blue-dashed box at the bottom-center of the illustration is a micromorphic continuum FE region that can be converted to a DNS region for adaptive high-fidelity material modeling as the projectile penetrates the target.

An outline of the report is as follows: section 2.1 summarizes the statement of work (SOW) and the tasks, 2.2 presents the formulation of the nonlinear (finite deformation) micromorphic continuum mechanics balance equations, section 2.3 presents the finite strain elastoplasticity modeling framework based on a multiplicative decomposition of the deformation gradient and microdeformation tensor, sections 2.4 and 2.5 describe how the micromorphic continuum mechanics fits into a multiscale modeling approach, section 3 summarizes the results, and section 4 provides the conclusions and future work.

1.4 Notation

Cartesian coordinates are assumed for easier presentation of concepts and also in order to define a Lagrangian elastic strain measure $\bar{\mathbf{E}}^e$ in the intermediate configuration $\bar{\mathcal{B}}$,

assuming a multiplicative decomposition of the deformation gradient \mathbf{F} and microdeformation tensor χ into elastic and plastic parts (section 2.3.1). See Regueiro (2010) for more details regarding finite strain micromorphic elastoplasticity in general curvilinear coordinates, and also Eringen (1962) for nonlinear continuum mechanics in general curvilinear coordinates and Clayton et al. (2004, 2005) for nonlinear crystal elastoplasticity in general curvilinear coordinates.

Index notation is used so as to be as clear as possible with regard to details of the formulation. Cartesian coordinates are assumed, so all indices are subscripts, and spatial partial derivative is the same as covariant derivative (Eringen, 1962). Some symbolic/direct notation is also given, such that $(\mathbf{ab})_{ik} = a_{ij}b_{jk}$, $(\mathbf{a} \otimes \mathbf{b})_{ijkl} = a_{ij}b_{kl}$, $(\mathbf{a} \odot \mathbf{c})_{ijk} = a_{im}c_{jmk}$. Boldface denotes a tensor or vector, where its index notation is given. Generally, variables in uppercase letters and no overbar live in the reference configuration \mathcal{B}_0 (such as the reference differential volume dV), variables in lowercase live in the current configuration \mathcal{B} (such as the current differential volume dv), and variables in uppercase with overbar live in the intermediate configuration $\bar{\mathcal{B}}$ (such as the intermediate differential volume $d\bar{V}$). The same applies to their indices, such that a differential line segment in the current configuration dx_i is related to a differential line segment in the reference configuration dX_I through the deformation gradient: $dx_i = F_{iI}dX_I$ (Einstein's summation convention assumed [see Eringen, 1962; Holzapfel, 2000]). In addition, the multiplicative decomposition of the deformation gradient is written as $F_{iI} = F_{i\bar{I}}^e F_{\bar{I}I}^p$ ($\mathbf{F} = \mathbf{F}^e \mathbf{F}^p$), where superscripts e and p denote elastic and plastic parts, respectively. Subscripts $(\bullet)_{,i}$, $(\bullet)_{,\bar{I}}$ and $(\bullet)_{,I}$ imply spatial partial derivatives in the current, intermediate, and reference configurations, respectively. A superscript prime symbol $(\bullet)'$ denotes a variable associated with the microelement for micromorphic continuum mechanics. Superposed dot $(\dot{\square}) = D(\square)/Dt$ denotes material time derivative. The symbol $\stackrel{\text{def}}{=}$ implies a definition.

2. Technical Discussion

2.1 Statement of Work (SOW) and Specific Tasks

Bound particulate materials are commonly found in industrial products, construction materials, and nature (e.g., geological materials). They include polycrystalline ceramics (e.g., crystalline grains with amorphous grain boundary phases), energetic materials (high explosives and solid rocket propellant), hot asphalt, asphalt pavement (after asphalt has cured), mortar, conventional quasi-brittle concrete, ductile fiber composite concretes, and sandstones, for instance. Bound particulate materials contain particles[§] (quasi-brittle or ductile) bound by binder material often called the “matrix.”

[§]We use “particle” and “grain” interchangeably.

The heterogeneous nature of bound particulate materials governs its mechanical behavior at the particle- to continuum-scales. The particle-scale is denoted as the scale at which particle-matrix mechanical behavior is dominant, thus necessitating that particles and matrix material be resolved explicitly (i.e., meshed directly in a numerical model), accounting for their interfaces and differences in material properties. Currently, there is no approach enabling prediction of initiation and propagation of dynamic fracture in bound particulate materials—for example, polycrystalline ceramics, particulate energetic materials, mortar, and sandstone—accounting for their underlying particulate microstructure across multiple length-scales concurrently. Traditional continuum methods have provided the basis for understanding the dynamic fracture of these materials, but cannot predict the initiation of dynamic fracture without accounting for the material’s particulate nature. DNS of deformation, intra-particle cracking, and inter-particle-matrix/binder debonding at the particle-scale is limited by current computing power (even massively parallel computing) to a small RVE of the material, and usually must assume overly-restrictive BCs on the RVE (e.g., fixed normal displacement).

Multiscale modeling techniques are clearly needed to accurately capture the response of bound particulate materials in a way accounting simultaneously for effects of the microstructure at the particle-scale and BCs applied to the engineering structure of interest, at the continuum-scale. The services of a scientist or engineer are required to develop the mathematical theory and numerical methodology for multiscale modeling of bound particulate materials of interest to the U.S. Army Research Laboratory (ARL).

The overall objective of the proposed research is to develop a concurrent multiscale computational modeling approach that couples regions of continuum deformation to regions of particle-matrix deformation, cracking, and debonding, while bridging the particle- to continuum-scale mechanics to allow numerical adaptivity in modeling initiation of dynamic fracture and degradation in bound particulate materials.

For computational efficiency, the solicited research use DNSs only in the spatial regions of interest, such as the initiation site of a crack and its tip during propagation, and uses a micromorphic continuum approach in the overlap and adjacent regions to provide proper BCs on the DNS region, as well as an overlay continuum to which to project the underlying particle-scale mechanical response (stress, internal state variables [ISVs]). The micromorphic continuum constitutive model accounts for the inherent length-scale of damaged fracture zone at the particle-scale, and thus includes the kinematics to enable the proper coupling with the fractured DNS particle region. Outside of the DNS region, a micromorphic extension of existing continuum model(s), with the particular model(s) to be determined based on ARL needs, of material behavior is used.

This SOW calls for development of the formulation and finite element implementation of a

finite strain micromorphic inelastic constitutive model to bridge particle-scale mechanics to the continuum-scale. The desired result is formulation of a model that enables more complete understanding of the role of microstructure-scale physics on the thermomechanical properties and performance of heterogeneous materials of interest to ARL. These materials could include, but are not limited to, the following: ceramic materials, energetic materials, geological materials, and urban structural materials.

2.1.1 Specific Tasks

Specific tasks, and summary of what was accomplished for each task.

1. *Investigate and assess specific needs of ARL researchers with regards to multiscale modeling of heterogeneous particulate materials. Determine, following discussion with ARL materials researchers, the desired classical continuum constitutive model to be reformulated as a micromorphic continuum constitutive model and used in the region outside and overlapping partially the DNS window, for material(s) of interest to ARL. For example, polycrystalline ceramics models include those of Johnson and Holmquist (1999) or Rajendran and Grove (1996) and energetic materials include those following Dienes et al. (2006). A finite strain Drucker-Prager pressure-sensitive elastoplasticity model [Regueiro, 2009] was selected as a simple model approximation to start, with future extension to the more sophisticated constitutive model forms mentioned in the task 1. This model is presented in section 2.3.3.*
2. *Formulate theory and numerical algorithms for a finite strain micromorphic inelastic constitutive model to bridge particle-scale mechanics to the continuum-scale based on the decided constitutive equations from task 1.*

See the summary for task 1.

3. *Initiate finite element implementation of the formulated finite strain micromorphic inelastic constitutive model in a continuum mechanics code.*

The finite element implementation has been initiated in the password-protected version of Tahoe tahoe.colorado.edu, where the open source version is available at tahoe.cvs.sourceforge.net. This report focuses on the theory; while details of the finite element implementation and numerical examples will follow in journal articles and a future report.

4. *Interact with ARL researchers in order to improve mutual understanding (i.e., understanding of both principal investigators [PIs] and of ARL) with regards to dynamic fracture and material degradation in bound particulate materials and associated numerical modeling techniques.*

We are continuing to interact with ARL researchers regarding their needs for this research problem.

5. *Formulate an algorithm to couple finite strain micromorphic continuum finite elements to DNS finite elements of bound particulate material through an overlapping region.*

The formulated algorithm is presented in section 2.5.

6. *Initiate implementation of coupling algorithm in task 5 using FE code Tahoe (both for micromorphic continuum and DNS). Future extension can be made for coupling micromorphic model (Tahoe) to DNS model (ARL or other FE, or particle/meshfree, code).*

The coupling algorithm has been initiated for a finite element and discrete element coupling. Extension to other DNS models of the grain-scale response is part of future work (see section 2.5).

2.2 Nonlinear Micromorphic Continuum Mechanics

2.2.1 Kinematics

Figure 3 illustrates the mapping of the macroelement and microelement in the reference configuration to the current configuration through the deformation gradient \mathbf{F} and microdeformation tensor χ . The macroelement continuum point is denoted by $P(\mathbf{X}, \mathbf{\Xi})$ and $p(\mathbf{x}, \xi, t)$ in the reference and current configurations, respectively, with centroid C and c . The microelement continuum point centroid is denoted by C' and c' in the reference and current configurations, respectively. The microelement is denoted by an assembly of particles, but in general represents a grain/particle/fiber microstructural sub-volume of the heterogeneous material. The relative position vector of the microelement centroid with respect to the macroelement centroid is denoted by $\mathbf{\Xi}$ and $\xi(\mathbf{X}, \mathbf{\Xi}, t)$ in the reference and current configurations, respectively, such that the microelement centroid position vectors are written as (figure 3) (Eringen and Suhubi, 1964; Eringen, 1999)

$$X'_K = X_K + \Xi_K, \quad x'_k = x_k(\mathbf{X}, t) + \xi_k(\mathbf{X}, \mathbf{\Xi}, t) \quad (1)$$

Eringen and Suhubi (1964) assumed that for sufficiently small lengths $\|\mathbf{\Xi}\| \ll 1$ ($\|\bullet\|$ is the L_2 norm), ξ is linearly related to $\mathbf{\Xi}$ through the microdeformation tensor χ , such that

$$\xi_k(\mathbf{X}, \mathbf{\Xi}, t) = \chi_{kK}(\mathbf{X}, t) \Xi_K \quad (2)$$

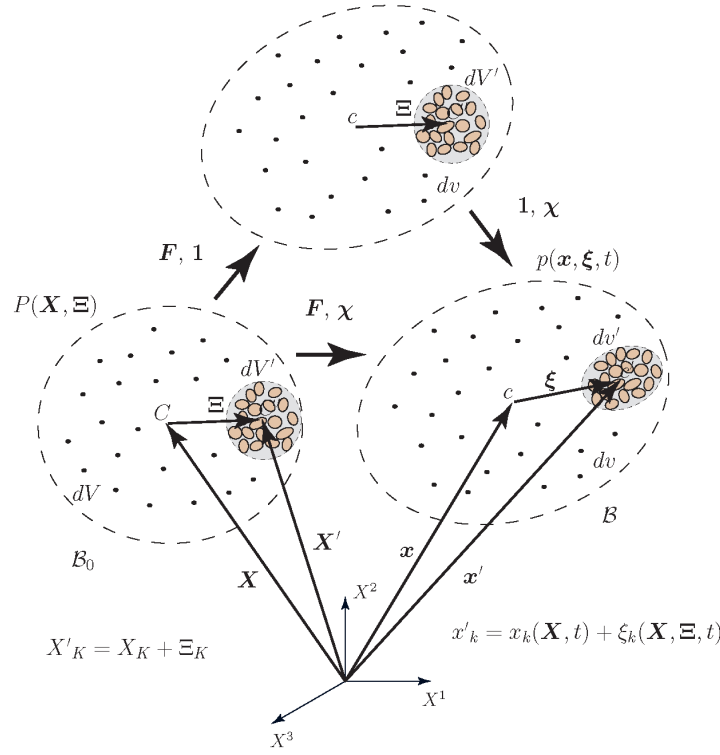


Figure 3. Map from reference \mathcal{B}_0 to current configuration \mathcal{B} accounting for relative position Ξ , ξ of microelement centroid C' , c' with respect to centroid of macroelement C , c . \mathbf{F} and χ can load and unload independently (although coupled through constitutive equations and balance equations), and thus the additional current configuration is shown.

where then the spatial position vector of the microelement centroid is written as

$$x'_k = x_k(\mathbf{X}, t) + \chi_{kK}(\mathbf{X}, t)\Xi_K \quad (3)$$

This is equivalent to assuming an affine, or homogeneous, deformation of the macroelement differential volume dV (but *not* the body \mathcal{B} ; i.e., the continuum body \mathcal{B} is expected to experience heterogeneous deformation because of χ , even if BCs are uniform). It also simplifies considerably the formulation of the micromorphic continuum balance equations as presented in (Eringen, 1964; Eringen, 1999). This microdeformation χ is analogous to the small strain microdeformation tensor ψ in Mindlin (1964), physically described in his figure 1. Eringen (1968) also provides a physical interpretation of χ generally, but then simplifies for the micropolar case. For example, χ can be interpreted as calculated from a microdisplacement gradient tensor Φ as $\chi = 1 + \Phi$, where Φ is not actually calculated from a microdisplacement vector \mathbf{u}' , but a \mathbf{u}' can be calculated once Φ is known (see equation 265). The microelement spatial velocity vector (holding \mathbf{X} and Ξ fixed) is then written as

$$v'_k = \dot{x}'_k = \dot{x}_k + \dot{\xi}_k = v_k + \nu_{kl}\xi_l \quad (4)$$

where $\dot{\xi}_k = \dot{\chi}_{kK}\Xi_K = \dot{\chi}_{kK}\chi_{Kl}^{-1}\xi_l = \nu_{kl}\xi_l$, v_k is the macroelement spatial velocity vector, $\nu_{kl} = \dot{\chi}_{kK}\chi_{Kl}^{-1}$ ($\nu = \dot{\chi}\chi^{-1}$) the microgyration tensor, similar in form to the velocity gradient $v_{k,l} = \dot{F}_{kK}F_{Kl}^{-1}$ ($\ell = \mathbf{F}\mathbf{F}^{-1}$).

Now we take the partial spatial derivative of (equation 3) with respect to the reference microelement position vector X'_K , to arrive at an expression for the microelement deformation gradient F'_{kK} as (see appendix A)

$$\begin{aligned} F'_{kK} &= F_{kK}(\mathbf{X}, t) + \frac{\partial \chi_{kL}(\mathbf{X}, t)}{\partial X_K} \Xi_L \\ &+ \left(\chi_{kA}(\mathbf{X}, t) - F_{kA}(\mathbf{X}, t) - \frac{\partial \chi_{kM}(\mathbf{X}, t)}{\partial X_A} \Xi_M \right) \frac{\partial \Xi_A}{\partial X_K} \end{aligned} \quad (5)$$

where the deformation gradient of the macroelement is $F_{kK} = \partial x_k(\mathbf{X}, t)/\partial X_K$. The microelement deformation gradient F'_{kK} maps microelement differential line segments $dx'_k = F'_{kK}dX'_K$ and volumes $dv' = J'dV'$, where $J' = \det \mathbf{F}'$ is the microelement Jacobian of deformation. This is presented for generality of mapping stresses between \mathcal{B}_0 and \mathcal{B} , \mathcal{B}_0 and $\bar{\mathcal{B}}$, $\bar{\mathcal{B}}$ and \mathcal{B} , but will not be used explicitly in the constitutive equations in section 2.3.3.

2.2.2 Micromorphic Balance Equations and Clausius-Duhem Inequality

Using the spatial integral-averaging approach in Eringen and Suhubi (1964), we can derive the balance equations and Clausius-Duhem inequality summarized in equation 57. The rationale of this integral-averaging approach over dv and \mathcal{B} in the current configuration is to assume the classical balance equations in the microelement differential volume dv' must hold over integrated macroelement differential volume dv , in turn integrated over the current configuration of the body in \mathcal{B} . This approach is applied repeatedly to derive the micromorphic balance equations in equation 57.

Balance of mass: The microelement mass m' over dv can be expressed as

$$m' = \int_{dv} \rho' dv' = \int_{dV} \rho'_0 dV' \quad (6)$$

where $\rho'_0 = \rho' J'$, $J' = \det \mathbf{F}'$. Then, the conservation of microelement mass m' is

$$\begin{aligned}
\frac{Dm'}{Dt} &= 0 \\
&= \frac{D}{Dt} \int_{dv} \rho' dv' = \frac{D}{Dt} \int_{dV} \rho' J' dV' \\
&= \int_{dV} \left(\frac{D\rho'}{Dt} J' + \rho' \frac{DJ'}{Dt} \right) dV' \\
&= \int_{dv} \left(\frac{D\rho'}{Dt} + \rho' \frac{\partial v'_l}{\partial x'_l} \right) dv' = 0
\end{aligned} \tag{7}$$

Thus, the pointwise (localized) balance of mass over dv is

$$\frac{D\rho'}{Dt} + \rho' \frac{\partial v'_l}{\partial x'_l} = 0 \tag{8}$$

Now, consider the balance of mass of solid over the whole body \mathcal{B} . We start with the integral-average definition of mass density:

$$\rho dv \stackrel{\text{def}}{=} \int_{dv} \rho' dv' \tag{9}$$

The total mass m of body \mathcal{B} is expressed as

$$m = \int_{\mathcal{B}} \rho dv = \int_{\mathcal{B}} \left[\int_{dv} \rho' dv' \right] = \int_{\mathcal{B}_0} \left[\int_{dV} \rho' J' dV' \right] \tag{10}$$

Then, for conservation of mass over the body \mathcal{B} , we have

$$\begin{aligned}
\frac{Dm}{Dt} &= \int_{\mathcal{B}_0} \left[\int_{dV} \frac{D(\rho' J')}{Dt} dV' \right] \\
&= \int_{\mathcal{B}} \left[\int_{dv} \underbrace{\left(\frac{D\rho'}{Dt} + \rho' \frac{\partial v'_l}{\partial x'_l} \right)}_{=0} dv' \right] = 0
\end{aligned} \tag{11}$$

Then, the balance of mass in \mathcal{B} leads to the standard result

$$\begin{aligned}
\frac{Dm}{Dt} &= \frac{D}{Dt} \int_{\mathcal{B}} \rho dv = 0 \\
&= \int_{\mathcal{B}_0} \frac{D(\rho J)}{Dt} dV \\
&= \int_{\mathcal{B}} \left(\frac{D\rho}{Dt} + \rho \frac{\partial v_l}{\partial x_l} \right) dv = 0
\end{aligned} \tag{12}$$

Localizing the integral, we have the pointwise satisfaction of balance of mass for a single constituent (in this case, solid) material:

$$\frac{D\rho}{Dt} + \rho \frac{\partial v_l}{\partial x_l} = 0 \tag{13}$$

Balance of microinertia:

Given that Ξ_K is the position of microelement dV' centroid C' in the reference configuration with respect to the *mass center* of the macroelement dV centroid C (see figure 3), we have the result

$$\int_{dV} \rho'_0 \Xi_K dV' = 0 \tag{14}$$

This can be thought of as the first mass moment being zero because of the definition Ξ_K as the “relative” position of C' with respect to C (the mass center of dV) (Eringen, 1999).

The second mass moment is not zero, and in the process a microinertia I_{KL} in \mathcal{B}_0 is defined as

$$\rho_0 I_{KL} dV \stackrel{\text{def}}{=} \int_{dV} \rho'_0 \Xi_K \Xi_L dV' \tag{15}$$

Likewise, a microinertia i_{kl} in \mathcal{B} is defined as

$$\rho i_{kl} dv \stackrel{\text{def}}{=} \int_{dv} \rho' \xi_k \xi_l dv' \quad (16)$$

$$\begin{aligned} &= \int_{dv} \rho' \chi_{kK} \Xi_K \chi_{lL} \Xi_L dv' \\ &= \chi_{kK} \chi_{lL} \int_{dv} \rho'_0 \Xi_K \Xi_L dV' \\ &= \chi_{kK} \chi_{lL} \rho_0 I_{KL} dV = \chi_{kK} \chi_{lL} \rho I_{KL} dv \\ &\implies I_{KL} = \chi_{Kk}^{-1} \chi_{Ll}^{-1} i_{kl} \end{aligned} \quad (17)$$

The balance of microinertia in \mathcal{B}_0 is then defined as

$$\begin{aligned} \frac{D}{Dt} \int_{\mathcal{B}_0} \rho_0 I_{KL} dV &= \int_{\mathcal{B}_0} \rho_0 \frac{DI_{KL}}{Dt} dV = 0 \\ \frac{DI_{KL}}{Dt} &= \chi_{Kk}^{-1} \chi_{Ll}^{-1} \left(\frac{Di_{kl}}{Dt} - \nu_{ka} i_{al} - \nu_{la} i_{ak} \right) \\ &= \int_{\mathcal{B}} \rho \chi_{Kk}^{-1} \chi_{Ll}^{-1} \left(\frac{Di_{kl}}{Dt} - \nu_{ka} i_{al} - \nu_{la} i_{ak} \right) dv = 0 \end{aligned} \quad (18)$$

Localizing the integral, and factoring out $\rho \chi_{Kk}^{-1} \chi_{Ll}^{-1}$, the pointwise balance of microinertia in \mathcal{B} is

$$\frac{Di_{kl}}{Dt} - \nu_{ka} i_{al} - \nu_{la} i_{ak} = 0 \quad (19)$$

Balance of linear momentum and the first moment of momentum: To derive the micromorphic balance of linear momentum and the first moment of momentum (different than angular momentum), Eringen and Suhubi (1964) followed a weighted residual approach, where the point of departure is that balance of linear and angular momentum in the microelement dv' over dv are satisfied:

$$\sigma'_{lk,l} + \rho'(f'_k - a'_k) = 0 \quad (20)$$

$$\sigma'_{lk} = \sigma'_{kl} \quad (21)$$

where microelement Cauchy stress σ' is symmetric (macroelement Cauchy stress σ will be shown to be symmetric). Using a smooth weighting function ϕ' (to be defined for three

cases), the weighted average over \mathcal{B} of the balance of linear momentum on dv is expressed as

$$\int_{\mathcal{B}} \left\{ \int_{dv} \phi' [\sigma'_{lk,l} + \rho'(f'_k - a'_k)] dv' \right\} = 0 \quad (22)$$

where $(\bullet)'_{,l} = \partial(\bullet)' / \partial x'_l$. Applying the chain rule $(\phi' \sigma'_{lk})_{,l} = \phi'_{,l} \sigma'_{lk} + \phi' \sigma'_{lk,l}$, we can rewrite equation 22 as

$$\int_{\mathcal{B}} \left\{ \int_{dv} [(\phi' \sigma'_{lk})_{,l} - \phi'_{,l} \sigma'_{lk} + \rho' \phi' (f'_k - a'_k)] dv' \right\} = 0 \quad (23)$$

$$\int_{\partial \mathcal{B}} \left\{ \int_{da} (\phi' \sigma'_{lk}) n'_l da' \right\} + \int_{\mathcal{B}} \left\{ \int_{dv} [-\phi'_{,l} \sigma'_{lk} + \rho' \phi' (f'_k - a'_k)] dv' \right\} = 0 \quad (24)$$

We consider three cases for the weighting function ϕ' leading to three separate micromorphic balance equations on \mathcal{B} :

1. $\phi' = 1$, balance of linear momentum
2. $\phi' = e_{nmk} x'_m$, balance of angular momentum, where e_{nmk} is the permutation tensor (Holzapfel, 2000)
3. $\phi' = x'_m$, balance of the first moment of momentum

Substituting these three choices for ϕ' into equation 24, we can derive the respective micromorphic balance equations on \mathcal{B} :

1. $\phi' = 1$, balance of linear momentum:

$$\int_{\partial \mathcal{B}} \left\{ \int_{da} \sigma'_{lk} n'_l da' \right\} + \int_{\mathcal{B}} \left\{ \int_{dv} [\rho' (f'_k - a'_k)] dv' \right\} = 0 \quad (25)$$

The spatial-averaged definitions of unsymmetric Cauchy stress σ_{lk} , body force f_k , and acceleration a_k are used to derive the micromorphic balance of linear momentum:

$$\sigma_{lk} n_l da \stackrel{\text{def}}{=} \int_{da} \sigma'_{lk} n'_l da' \quad (26)$$

$$\rho f_k dv \stackrel{\text{def}}{=} \int_{dv} \rho' f'_k dv' \quad (27)$$

$$\rho a_k dv \stackrel{\text{def}}{=} \int_{dv} \rho' a'_k dv' \quad (28)$$

From equation 25 and equations 26–28, there results

$$\int_{\partial\mathcal{B}} \sigma_{lk} n_l da + \int_{\mathcal{B}} \rho(f_k - a_k) dv = 0 \quad (29)$$

$$\int_{\mathcal{B}} [\sigma_{lk,l} + \rho(f_k - a_k)] dv = 0 \quad (30)$$

Localizing the integral, we have the pointwise expression for micromorphic balance of linear momentum

$$\sigma_{lk,l} + \rho(f_k - a_k) = 0 \quad (31)$$

Note that the macroscopic Cauchy stress σ_{lk} is unsymmetric.

2. $\phi' = e_{nmk} x'_m$, $x'_m = x_m + \xi_m$, balance of angular momentum:

$$\begin{aligned} & \int_{\partial\mathcal{B}} \left\{ \int_{da} e_{nmk} (x'_m \sigma'_{lk}) n'_l da' \right\} + \int_{\mathcal{B}} \left\{ \int_{dv} e_{nmk} [-x'_{m,l} \sigma'_{lk} + \rho' x'_m (f'_k - a'_k)] dv' \right\} = 0 \\ & \int_{\partial\mathcal{B}} \left\{ \int_{da} e_{nmk} ((x_m + \xi_m) \sigma'_{lk}) n'_l da' \right\} \\ & + \int_{\mathcal{B}} \left\{ \int_{dv} e_{nmk} [-\sigma'_{mk} + \rho' (x_m + \xi_m) (f'_k - a'_k)] dv' \right\} = 0 \end{aligned} \quad (32)$$

where $x'_{m,l} = \partial x'_m / \partial x'_l = \delta_{ml}$. We analyze the terms in equation 32, using $a'_k = a_k + \ddot{\xi}_k$ and $\ddot{\xi}_k = (\dot{\nu}_{kc} + \nu_{kb} \nu_{bc}) \xi_c$, such that

$$\begin{aligned} \int_{\partial\mathcal{B}} \left\{ \int_{da} e_{nmk} ((x_m + \xi_m) \sigma'_{lk}) n'_l da' \right\} &= \int_{\partial\mathcal{B}} e_{nmk} x_m \underbrace{\int_{da} \sigma'_{lk} n'_l da'}_{\stackrel{\text{def}}{=} \sigma_{lk} n_l da} \\ &+ \int_{\partial\mathcal{B}} e_{nmk} \underbrace{\int_{da} \sigma'_{lk} \xi_m n'_l da'}_{\stackrel{\text{def}}{=} m_{lkm} n_l da} \\ &= e_{nmk} \int_{\partial\mathcal{B}} [x_m \sigma_{lk} n_l + m_{lkm} n_l] da \\ &= e_{nmk} \int_{\mathcal{B}} [\sigma_{mk} + x_m \sigma_{lk,l} + m_{lkm,l}] dv \end{aligned} \quad (33)$$

$$\int_{\mathcal{B}} \left\{ \int_{dv} e_{nmk} [-\sigma'_{mk}] dv' \right\} = -e_{nmk} \underbrace{\int_{\mathcal{B}} \int_{dv} \sigma'_{mk} dv'}_{\stackrel{\text{def}}{=} s_{mk} dv} = -e_{nmk} \int_{\mathcal{B}} s_{mk} dv \quad (34)$$

$$\begin{aligned}
\int_{\mathcal{B}} \left\{ \int_{dv} e_{nmk} [\rho'(x_m + \xi_m) f'_k] dv' \right\} &= \int_{\mathcal{B}} e_{nmk} x_m \underbrace{\int_{dv} \rho' f'_k dv'}_{\stackrel{\text{def}}{=} \rho f_k dv} \\
&\quad + \int_{\mathcal{B}} e_{nmk} \underbrace{\int_{dv} \rho' f'_k \xi_m dv'}_{\stackrel{\text{def}}{=} \rho \ell_{km} dv} \\
&= e_{nmk} \int_{\mathcal{B}} (x_m \rho f_k + \rho \ell_{km}) dv \tag{35}
\end{aligned}$$

$$\begin{aligned}
\int_{\mathcal{B}} \left\{ \int_{dv} e_{nmk} [\rho'(x_m + \xi_m) (-a'_k)] dv' \right\} &= -e_{nmk} \int_{\mathcal{B}} \left\{ \int_{dv} \rho' (x_m a_k + x_m \ddot{\xi}_k + \xi_m a_k \right. \\
&\quad \left. + \xi_m \ddot{\xi}_k) dv' \right\} \\
&= -e_{nmk} \int_{\mathcal{B}} \left[x_m a_k \underbrace{\int_{dv} \rho' dv'}_{\stackrel{\text{def}}{=} \rho dv} \right. \\
&\quad + x_m (\dot{\nu}_{kc} + \nu_{kb} \nu_{bc}) \underbrace{\int_{dv} \rho' \xi_c dv'}_{=0} + a_k \underbrace{\int_{dv} \rho' \xi_m dv'}_{=0} \\
&\quad \left. + \underbrace{\int_{dv} \rho' \ddot{\xi}_k \xi_m dv'}_{\stackrel{\text{def}}{=} \rho \omega_{km} dv} \right] \\
&= -e_{nmk} \int_{\mathcal{B}} [x_m \rho a_k + \rho \omega_{km}] dv \tag{36}
\end{aligned}$$

where m_{lkm} is the higher order (couple) stress, s_{mk} is the symmetric microstress, ℓ_{km} is the body force couple, and ω_{km} is the micro-spin inertia. Combining the terms, we have

$$\begin{aligned}
e_{nmk} \int_{\mathcal{B}} \left[x_m \underbrace{(\sigma_{lk,l} + \rho(f_k - a_k))}_{=0} + \sigma_{mk} - s_{mk} + m_{lkm,l} + \rho(\ell_{km} - \omega_{km}) \right] dv &= 0 \\
e_{nmk} \int_{\mathcal{B}} [\sigma_{mk} - s_{mk} + m_{lkm,l} + \rho(\ell_{km} - \omega_{km})] dv &= 0 \tag{37}
\end{aligned}$$

Thus, upon localizing the integral,

$$e_{nmk} [\sigma_{mk} - s_{mk} + m_{lkm,l} + \rho(\ell_{km} - \omega_{km})] = 0 \quad (38)$$

$$\sigma_{[mk]} - \underbrace{s_{[mk]}}_{=0} + m_{l[km],l} + \rho(\ell_{[km]} - \omega_{[km]}) = 0 \quad (39)$$

resulting in

$$\sigma_{[mk]} + m_{l[km],l} + \rho(\ell_{[km]} - \omega_{[km]}) = 0 \quad (40)$$

where the antisymmetric definition $\sigma_{[mk]} = (\sigma_{mk} - \sigma_{km})/2$. Equation 40 is the pointwise balance of angular momentum on \mathcal{B} , providing three equations to solve for a microrotation vector φ_k (Eringen, 1968). But we want to solve for the general nine-dimensional microdeformation tensor χ_{kK} , thus we need six more equations. The balance of the first moment of momentum provides these additional equations.

3. $\phi' = x'_m$, balance of the first moment of momentum: The analysis follows that used for the balance of angular momentum, except we do not multiply by the permutation tensor e_{nmk} . Thus, we may write equation 38 directly without e_{nmk} :

$$\sigma_{mk} - s_{mk} + m_{lkm,l} + \rho(\ell_{km} - \omega_{km}) = 0 \quad (41)$$

This, in general, provides nine equations to solve for a microdisplacement gradient tensor Φ_{kK} through the definition $\chi_{kK} = \delta_{kK} + \Phi_{kK}$. We note that equation 41 encompasses equation 40 (the three antisymmetric equations), and provides six additional equations (the symmetric part of equation 41) (Eringen and Suhubi, 1964).

Balance of energy: It is assumed the classical balance of energy equation holds in microelement dv' over macroelement dv as

$$\int_{dv} \rho' \dot{e}' dv' = \int_{dv} (\sigma'_{kl} v'_{l,k} + q'_{k,k} + \rho' r') dv' \quad (42)$$

where \dot{e}' is the microinternal energy density per unit mass, q'_k the micro-heat flux, and r' the micro-heat source density per unit mass. This is then integrated to hold over the whole body \mathcal{B} as

$$\int_{\mathcal{B}} \left\{ \int_{dv} \rho' \dot{e}' dv' \right\} = \int_{\mathcal{B}} \left\{ \int_{dv} (\sigma'_{kl} v'_{l,k} + q'_{k,k} + \rho' r') dv' \right\} \quad (43)$$

The individual terms in equation 43 can be analyzed, using $v'_l = v_l + \dot{\xi}_l = v_l + \nu_{lm}\xi_m$, $a'_l = a_l + \ddot{\xi}_l$, and $\sigma'_{kl,k} = \rho'(a'_l - f'_l)$:

$$\int_{dv} \rho' \dot{e}' dv' = \int_{dV} \rho'_0 \dot{e}' dV' = \frac{D}{Dt} \underbrace{\int_{dV} \rho'_0 \dot{e}' dV'}_{\stackrel{\text{def}}{=} \rho_0 e dV = \rho e dv} = \frac{D}{Dt} (\rho_0 e dV) = \rho_0 \dot{e} dV = \rho \dot{e} dv \quad (44)$$

$$\begin{aligned} \int_{dv} \sigma'_{kl} v'_{l,k} dv' &= \int_{dv} [(\sigma'_{kl} v'_l)_{,k} - \sigma'_{kl,k} v'_l] dv' \\ &= \int_{da} \sigma'_{kl} v'_l n'_k da' - \int_{dv} \sigma'_{kl,k} v'_l dv' \\ &= \int_{da} \sigma'_{kl} (v_l + \nu_{lm} \xi_m) n'_k da' - \int_{dv} \rho' (a'_l - f'_l) (v_l + \nu_{lm} \xi_m) dv' \\ &= \underbrace{v_l \int_{da} \sigma'_{kl} n'_k da'}_{\stackrel{\text{def}}{=} \sigma_{kl} n_k da} + \underbrace{\nu_{lm} \int_{da} \sigma'_{kl} \xi_m n'_k da'}_{\stackrel{\text{def}}{=} m_{klm} n_k da} - \underbrace{v_l \int_{dv} \rho' a'_l dv'}_{\stackrel{\text{def}}{=} \rho a_l dv} + \underbrace{v_l \int_{dv} \rho' f'_l dv'}_{\stackrel{\text{def}}{=} \rho f_l dv} \\ &\quad - \underbrace{\nu_{lm} a_l \int_{dv} \rho' \xi_m dv'}_{=0} - \underbrace{\nu_{lm} \int_{dv} \rho' \ddot{\xi}_l \xi_m dv'}_{\stackrel{\text{def}}{=} \rho \omega_{lm} dv} + \underbrace{\nu_{lm} \int_{dv} \rho' f'_l \xi_m dv'}_{\stackrel{\text{def}}{=} \rho \ell_{lm} dv} \end{aligned} \quad (45)$$

$$\int_{dv} q'_{k,k} dv' = \int_{da} q'_k n'_k da' \stackrel{\text{def}}{=} q_k n_k da \quad (46)$$

$$\int_{dv} \rho' r' dv' \stackrel{\text{def}}{=} \rho r dv \quad (47)$$

Substituting these terms back into equation 43, we have

$$\begin{aligned} \int_{\mathcal{B}} \rho \dot{e} dv &= \int_{\partial \mathcal{B}} (v_l \sigma_{kl} n_k + \nu_{lm} m_{klm} n_k) da - \int_{\mathcal{B}} v_l \rho (a_l - f_l) dv - \int_{\mathcal{B}} \nu_{lm} \rho (\omega_{lm} - \ell_{lm}) dv \\ &\quad + \int_{\partial \mathcal{B}} q_k n_k da + \int_{\mathcal{B}} \rho r dv \\ &= \int_{\mathcal{B}} \left[v_l \underbrace{(\sigma_{kl,k} + \rho(f_l - a_l))}_{=0} + \nu_{lm} \underbrace{(m_{klm,k} + \rho(\ell_{lm} - \omega_{lm}))}_{=s_{ml} - \sigma_{ml}} \right. \\ &\quad \left. + v_{l,k} \sigma_{kl} + \nu_{lm,k} m_{klm} + q_{k,k} + \rho r \right] dv \end{aligned} \quad (48)$$

Localizing the integral, the pointwise balance of energy over \mathcal{B} becomes

$$\rho \dot{e} = \nu_{lm} (s_{ml} - \sigma_{ml}) + v_{l,k} \sigma_{kl} + \nu_{lm,k} m_{klm} + q_{k,k} + \rho r \quad (49)$$

Second Law of Thermodynamics and Clausius-Duhem Inequality: We assume the second law is valid in microelement dv' over dv such that

$$\underbrace{\frac{D}{Dt} \int_{dv} \rho' \eta' dv'}_{\int_{dv} \rho' \dot{\eta}' dv' \stackrel{\text{def}}{=} \rho \dot{\eta} dv} - \underbrace{\int_{da} \frac{1}{\theta} q'_k n'_k da'}_{\int_{dv} (\frac{q'_k}{\theta})_{,k} dv' \stackrel{\text{def}}{=} (\frac{q_k}{\theta})_{,k} dv} - \underbrace{\int_{dv} \frac{\rho' r'}{\theta} dv'}_{\stackrel{\text{def}}{=} \frac{\rho r}{\theta} dv} \geq 0 \quad (50)$$

Note that no microtemperature θ' is currently introduced (Eringen. 1999). Integrating over \mathcal{B} , localizing the integral, and multiplying by macrotemperature θ , we arrive at the pointwise form of the second law as

$$\int_{\mathcal{B}} \rho \dot{\eta} dv - \int_{\mathcal{B}} \left(\frac{1}{\theta} q_{k,k} - \frac{q_k}{\theta^2} \theta_{,k} \right) dv - \int_{\mathcal{B}} \frac{\rho r}{\theta} dv \geq 0 \quad (51)$$

$$\rho \theta \dot{\eta} - q_{k,k} + \frac{1}{\theta} q_k \theta_{,k} - \rho r \geq 0 \quad (52)$$

We derive the micromorphic Clausius-Duhem inequality by introducing the Helmholtz free energy function ψ , and using the balance of energy in equation 49. Recall the definition of ψ (Holzapfel, 2000), and its material time derivative leading to an expression for $\rho \theta \dot{\eta}$ in equation 52 as

$$\psi = e - \theta \eta \quad (53)$$

$$\dot{\psi} = \dot{e} - \dot{\theta} \eta - \theta \dot{\eta} \quad (54)$$

$$\rho \theta \dot{\eta} = \rho \dot{e} - \rho \dot{\theta} \eta - \rho \dot{\psi} \quad (55)$$

Upon substitution into equation 52 and using equation 49, we arrive at the micromorphic Clausius-Duhem inequality:

$$-\rho(\dot{\psi} + \eta \dot{\theta}) + \sigma_{kl}(v_{l,k} - \nu_{lk}) + s_{kl} \nu_{lk} + m_{klm} \nu_{lm,k} + \frac{1}{\theta} q_k \theta_{,k} \geq 0 \quad (56)$$

Summary of balance equations: The equations are now summarized over the current configuration \mathcal{B} as

$$\left. \begin{aligned}
 &\text{balance of mass : } \frac{D\rho}{Dt} + \rho v_{k,k} = 0 \\
 &\quad \rho dv \stackrel{\text{def}}{=} \int_{dv} \rho' dv' \\
 &\text{balance of microinertia : } \frac{Di_{kl}}{Dt} - \nu_{km} i_{ml} - \nu_{lm} i_{mk} = 0 \\
 &\quad \rho i_{kl} dv \stackrel{\text{def}}{=} \int_{dv} \rho' \xi_k \xi_l dv' \\
 &\text{balance of linear momentum : } \sigma_{lk,l} + \rho(f_k - a_k) = 0 \\
 &\quad \sigma_{lk} n_l da \stackrel{\text{def}}{=} \int_{da} \sigma'_{lk} n'_l da' \\
 &\quad \rho f_k dv \stackrel{\text{def}}{=} \int_{dv} \rho' f'_k dv' \\
 &\quad \rho a_k dv \stackrel{\text{def}}{=} \int_{dv} \rho' a'_k dv' \\
 &\text{balance of first moment of momentum : } \sigma_{ml} - s_{ml} + m_{klm,k} + \rho(\ell_{lm} - \omega_{lm}) = 0 \\
 &\quad s_{ml} dv \stackrel{\text{def}}{=} \int_{dv} \sigma'_{ml} dv' \\
 &\quad m_{klm} n_k da \stackrel{\text{def}}{=} \int_{da} \sigma'_{kl} \xi_m n'_k da' \\
 &\quad \rho \ell_{lm} dv \stackrel{\text{def}}{=} \int_{dv} \rho' f'_l \xi_m dv' \\
 &\quad \rho \omega_{lm} dv \stackrel{\text{def}}{=} \int_{dv} \rho' \ddot{\xi}_l \xi_m dv' \\
 &\text{balance of energy : } \rho \dot{e} = (s_{kl} - \sigma_{kl}) \nu_{lk} + \sigma_{kl} \nu_{l,k} \\
 &\quad + m_{klm} \nu_{lm,k} + q_{k,k} + \rho r \\
 &\text{Clausius – Duhem inequality : } -\rho(\dot{\psi} + \eta \dot{\theta}) + \sigma_{kl}(\nu_{l,k} - \nu_{lk}) + s_{kl} \nu_{lk} \\
 &\quad + m_{klm} \nu_{lm,k} + \frac{1}{\theta} q_k \theta_{,k} \geq 0
 \end{aligned} \right\} \quad (57)$$

where $D(\bullet)/Dt$ is the material time derivative, i_{kl} is the symmetric microinertia tensor, σ_{lk} is the unsymmetric Cauchy stress, f_k the body force vector per unit mass, f'_l is the body force vector per unit mass over the microelement, a_k is the acceleration, s_{ml} is the symmetric microstress, m_{klm} the higher order couple stress, ℓ_{lm} the body force couple per unit mass, ω_{lm} the microspin inertia per unit mass, e is the internal energy per unit mass, ν_{lk} is the microgyration tensor, $\nu_{l,k}$ is the velocity gradient, $\nu_{lm,k}$ is the spatial derivative of the microgyration tensor, q_k is the heat flux vector, r is the heat supply per unit mass, ψ is the Helmholtz free energy per unit mass, η is the entropy per unit mass, and θ is the absolute temperature. Note that the balance of first moment of momentum is more general than the balance of angular momentum (or “moment of momentum” [Eringen, 1962]), such that its skew-symmetric part is the angular momentum balance of a micropolar continuum (see equation 40)). Recall that the Cauchy stress σ'_{ml} over the microelement is symmetric

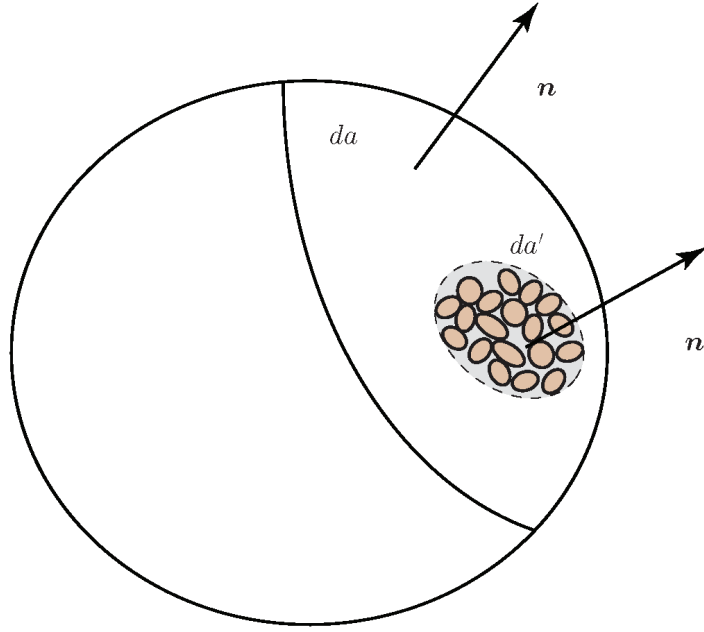


Figure 4. Differential area of microelement da' within macroelement da in current configuration \mathcal{B} .

because the balance of angular momentum is satisfied over the microelement (Eringen and Suhubi, 1964).

Physically, the microstress \mathbf{s} defined in equation 57₄ as the volume average of the Cauchy stress σ' over the microelement, can be interpreted in the context of its difference with the unsymmetric Cauchy stress as $\mathbf{s} - \sigma$ (Mindlin (1964) called this the “relative stress”). This is the energy conjugate driving stress for the microdeformation χ through its microgyration tensor $\nu = \dot{\chi}\chi^{-1}$ in equation 57₅, and also the reduced dissipation inequality in the intermediate configuration equations 95 and 98 as $\bar{\Sigma} - \bar{\mathbf{S}}$ (the analogous stress difference in $\bar{\mathcal{B}}$). In fact, we do not solve for \mathbf{s} or $\bar{\Sigma}$ directly, but constitutively we solve for the difference $\mathbf{s} - \sigma$ or $\bar{\Sigma} - \bar{\mathbf{S}}$ (see equation 118). The higher-order stress \mathbf{m} is analogous to the double stress μ in Mindlin (1964) with physical components of microstretch, microshear, and microrotation shown in his figure 2. For example, m_{112} is the higher order shear stress in the x_2 direction based on a stretch in the x_1 direction. Using the area average definition for m_{klm} , we have $m_{112}n_1 \stackrel{\text{def}}{=} (1/da) \int_{da} \sigma'_{11}\xi_2 n'_1 da'$, where σ'_{11} is the normal microelement stress in the x_1 direction, and ξ_2 is the shear couple in the x_2 direction.

2.3 Finite Strain Micromorphic Elastoplasticity

This section proposes a phenomenological bridging-scale constitutive modeling framework in the context of finite strain micromorphic elastoplasticity based on a multiplicative

decomposition of the deformation gradient \mathbf{F} and microdeformation tensor χ into elastic and plastic parts. In addition to the three translational displacement vector \mathbf{u} degrees of freedom (DOFs), there are nine DOFs associated with the unsymmetric microdeformation tensor χ (microrotation, microstretch, and microshear). We leave the formulation general in terms of χ , which can be further simplified depending on the material and associated constitutive assumptions (see Forest and Sievert (2003, 2006)). The Clausius-Duhem inequality formulated in the intermediate configuration yields the mathematical form of three levels of plastic evolutions equations in either (1) Mandel-stress form (Mandel, 1974), or (2) an alternate ‘metric’ form. For demonstration of the micromorphic elastoplasticity modeling framework, J_2 flow plasticity and linear isotropic elasticity are initially assumed, extended to a pressure-sensitive Drucker-Prager plasticity model, and then mapped to the current configuration for semi-implicit numerical time integration.

The formulation presented here differs from other works on finite strain micromorphic elastoplasticity that consider a multiplicative decomposition into elastic and plastic parts (Sansour 1998, Forest and Sievert, 2003, 2006) and those that do not (Lee and Chen, 2003; Vernerey et al., 2007).

Sansour (1998) considered a finite strain Cosserat and micromorphic plastic continuum, redefining the micromorphic strain measures (see equation B-) in appendix B) to be invariant with respect to rigid rotations only, not also translations. Sansour did not extend his formulation to include details on a finite strain micromorphic elastoplasticity constitutive model formulation, as this report does. Sansour proposed to arrive at the higher-order macro-continuum by integrally-averaging micro-continuum plasticity behavior using computation. Such an approach is similar to computational homogenization, as proposed by Forest and Sievert (2006) to estimate material parameters for generalized continuum plasticity models. On a side note, one advantage to the micromorphic continuum approach by Eringen and Suhubi (1964) is that the integral-averaging of certain stresses, body forces, and microinertia terms are already part of the formulation. This becomes especially useful when computationally homogenizing the underlying microstructural mechanical response (e.g., provided by a microstructural FE or DE simulation) in regions of interest, such as overlapping between micromorphic continuum and grain/particle/fiber representations for a concurrent multiscale modeling approach (figure 12).

Forest and Sievert (2003, 2006) established a hierarchy of elastoplastic models for generalized continua, including Cosserat, higher grade, and micromorphic at small and finite strain. Specifically with regard to micromorphic finite strain theory, Forest and Sievert (2003) follows the approach of Germain (1973), which leads to different stress power terms in the balance of energy and, in turn, Clausius-Duhem inequality than presented by Eringen (1999). Also, the invariant elastic deformation measures do not

match the sets 89 and B-1 proposed by Eringen (1999). Upon analyzing the change in square of microelement arc-lengths $(ds')^2 - (d\bar{S}')^2$ between current \mathcal{B} and intermediate configurations $\bar{\mathcal{B}}$ (cf. appendix C), then either set 89 or B-1 is unique. Forest and Sievert (2003, 2006) proposed to use a mix of the two sets, i.e. equations 8)₁, B-1₂, and B-1₃, in their Helmholtz free energy function. When analyzing $(ds')^2 - (d\bar{S}')^2$, they would also need (B-1)₁ as a fourth elastic deformation measure. As Eringen proposed, however, it is more straightforward to use either set 89 or B-1 when representing elastic deformation. The report presents both sets, but we use equation 89. Mandel stress tensors are identified in Forest and Sievert (2003, 2006) to use in the plastic evolution equations. This report presents additional Mandel stresses and considers also an alternate “metric”-form often used in finite deformation elastoplasticity modeling.

Vernerey et al. (2007) treated micromorphic plasticity modeling similar to Germain (1973) and Mindlin (1964), which leads to different stress power terms and balance equations than in Eringen (1999). The resulting plasticity model form is thus similar to Forest and Sievert (2003), although does not use a multiplicative decomposition and thus does not assume the existence of an intermediate configuration. An extension presented by Vernerey et al. (2007) is to consider multiple scale micromorphic kinematics, stresses, and balance equations, where the number of scales is a choice made by the constitutive modeler. A multiple scale averaging procedure is introduced to determine material parameters at the higher scales based on lower scale response.

In general, in terms of a multiplicative decomposition of the deformation gradient and microdeformation, as compared to recent formulations of finite strain micromorphic elastoplasticity reported in the literature (just reviewed in preceding paragraphs), we view our approach to be more in line with the original concept and formulation presented by Eringen and Suhubi (1964), Eringen (1999), which provide a clear link between microelement and macroelement deformation, balance equations, and stresses. Thus, we believe our formulation and resulting elastoplasticity model framework is more general than what has been presented previously. The paper by Lee and Chen (2003) also follows closely Eringen’s micromorphic kinematics and balance laws, but does not treat multiplicative decomposition kinematics and subsequent constitutive model form in the intermediate configuration, as this report does. We demonstrate the formulation for three levels of J_2 plasticity and linear isotropic elasticity, as well as pressure-sensitive Drucker-Prager plasticity, and numerical time integration by a semi-implicit scheme in the current configuration \mathcal{B} .

2.3.1 Kinematics

We assume a multiplicative decomposition of the deformation gradient (Lee, 1969) and microdeformation (Sansour, 1998; Forest and Sievert, 2003, 2006) (figures 5), such that

$$\begin{aligned}\mathbf{F} &= \mathbf{F}^e \mathbf{F}^p, & \chi &= \chi^e \chi^p \\ F_{kK} &= F_{k\bar{K}}^e F_{\bar{K}K}^p, & \chi_{kK} &= \chi_{k\bar{K}}^e \chi_{\bar{K}K}^p\end{aligned}\tag{58}$$

Given the multiplicative decompositions of \mathbf{F} and χ , the velocity gradient and microgyration tensors can be expressed as

$$\ell = \dot{\mathbf{F}}\mathbf{F}^{-1} = \dot{\mathbf{F}}^e \mathbf{F}^{e-1} + \mathbf{F}^e \bar{\mathbf{L}}^p \mathbf{F}^{e-1} = \ell^e + \ell^p \tag{59}$$

$$\begin{aligned}v_{l,k} &= \dot{F}_{l\bar{A}}^e F_{\bar{A}k}^{e-1} + F_{l\bar{B}}^e \bar{L}_{\bar{B}\bar{C}}^p F_{\bar{C}k}^{e-1} = \ell_{lk}^e + \ell_{lk}^p \\ \bar{L}_{\bar{B}\bar{C}}^p &= \dot{F}_{\bar{B}\bar{B}}^p F_{\bar{B}\bar{C}}^{p-1} \\ \nu &= \dot{\chi}\chi^{-1} = \dot{\chi}^e \chi^{e-1} + \chi^e \bar{\mathbf{L}}^{\chi,p} \chi^{e-1} = \nu^e + \nu^p \\ \nu_{lk} &= \dot{\chi}_{l\bar{A}}^e \chi_{\bar{A}k}^{e-1} + \chi_{l\bar{B}}^e \bar{L}_{\bar{B}\bar{C}}^{\chi,p} \chi_{\bar{C}k}^{e-1} = \nu_{lk}^e + \nu_{lk}^p \\ \bar{L}_{\bar{B}\bar{C}}^{\chi,p} &= \dot{\chi}_{\bar{B}\bar{B}}^p \chi_{\bar{B}\bar{C}}^{p-1}\end{aligned}\tag{60}$$

In the next section, the Clausius-Duhem inequality requires the spatial derivative of the microgyration tensor, which split into elastic and plastic parts based on (60). Thus, it is written as

$$\nabla \nu = \nabla \nu^e + \nabla \nu^p \tag{61}$$

$$\begin{aligned}\nu_{lm,k} &= \nu_{lm,k}^e + \nu_{lm,k}^p \\ \nu_{lm,k}^e &= \dot{\chi}_{l\bar{A},k}^e \chi_{\bar{A}m}^{e-1} - \nu_{ln}^e \chi_{n\bar{D},k}^e \chi_{\bar{D}m}^{e-1}\end{aligned}\tag{62}$$

$$\begin{aligned}\nu_{lm,k}^p &= \left(\chi_{l\bar{C},k}^e \dot{\chi}_{\bar{C}A}^p + \chi_{l\bar{E}}^e \dot{\chi}_{\bar{E}A,k}^p - \chi_{l\bar{F}}^e \bar{L}_{\bar{F}\bar{G}}^{\chi,p} \chi_{\bar{G}A,k}^p \right) \chi_{\bar{A}m}^{-1} \\ &\quad - \nu_{la}^p \chi_{a\bar{A},k}^e \chi_{\bar{A}m}^{e-1}\end{aligned}\tag{63}$$

The spatial derivative of the elastic microdeformation tensor $\nabla \chi^e$ is analogous to the small strain microdeformation gradient \aleph in Mindlin (1964), and its physical interpretation in figure 2 of Mindlin (1964). For example, $\chi_{11,2}^e$ is an elastic microshear gradient in the x_2 direction based on a microstretch in the x_1 direction. Furthermore, just as differential macroelement volumes map as

$$dv = JdV = J^e J^p dV = J^e d\bar{V} \tag{64}$$

where $J^e = \det \mathbf{F}^e$ and $J^p = \det \mathbf{F}^p$, then microelement differential volumes map as

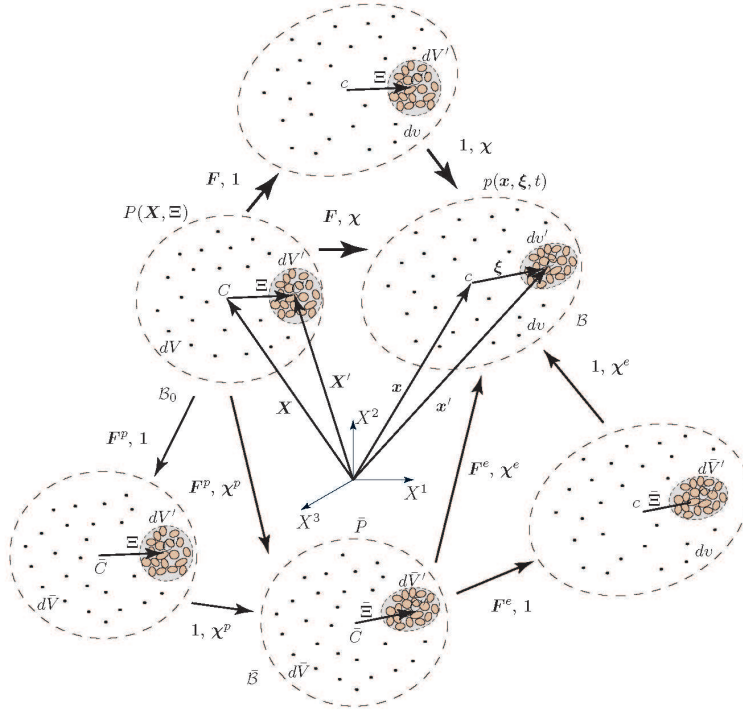


Figure 5. Multiplicative decomposition of deformation gradient \mathbf{F} and microdeformation tensor χ into elastic and plastic parts, and the existence of an intermediate configuration $\tilde{\mathcal{B}}$. Since \mathbf{F}^e , \mathbf{F}^p , χ^e , and χ^p can load and unload independently (although coupled through constitutive equations and balance equations), additional configurations are shown. The constitutive equations and balance equations presented in the report govern these deformation processes, and so generality is preserved.

$$dv' = J' dV' = J^{e'} J^{p'} dV' = J^{e'} d\bar{V}' \quad (65)$$

where $J^{e'} = \det \mathbf{F}^{e'}$ and $J^{p'} = \det \mathbf{F}^{p'}$. $\mathbf{F}^{e'}$ and $\mathbf{F}^{p'}$ have not been defined from equation 5), and are not required for formulating the final constitutive equations. Likewise, according to micro- and macroelement mass conservation, mass densities map as

$$\rho_0 = \rho J = \rho J^e J^p = \bar{\rho} J^p \quad (66)$$

$$\rho'_0 = \rho' J' = \rho' J^{e'} J^{p'} = \bar{\rho}' J^{p'} \quad (67)$$

This last result was achieved by using a volume-average definition relating macroelement mass density to microelement mass density as

$$\rho dv \stackrel{\text{def}}{=} \int_{dv} \rho' dv' , \quad \rho_0 dV \stackrel{\text{def}}{=} \int_{dV} \rho'_0 dV' , \quad \bar{\rho} d\bar{V} \stackrel{\text{def}}{=} \int_{d\bar{V}} \bar{\rho}' d\bar{V}' \quad (68)$$

This volume averaging approach by Eringen and Suhubi (1964) is used extensively in formulating the balance equations and Clausius-Duhem inequality in section 2.2.2.

2.4 Clausius-Duhem Inequality in $\bar{\mathcal{B}}$

This section focusses on the Clausius-Duhem inequality mapped to the intermediate configuration to identify evolution equations for various plastic deformation rates that must be defined constitutively, and their appropriate conjugate stress arguments in $\bar{\mathcal{B}}$.

From a materials modeling perspective, it is often preferred to write the Clausius-Duhem inequality in the intermediate configuration $\bar{\mathcal{B}}$, which is considered naturally elastically unloaded, and formulate constitutive equations there. The physical motivation lies with earlier work by Kondo (1952), Bilby et al. (1955), Kroner (1960), and others, who viewed dislocations in crystals as defects with associated local elastic deformation, where macroscopic elastic deformation could be applied and removed without disrupting the dislocation structure of a crystal. More recent models extend this concept, such as papers by Clayton et al. (2005, 2006) and references therein. The intermediate configuration $\bar{\mathcal{B}}$ can be considered a “reference” material configuration in which fabric/texture anisotropy and other inelastic material properties can be defined. Thus, details on the mapping to $\bar{\mathcal{B}}$ are given in this section. Recall that the Clausius-Duhem inequality in equation 57₆ was written using localization of an integral over the current configuration \mathcal{B} , such that

$$\int_{\mathcal{B}} \left[-\rho(\dot{\psi} + \eta\dot{\theta}) + \sigma_{kl}(\nu_{l,k} - \nu_{lk}) + s_{kl}\nu_{lk} + m_{klm}\nu_{lm,k} + \frac{1}{\theta}q_k\theta_{,k} \right] dv \geq 0 \quad (69)$$

Using the microelement Piola transform $\sigma'_{kl} = F^{e'}_{k\bar{K}} \bar{S}'_{\bar{K}\bar{L}} F^{e'}_{l\bar{L}} / J^{e'}$ and Nanson's formula $n'_k da' = J^{e'} F^{e'}_{\bar{A}k}{}^{-1} \bar{N}'_{\bar{A}} d\bar{A}'$, the following mappings of the area-averaged unsymmetric Cauchy stress σ , volume-averaged symmetric microstress \mathbf{s} , and area-averaged higher order couple stress \mathbf{m} terms are obtained as

$$\begin{aligned} \sigma_{ml} n_m da &\stackrel{\text{def}}{=} \int_{da} \sigma'_{ml} n'_m da' \\ &= \int_{d\bar{A}} \frac{1}{J^{e'}} F^{e'}_{m\bar{M}} \bar{S}'_{\bar{M}\bar{N}} F^{e'}_{l\bar{N}} J^{e'} F^{e'}_{\bar{A}m}{}^{-1} \bar{N}'_{\bar{A}} d\bar{A}' \\ &= \int_{d\bar{A}} F^{e'}_{l\bar{N}} \bar{S}'_{\bar{M}\bar{N}} \bar{N}'_{\bar{M}} d\bar{A}' \\ &= F^e_{l\bar{N}} \bar{S}_{\bar{M}\bar{N}} \bar{N}_{\bar{M}} d\bar{A} \\ &\quad \text{where } \bar{S}_{\bar{M}\bar{N}} \bar{N}_{\bar{M}} d\bar{A} \stackrel{\text{def}}{=} F^{e'}_{\bar{N}a}{}^{-1} \int_{d\bar{A}} F^{e'}_{a\bar{B}} \bar{S}'_{\bar{A}\bar{B}} \bar{N}'_{\bar{A}} d\bar{A}' \\ &\quad \text{recall } \bar{N}_{\bar{M}} d\bar{A} = \frac{1}{J^e} F^e_{m\bar{M}} n_m da \\ &= \underbrace{\frac{1}{J^e} F^e_{m\bar{M}} \bar{S}_{\bar{M}\bar{N}} F^e_{l\bar{N}} n_m da}_{=\sigma_{ml}} \end{aligned} \quad (70)$$

$$\begin{aligned} s_{kl} dv &\stackrel{\text{def}}{=} \int_{dv} \sigma'_{kl} dv' = \int_{d\bar{V}} \frac{1}{J^{e'}} F^{e'}_{k\bar{K}} \bar{S}'_{\bar{K}\bar{L}} F^{e'}_{l\bar{L}} J^{e'} d\bar{V}' \\ &= F^e_{k\bar{K}} F^e_{l\bar{L}} \bar{\Sigma}_{\bar{K}\bar{L}} d\bar{V} \\ &\quad \text{where } \bar{\Sigma}_{\bar{K}\bar{L}} d\bar{V} \stackrel{\text{def}}{=} F^{e'}_{\bar{K}i}{}^{-1} F^{e'}_{\bar{L}j}{}^{-1} \int_{d\bar{V}} F^{e'}_{i\bar{I}} F^{e'}_{j\bar{J}} \bar{S}'_{\bar{I}\bar{J}} d\bar{V}' \\ &= \underbrace{\frac{1}{J^e} F^e_{k\bar{K}} \bar{\Sigma}_{\bar{K}\bar{L}} F^e_{l\bar{L}}}_{=s_{kl}} dv \end{aligned} \quad (71)$$

$$\begin{aligned}
m_{klm}n_k da &\stackrel{\text{def}}{=} \int_{da} \sigma'_{kl} \xi_m n'_k da' \\
&= \int_{d\bar{A}} \frac{1}{J^{e'}} F_{k\bar{K}}^{e'} \bar{S}'_{\bar{K}\bar{L}} F_{l\bar{K}}^{e'} \chi_{m\bar{M}}^e \bar{\Xi}_{\bar{M}} J^{e'} F_{\bar{A}k}^{e'}{}^{-1} \bar{N}'_{\bar{A}} d\bar{A}' \\
&= \int_{d\bar{A}} F_{l\bar{L}}^{e'} \chi_{m\bar{M}}^e \bar{S}'_{\bar{K}\bar{L}} \bar{\Xi}_{\bar{M}} \bar{N}'_{\bar{K}} d\bar{A}' \\
&= F_{l\bar{L}}^e \chi_{m\bar{M}}^e \bar{M}_{\bar{K}\bar{L}\bar{M}} \bar{N}_{\bar{K}} d\bar{A} \\
&\quad \text{where } \bar{M}_{\bar{K}\bar{L}\bar{M}} \bar{N}_{\bar{K}} d\bar{A} \stackrel{\text{def}}{=} F_{\bar{L}a}^e{}^{-1} \int_{d\bar{A}} F_{a\bar{B}}^{e'} \bar{S}'_{\bar{K}\bar{B}} \bar{\Xi}_{\bar{M}} \bar{N}'_{\bar{K}} d\bar{A}' \\
&\quad \text{recall } \bar{N}_{\bar{K}} d\bar{A} = \frac{1}{J^e} F_{k\bar{K}}^e n_k da \\
&= \underbrace{\frac{1}{J^e} F_{k\bar{K}}^e F_{l\bar{L}}^e \chi_{m\bar{M}}^e \bar{M}_{\bar{K}\bar{L}\bar{M}}}_{=m_{klm}} n_k da
\end{aligned} \tag{72}$$

where $\bar{S}'_{\bar{K}\bar{L}}$ is the symmetric second Piola-Kirchhoff stress in the microelement intermediate configuration (over $d\bar{V}$), $\bar{S}_{\bar{K}\bar{L}}$ is the unsymmetric second Piola-Kirchhoff stress in the intermediate configuration $\bar{\mathcal{B}}$, $\bar{\Sigma}_{\bar{K}\bar{L}}$ is the symmetric second Piola-Kirchhoff microstress in the intermediate configuration $\bar{\mathcal{B}}$, $\bar{M}_{\bar{K}\bar{L}\bar{M}}$ is the higher order couple stress written in the intermediate configuration, and $\bar{N}_{\bar{K}}$ the unit normal on $d\bar{A}$. In general, $\mathbf{F}^{e'} \neq \mathbf{F}^e$, but the constitutive equations in section 2.3.3 do not require that $\mathbf{F}^{e'}$ be defined or solved.

Using the mappings for ρ and dv , and the Piola transform on q_k , the Clausius-Duhem inequality can be rewritten in the intermediate configuration as

$$\begin{aligned}
&\int_{\bar{\mathcal{B}}} \left[-\bar{\rho}(\dot{\bar{\psi}} + \bar{\eta}\dot{\bar{\theta}}) + J^e \sigma_{kl}(v_{l,k} - \nu_{lk}) + J^e s_{kl} \nu_{lk} \right. \\
&\quad \left. + \nu_{lm,k} (F_{k\bar{K}}^e F_{l\bar{L}}^e \chi_{m\bar{M}}^e \bar{M}_{\bar{K}\bar{L}\bar{M}}) + \frac{1}{\bar{\theta}} \bar{Q}_{\bar{K}} \bar{\theta}_{,\bar{K}} \right] d\bar{V} \geq 0
\end{aligned} \tag{73}$$

Individual stress power terms in equation 73 can be additively decomposed into elastic and plastic parts based on equations 59–61. Using equation 61, the higher order couple stress power can be written as

$$\begin{aligned}
\nu_{lm,k} \left(F_{k\bar{K}}^e F_{l\bar{L}}^e \chi_{m\bar{M}}^e \bar{M}_{\bar{K}\bar{L}\bar{M}} \right) = \\
\bar{M}_{\bar{K}\bar{L}\bar{M}} F_{l\bar{L}}^e \left(\dot{\chi}_{a\bar{M},\bar{K}}^e - \nu_{ln}^e \chi_{n\bar{M},\bar{K}}^e \right) \Big\} \text{elastic} \\
+ M_{\bar{K}\bar{L}\bar{M}} F_{l\bar{L}}^e \left(-\nu_{ln}^p \chi_{n\bar{M},\bar{K}}^e \right) \Big\} \text{plastic} \\
+ \left[\chi_{a\bar{C},\bar{K}}^e \dot{\chi}_{\bar{C}A}^p + \chi_{a\bar{D}}^e \dot{\chi}_{\bar{D}A,\bar{K}}^p - \chi_{a\bar{B}}^e \bar{L}_{\bar{B}\bar{E}}^{\chi,p} \chi_{\bar{E}A,\bar{K}}^p \right] \chi_{A\bar{M}}^{p-1} \Big\} \text{plastic}
\end{aligned} \tag{74}$$

where the spatial derivative with respect to the intermediate configuration $\bar{\mathcal{B}}$ can be defined as

$$(\bullet)_{,\bar{K}} \stackrel{\text{def}}{=} (\bullet)_{,k} F_{k\bar{K}}^e \tag{75}$$

The other stress power terms using equations 59 and 60 are written as

$$J^e \sigma_{kl} v_{l,k} = \underbrace{F_{k\bar{L}}^e \dot{F}_{k\bar{K}}^e \bar{S}_{\bar{K}\bar{L}}}_{\text{elastic}} + \underbrace{\bar{C}_{\bar{L}\bar{B}}^e \bar{L}_{\bar{B}\bar{K}}^p \bar{S}_{\bar{K}\bar{L}}}_{\text{plastic}} \tag{76}$$

$$J^e \sigma_{kl} \nu_{lk} = \underbrace{(F_{l\bar{L}}^e \nu_{lk}^e F_{k\bar{K}}^e) \bar{S}_{\bar{K}\bar{L}}}_{\text{elastic}} + \underbrace{\bar{\Psi}_{\bar{L}\bar{E}}^e \bar{L}_{\bar{E}\bar{F}}^{\chi,p} \chi_{\bar{F}k}^{e-1} F_{k\bar{K}}^e \bar{S}_{\bar{K}\bar{L}}}_{\text{plastic}} \tag{77}$$

$$J^e s_{kl} \nu_{lk} = \underbrace{(F_{l\bar{L}}^e \nu_{lk}^e F_{k\bar{K}}^e) \bar{\Sigma}_{\bar{K}\bar{L}}}_{\text{elastic}} + \underbrace{\bar{\Psi}_{\bar{L}\bar{E}}^e \bar{L}_{\bar{E}\bar{F}}^{\chi,p} \chi_{\bar{F}k}^{e-1} F_{k\bar{K}}^e \bar{\Sigma}_{\bar{K}\bar{L}}}_{\text{plastic}} \tag{78}$$

where $\bar{C}_{\bar{L}\bar{B}}^e = F_{a\bar{L}}^e F_{a\bar{B}}^e$ is the right elastic Cauchy-Green tensor $\bar{\mathbf{C}}^e = \mathbf{F}^{eT} \mathbf{F}^e$ in $\bar{\mathcal{B}}$, and $\bar{\Psi}_{\bar{L}\bar{E}}^e = F_{l\bar{L}}^e \chi_{l\bar{E}}^e$ an elastic deformation measure in $\bar{\mathcal{B}}$ as $\bar{\Psi}^e = \mathbf{F}^{eT} \chi^e$ (cf. appendix C).

Similar to Eringen and Suhubi (1964) for a micromorphic elastic material, the Helmholtz free energy function in $\bar{\mathcal{B}}$ is assumed to take the following functional form for micromorphic elastoplasticity as

$$\begin{aligned}
\bar{\rho} \bar{\psi}(\mathbf{F}^e, \chi^e, \bar{\nabla} \chi^e, \bar{\mathbf{Z}}, \bar{\mathbf{Z}}^\chi, \bar{\nabla} \bar{\mathbf{Z}}^\chi, \theta) \\
\bar{\rho} \bar{\psi}(F_{k\bar{K}}^e, \chi_{k\bar{K}}^e, \chi_{k\bar{M},\bar{K}}^e, \bar{Z}_{\bar{K}}, \bar{Z}_{\bar{K}}^\chi, \bar{Z}_{\bar{K},\bar{L}}^\chi, \theta)
\end{aligned} \tag{79}$$

where $\bar{Z}_{\bar{K}}$ is a vector of macro strain-like ISVs in $\bar{\mathcal{B}}$, $\bar{Z}_{\bar{K}}^\chi$ is a vector of micro strain-like ISVs, and $\bar{Z}_{\bar{K},\bar{L}}^\chi$ is a spatial derivative of a vector of micro strain-like ISVs. Then, by the chain rule

$$\begin{aligned}
\frac{D(\bar{\rho}\bar{\psi})}{Dt} &= \frac{\partial(\bar{\rho}\bar{\psi})}{\partial F_{k\bar{K}}^e} \dot{F}_{k\bar{K}}^e + \frac{\partial(\bar{\rho}\bar{\psi})}{\partial \chi_{k\bar{K}}^e} \dot{\chi}_{k\bar{K}}^e + \frac{\partial(\bar{\rho}\bar{\psi})}{\partial \chi_{k\bar{M},\bar{K}}^e} \frac{D(\chi_{k\bar{M},\bar{K}}^e)}{Dt} \\
&+ \frac{\partial(\bar{\rho}\bar{\psi})}{\partial \bar{Z}_{\bar{K}}} \dot{\bar{Z}}_{\bar{K}} + \frac{\partial(\bar{\rho}\bar{\psi})}{\partial \bar{Z}_{\bar{K}}^x} \dot{\bar{Z}}_{\bar{K}}^x + \frac{\partial(\bar{\rho}\bar{\psi})}{\partial \bar{Z}_{\bar{K},\bar{L}}^x} \frac{D(\bar{Z}_{\bar{K},\bar{L}}^x)}{Dt} + \frac{\partial(\bar{\rho}\bar{\psi})}{\partial \theta} \dot{\theta}
\end{aligned} \tag{80}$$

where an artifact of the “free energy per unit mass” assumption is that

$$\frac{D(\bar{\rho}\bar{\psi})}{Dt} = \dot{\bar{\rho}}\bar{\psi} + \bar{\rho}\dot{\bar{\psi}} = -(\bar{\rho}\bar{\psi}) \frac{\dot{J}^p}{J^p} + \bar{\rho}\dot{\bar{\psi}} \implies \bar{\rho}\dot{\bar{\psi}} = (\bar{\rho}\bar{\psi}) \frac{\dot{J}^p}{J^p} + \frac{D(\bar{\rho}\bar{\psi})}{Dt} \tag{81}$$

where we used the result $\dot{\bar{\rho}} = D(\rho_0/J^p)/Dt = -\bar{\rho}\dot{J}^p/J^p$. Substituting equations 74–78 and equations 80, 81 into equation 73, and using the Coleman and Noll (1963) argument for independent rate processes (independent $\dot{F}_{k\bar{K}}^e$, $\dot{\chi}_{k\bar{K}}^e$, $D(\chi_{k\bar{M},\bar{K}}^e)/Dt$, and $\dot{\theta}$), the Clausius-Duhem inequality is satisfied if the following constitutive equations hold:

$$\bar{S}_{\bar{K}\bar{L}} = \frac{\partial(\bar{\rho}\bar{\psi})}{\partial F_{k\bar{K}}^e} F_{\bar{L}k}^{e-1} \tag{82}$$

$$\begin{aligned}
\bar{\Sigma}_{\bar{K}\bar{L}} &= \frac{\partial(\bar{\rho}\bar{\psi})}{\partial F_{k\bar{K}}^e} F_{\bar{L}k}^{e-1} + F_{\bar{K}c}^{e-1} \chi_{c\bar{A}}^e \frac{\partial(\bar{\rho}\bar{\psi})}{\partial \chi_{a\bar{A}}^e} F_{\bar{L}a}^{e-1} \\
&+ F_{\bar{K}d}^{e-1} \chi_{d\bar{M},\bar{E}}^e \frac{\partial(\bar{\rho}\bar{\psi})}{\partial \chi_{f\bar{M},\bar{E}}^e} F_{\bar{L}f}^{e-1}
\end{aligned} \tag{83}$$

$$\bar{M}_{\bar{K}\bar{L}\bar{M}} = \frac{\partial(\bar{\rho}\bar{\psi})}{\partial \chi_{k\bar{M},\bar{K}}^e} F_{\bar{L}k}^{e-1} \tag{84}$$

$$\bar{\rho}\bar{\eta} = -\frac{\partial(\bar{\rho}\bar{\psi})}{\partial \theta} \tag{85}$$

For comparison to the result reported in equation 6.3 of Eringen and Suhubi (1964), we map these stresses to the current configuration, using

$$\sigma_{kl} = \frac{1}{J^e} F_{k\bar{K}}^e \bar{S}_{\bar{K}\bar{L}} F_{l\bar{L}}^e = \frac{1}{J^e} F_{k\bar{K}}^e \frac{\partial(\bar{\rho}\bar{\psi})}{\partial F_{l\bar{K}}^e} \quad (86)$$

$$\begin{aligned} s_{kl} &= \frac{1}{J^e} F_{k\bar{K}}^e \bar{\Sigma}_{\bar{K}\bar{L}} F_{l\bar{L}}^e \\ &= \frac{1}{J^e} \left(F_{k\bar{K}}^e \frac{\partial(\bar{\rho}\bar{\psi})}{\partial F_{l\bar{K}}^e} + \chi_{k\bar{A}}^e \frac{\partial(\bar{\rho}\bar{\psi})}{\partial \chi_{l\bar{A}}^e} + \chi_{k\bar{M},\bar{E}}^e \frac{\partial(\bar{\rho}\bar{\psi})}{\partial \chi_{l\bar{M},\bar{E}}^e} \right) \end{aligned} \quad (87)$$

$$m_{klm} = \frac{1}{J^e} F_{k\bar{K}}^e F_{l\bar{L}}^e \chi_{m\bar{M}}^e \bar{M}_{\bar{K}\bar{L}\bar{M}} = \frac{1}{J^e} \frac{\partial(\bar{\rho}\bar{\psi})}{\partial \chi_{l\bar{M},\bar{K}}^e} F_{k\bar{K}}^e \chi_{m\bar{M}}^e \quad (88)$$

The equations match those in (6.3) of Eringen and Suhubi (1964) if elastic, i.e. $\mathbf{F}^e = \mathbf{F}$, $\chi^e = \chi$. We prefer, however, to express the Helmholtz free energy function in terms of invariant—with respect to rigid body motion on the current configuration \mathcal{B} —elastic deformation measures, such as the set proposed by Eringen and Suhubi (1964) as

$$\bar{C}_{\bar{K}\bar{L}}^e = F_{k\bar{K}}^e F_{k\bar{L}}^e, \quad \bar{\Psi}_{\bar{K}\bar{L}}^e = F_{k\bar{K}}^e \chi_{k\bar{L}}^e, \quad \bar{\Gamma}_{\bar{K}\bar{L}\bar{M}}^e = F_{k\bar{K}}^e \chi_{k\bar{L},\bar{M}}^e \quad (89)$$

We have good physical interpretation of \mathbf{F}^e (and \mathbf{F}^p) from crystal lattice mechanics (Bilby et al., 1955; Kroner, 1960; Lee and Liu, 1967; Lee, 1969), while the elastic microdeformation χ^e has its interpretation in figure 5 of this report (elastic deformation of microelement) and also figure 1 of Mindlin (1964) for small strain theory. The spatial derivative of elastic microdeformation $\bar{\nabla}\chi^e$ has its physical interpretation in figure 2 of Mindlin (1964), and was earlier in this report described for example, as $\chi_{11,2}^e$ is the microshear gradient in the x_2 direction based on a stretch in the x_1 direction (although directions are not exact here because of the spatial derivative with respect to the intermediate configuration $\bar{\mathcal{B}}$). The Helmholtz free energy function $\bar{\psi}$ per unit mass is then written as

$$\begin{aligned} \bar{\rho}\bar{\psi}(\bar{\mathbf{C}}^e, \bar{\Psi}^e, \bar{\Gamma}^e, \bar{\mathbf{Z}}, \bar{\mathbf{Z}}^\chi, \bar{\nabla}\bar{\mathbf{Z}}^\chi, \theta) \\ \bar{\rho}\bar{\psi}(\bar{C}_{\bar{K}\bar{L}}^e, \bar{\Psi}_{\bar{K}\bar{L}}^e, \bar{\Gamma}_{\bar{K}\bar{L}\bar{M}}^e, \bar{Z}_{\bar{K}}, \bar{Z}_{\bar{K}}^\chi, \bar{Z}_{\bar{K},\bar{L}}^\chi, \theta) \end{aligned} \quad (90)$$

and the constitutive equations for stress result from equations 82–84 as

$$\begin{aligned}\bar{S}_{\bar{K}\bar{L}} &= 2\frac{\partial(\bar{\rho}\bar{\psi})}{\partial\bar{C}_{\bar{K}\bar{L}}^e} + \frac{\partial(\bar{\rho}\bar{\psi})}{\partial\bar{\Psi}_{\bar{K}\bar{B}}^e}\bar{C}_{\bar{L}\bar{A}}^{e-1}\bar{\Psi}_{\bar{A}\bar{B}}^e \\ &\quad + \frac{\partial(\bar{\rho}\bar{\psi})}{\partial\bar{\Gamma}_{\bar{K}\bar{B}\bar{C}}^e}\bar{C}_{\bar{L}\bar{A}}^{e-1}\bar{\Gamma}_{\bar{A}\bar{B}\bar{C}}^e\end{aligned}\tag{91}$$

$$\begin{aligned}\bar{\Sigma}_{\bar{K}\bar{L}} &= 2\frac{\partial(\bar{\rho}\bar{\psi})}{\partial\bar{C}_{\bar{K}\bar{L}}^e} + 2\text{sym}\left[\frac{\partial(\bar{\rho}\bar{\psi})}{\partial\bar{\Psi}_{\bar{K}\bar{B}}^e}\bar{C}_{\bar{L}\bar{A}}^{e-1}\bar{\Psi}_{\bar{A}\bar{B}}^e\right] \\ &\quad + 2\text{sym}\left[\frac{\partial(\bar{\rho}\bar{\psi})}{\partial\bar{\Gamma}_{\bar{K}\bar{B}\bar{C}}^e}\bar{C}_{\bar{L}\bar{A}}^{e-1}\bar{\Gamma}_{\bar{A}\bar{B}\bar{C}}^e\right]\end{aligned}\tag{92}$$

$$\bar{M}_{\bar{K}\bar{L}\bar{M}} = \frac{\partial(\bar{\rho}\bar{\psi})}{\partial\bar{\Gamma}_{\bar{L}\bar{M}\bar{K}}^e}\tag{93}$$

where $\text{sym}[\bullet]$ denotes the symmetric part. These stress equations 91–93 when mapped to the current configuration are the same as equations 6.9–11 in Eringen and Suhubi (1964) if there is no plasticity, i.e. $\mathbf{F}^e = \mathbf{F}$ and $\chi^e = \chi$. To consider another set of elastic deformation measures and resulting stresses, refer to appendix B.

The thermodynamically-conjugate stress-like ISVs are defined as

$$\bar{Q}_{\bar{K}} \stackrel{\text{def}}{=} \frac{\partial(\bar{\rho}\bar{\psi})}{\partial\bar{Z}_{\bar{K}}}, \quad \bar{Q}_{\bar{K}}^\chi \stackrel{\text{def}}{=} \frac{\partial(\bar{\rho}\bar{\psi})}{\partial\bar{Z}_{\bar{K}}^\chi}, \quad \bar{Q}_{\bar{K}\bar{L}}^{\nabla\chi} \stackrel{\text{def}}{=} \frac{\partial(\bar{\rho}\bar{\psi})}{\partial\bar{Z}_{\bar{K},\bar{L}}^\chi}\tag{94}$$

which are used in the evolution equations for plastic deformation rates, as well as multiple scale yield functions, where we assume scalar \bar{Z} , \bar{Z}^χ , $\bar{\nabla}\bar{Z}^\chi$, and \bar{Q} , \bar{Q}^χ , $\bar{\mathbf{Q}}^{\nabla\chi}$. The stress-like ISVs in section 2.3.3 are physically interpreted as yield stress \bar{Q} and \bar{Q}^χ for macro-plasticity (stress $\bar{\mathbf{S}}$ calculated from elastic deformation) and micro-plasticity (stress difference $\bar{\Sigma} - \bar{\mathbf{S}}$ calculated from elastic deformation), respectively, while $\bar{\mathbf{Q}}^{\nabla\chi}$ is a higher order yield stress for microgradient plasticity (higher order stress $\bar{\mathbf{M}}$ calculated from gradient elastic deformation).

The remaining terms in the Clausius-Duhem inequality lead to the reduced dissipation inequality expressed in localized form in two ways: (1) Mandel form with Mandel-like stresses (Mandel, 1974), and (2) an alternate ‘metric’ form. Each leads to different ways of writing the plastic evolution equations, and stresses that are used in these evolution equations. From equation 73, the reduced dissipation inequality in Mandel form is written as

$$\begin{aligned}
& (\bar{\rho}\bar{\psi}) \frac{j^p}{j^p} + \frac{1}{\theta} \bar{Q}_{\bar{K}} \theta_{,\bar{K}} - \bar{Q}_{\bar{K}} \dot{\bar{Z}}_{\bar{K}} - \bar{Q}_{\bar{K}}^{\chi} \dot{\bar{Z}}_{\bar{K}}^{\chi} - \bar{Q}_{\bar{K}\bar{L}}^{\nabla\chi} \frac{D(\bar{Z}_{\bar{K},\bar{L}}^{\chi})}{Dt} \\
& + (\bar{S}_{\bar{K}\bar{B}} \bar{C}_{\bar{B}\bar{L}}^e) \bar{L}_{\bar{L}\bar{K}}^p + [\bar{C}_{\bar{K}\bar{N}}^{\chi,e-1} \bar{\Psi}_{\bar{A}\bar{N}}^e (\bar{\Sigma}_{\bar{A}\bar{B}} - \bar{S}_{\bar{A}\bar{B}}) \bar{\Psi}_{\bar{B}\bar{L}}^e] \bar{L}_{\bar{L}\bar{K}}^{\chi,p} \\
& + (\bar{M}_{\bar{K}\bar{L}\bar{M}} \bar{\Psi}_{\bar{L}\bar{D}}^e) \left\{ \bar{L}_{\bar{D}\bar{M},\bar{K}}^{\chi,p} - 2\text{skw} [\bar{L}_{\bar{D}\bar{C}}^{\chi,p} \bar{\Psi}_{\bar{C}\bar{F}}^{e-1} \bar{\Gamma}_{\bar{F}\bar{M}\bar{K}}^e] \right\} \geq 0
\end{aligned} \tag{95}$$

where $\bar{C}_{\bar{K}\bar{N}}^{\chi,e-1} = \chi^{e-1}_{\bar{K}k} \chi^{e-1}_{\bar{N}k}$, $\bar{\Psi}_{\bar{C}\bar{F}}^{e-1} = \chi^{e-1}_{\bar{C}i} F^{e-1}_{\bar{F}i}$, $\text{skw}[\bullet]$ denotes the skew-symmetric part defined as

$$2\text{skw}[\bullet] \stackrel{\text{def}}{=} [\bar{L}_{\bar{D}\bar{C}}^{\chi,p} \bar{\Psi}_{\bar{C}\bar{F}}^{e-1} \bar{\Gamma}_{\bar{F}\bar{M}\bar{K}}^e] - [\bar{L}_{\bar{B}\bar{M}}^{\chi,p} \bar{\Psi}_{\bar{D}\bar{G}}^{e-1} \bar{\Gamma}_{\bar{G}\bar{B}\bar{K}}^e] \tag{96}$$

and the spatial derivative of the micro-scale plastic velocity gradient is

$$\bar{L}_{\bar{D}\bar{M},\bar{K}}^{\chi,p} = [\dot{\chi}_{\bar{D}\bar{B}}^p \chi_{\bar{B}\bar{M}}^{p-1}]_{,\bar{K}} = \left(\dot{\chi}_{\bar{D}\bar{B},\bar{K}}^p - \bar{L}_{\bar{D}\bar{B}}^{\chi,p} \chi_{\bar{B}\bar{B},\bar{K}}^p \right) \chi_{\bar{B}\bar{M}}^{p-1} \tag{97}$$

The Mandel stresses are $\bar{S}_{\bar{K}\bar{B}} \bar{C}_{\bar{B}\bar{L}}^e$, $\bar{C}_{\bar{K}\bar{N}}^{\chi,e-1} \bar{\Psi}_{\bar{A}\bar{N}}^e (\bar{\Sigma}_{\bar{A}\bar{B}} - \bar{S}_{\bar{A}\bar{B}}) \bar{\Psi}_{\bar{B}\bar{L}}^e$, and $\bar{M}_{\bar{K}\bar{L}\bar{M}} \bar{\Psi}_{\bar{L}\bar{D}}^e$, where the first one is well known as the ‘‘Mandel stress,’’ whereas the second and third are the relative micro-Mandel-stress and the higher order Mandel couple stress, respectively. We rewrite the reduced dissipation inequality equatin 95 in an alternate ‘‘metric’’ form as

$$\begin{aligned}
& -(\bar{\rho}\bar{\psi}) \frac{j^p}{j^p} + \frac{1}{\theta} \bar{Q}_{\bar{K}} \theta_{,\bar{K}} - \bar{Q}_{\bar{K}} \dot{\bar{Z}}_{\bar{K}} - \bar{Q}_{\bar{K}}^{\chi} \dot{\bar{Z}}_{\bar{K}}^{\chi} - \bar{Q}_{\bar{K}\bar{L}}^{\nabla\chi} \frac{D}{Dt} (\bar{Z}_{\bar{K},\bar{L}}^{\chi}) \\
& + \bar{S}_{\bar{K}\bar{L}} (\bar{C}_{\bar{L}\bar{B}}^e \bar{L}_{\bar{B}\bar{K}}^p) + (\bar{\Sigma}_{\bar{K}\bar{L}} - \bar{S}_{\bar{K}\bar{L}}) [\bar{\Psi}_{\bar{L}\bar{E}}^e \bar{L}_{\bar{E}\bar{F}}^{\chi,p} \bar{C}_{\bar{F}\bar{N}}^{\chi,e-1} \bar{\Psi}_{\bar{K}\bar{N}}^e] \\
& + \bar{M}_{\bar{K}\bar{L}\bar{M}} \left\{ \bar{\Psi}_{\bar{L}\bar{D}}^e \bar{L}_{\bar{D}\bar{M},\bar{K}}^{\chi,p} - 2\bar{\Psi}_{\bar{L}\bar{D}}^e \text{skw} [\bar{L}_{\bar{D}\bar{C}}^{\chi,p} \bar{\Psi}_{\bar{C}\bar{F}}^{e-1} \bar{\Gamma}_{\bar{F}\bar{M}\bar{K}}^e] \right\} \geq 0
\end{aligned} \tag{98}$$

Form of plastic evolution equations: Based on equation 95, in order to satisfy the reduced dissipation inequality, we can write plastic evolution equations to solve for $F_{\bar{K}\bar{K}}^p$, $\chi_{\bar{K}\bar{K}}^p$, and $\chi_{\bar{K}\bar{K},\bar{L}}^p$ in Mandel stress form as

$$\bar{L}_{\bar{L}\bar{K}}^p = \bar{H}_{\bar{L}\bar{K}}(\bar{\mathbf{S}}\bar{\mathbf{C}}^e, \bar{\mathbf{Q}}) \quad (99)$$

$$\begin{aligned} & \text{solve for } F_{\bar{K}\bar{K}}^p \text{ and } F_{k\bar{K}}^e = F_{kK}F_{K\bar{K}}^{p-1} \\ \bar{L}_{\bar{L}\bar{K}}^{\chi,p} &= \bar{H}_{\bar{L}\bar{K}}^\chi((\bar{\mathbf{C}}^{\chi,e})^{-1}\bar{\Psi}^{eT}(\bar{\Sigma} - \bar{\mathbf{S}})\bar{\Psi}^e, \bar{\mathbf{Q}}^\chi) \\ & \text{solve for } \chi_{\bar{K}\bar{K}}^p \text{ and } \chi_{k\bar{K}}^e = \chi_{kK}\chi_{K\bar{K}}^{p-1} \end{aligned} \quad (100)$$

$$\begin{aligned} \bar{L}_{\bar{D}\bar{M},\bar{K}}^{\chi,p} - 2\text{skw}[\bar{L}_{\bar{D}\bar{C}}^{\chi,p}\bar{\Psi}_{\bar{C}\bar{F}}^{e-1}\bar{\Gamma}_{\bar{F}\bar{M}\bar{K}}^e] &= \bar{H}_{\bar{D}\bar{M}\bar{K}}^{\nabla\chi}(\bar{\mathbf{M}}\bar{\Psi}^e, \bar{\mathbf{Q}}^{\nabla\chi}) \\ & \text{solve for } \chi_{\bar{K}\bar{K},\bar{L}}^p \text{ and } \chi_{k\bar{K},\bar{L}}^e = (\chi_{kK,\bar{L}} - \chi_{k\bar{A}}^e\chi_{\bar{A}K,\bar{L}}^p)\chi_{K\bar{K}}^{p-1} \end{aligned} \quad (101)$$

where the arguments in parentheses (\bullet) denote the Mandel stress and stress-like ISV to use in the respective plastic evolution equation, where $\bar{\mathbf{H}}$, $\bar{\mathbf{H}}^\chi$, and $\bar{\mathbf{H}}^{\nabla\chi}$ denote tensor functions for the evolution equations, chosen to ensure that convexity is satisfied, and the dissipation is positive. This can be seen for the evolution equations in 102–104 by the constitutive definitions in equations 120, 124, and 128 in terms of stress gradients of potential functions (i.e., the yield functions for associative plasticity). In an alternate “metric” form, from equation 98, we can solve for the plastic deformation variables as

$$\bar{C}_{\bar{L}\bar{B}}^e\bar{L}_{\bar{B}\bar{K}}^p = \bar{H}_{\bar{L}\bar{K}}(\bar{\mathbf{S}}, \bar{\mathbf{Q}}) \quad (102)$$

$$\begin{aligned} & \text{solve for } F_{\bar{K}\bar{K}}^p \text{ and } F_{k\bar{K}}^e = F_{kK}F_{K\bar{K}}^{p-1} \\ \bar{\Psi}_{\bar{L}\bar{E}}^e\bar{L}_{\bar{E}\bar{F}}^{\chi,p}\bar{C}_{\bar{F}\bar{N}}^{\chi,e-1}\bar{\Psi}_{\bar{K}\bar{N}}^e &= \bar{H}_{\bar{L}\bar{K}}^\chi(\bar{\Sigma} - \bar{\mathbf{S}}, \bar{\mathbf{Q}}^\chi) \end{aligned} \quad (103)$$

$$\begin{aligned} & \text{solve for } \chi_{\bar{K}\bar{K}}^p \text{ and } \chi_{k\bar{K}}^e = \chi_{kK}\chi_{K\bar{K}}^{p-1} \\ \bar{\Psi}_{\bar{L}\bar{D}}^e\bar{L}_{\bar{D}\bar{M},\bar{K}}^{\chi,p} - 2\bar{\Psi}_{\bar{L}\bar{D}}^e\text{skw}[\bar{L}_{\bar{D}\bar{C}}^{\chi,p}\bar{\Psi}_{\bar{C}\bar{F}}^{e-1}\bar{\Gamma}_{\bar{F}\bar{M}\bar{K}}^e] &= \bar{H}_{\bar{L}\bar{M}\bar{K}}^{\nabla\chi}(\bar{\mathbf{M}}, \bar{\mathbf{Q}}^{\nabla\chi}) \end{aligned} \quad (104)$$

$$\text{solve for } \chi_{\bar{K}\bar{K},\bar{L}}^p \text{ and } \chi_{k\bar{K},\bar{L}}^e = (\chi_{kK,\bar{L}} - \chi_{k\bar{A}}^e\chi_{\bar{A}K,\bar{L}}^p)\chi_{K\bar{K}}^{p-1}$$

We use this “metric” form in defining evolution equations in section 2.3.3.

Remark 1. The reason that we propose the third plastic evolution equation 101 or 104 to solve for $\chi_{\bar{K}\bar{K},\bar{L}}^p$ directly (not calculating a spatial derivative of the tensor $\chi_{\bar{K}\bar{K}}^p$ from a FE interpolation of χ^p) is to potentially avoid requiring an additional balance equation to solve in weak form by a nonlinear FE method (refer to Regueiro et al. (2007) and references therein). With future FE implementation and numerical examples, we will attempt to determine whether equations 101 or 104 leads to an accurate calculation of $\chi_{\bar{K}\bar{K},\bar{L}}^p$. In Regueiro (2010), a simpler anti-plane shear version of the model demonstrates the two ways for calculating $\bar{\nabla}\chi^p$, either by an evolution equation like in equations 101 or 104, or a FE interpolation for χ^p and corresponding gradient calculation $\bar{\nabla}\chi^p$. Note that in Forest and Sievert (2003), for their equation 155₃, they also propose a direct evolution of a gradient of plastic microdeformation.

2.4.1 Constitutive Equations

The constitutive equations for linear isotropic elasticity, J_2 flow associative plasticity, and Drucker-Prager nonassociative plasticity with scalar ISV hardening/softening are formulated. We define a specific form of the Helmholtz free energy function, yield functions, and evolution equations for ISVs, and then conduct a semi-implicit numerical time integration presented in section 2.3.4.

2.4.2 Linear Isotropic Elasticity and J_2 Flow Isochoric Plasticity

Helmholtz free energy and stresses: Assuming linear elasticity and linear relation between stress-like and strain-like ISVs, a quadratic form for the Helmholtz free energy function results as

$$\begin{aligned} \bar{\rho}\bar{\psi} \stackrel{\text{def}}{=} & \frac{1}{2}\bar{E}_{\bar{K}\bar{L}}^e\bar{A}_{\bar{K}\bar{L}\bar{M}\bar{N}}\bar{E}_{\bar{M}\bar{N}}^e + \frac{1}{2}\bar{\mathcal{E}}_{\bar{K}\bar{L}}^e\bar{B}_{\bar{K}\bar{L}\bar{M}\bar{N}}\bar{\mathcal{E}}_{\bar{M}\bar{N}}^e \\ & + \frac{1}{2}\bar{\Gamma}_{\bar{K}\bar{L}\bar{M}}^e\bar{C}_{\bar{K}\bar{L}\bar{M}\bar{N}\bar{P}\bar{Q}}\bar{\Gamma}_{\bar{N}\bar{P}\bar{Q}}^e + \bar{E}_{\bar{K}\bar{L}}^e\bar{D}_{\bar{K}\bar{L}\bar{M}\bar{N}}\bar{\mathcal{E}}_{\bar{M}\bar{N}}^e \\ & + \frac{1}{2}\bar{H}\bar{Z}^2 + \frac{1}{2}\bar{H}^\chi(\bar{Z}^\chi)^2 + \frac{1}{2}\bar{Z}_{\bar{K}}^\chi\bar{H}_{\bar{K}\bar{L}}^{\nabla\chi}\bar{Z}_{\bar{L}}^\chi \end{aligned} \quad (105)$$

Note that the ISVs are scalar variables in this model, which are related to scalar yield strength of the material at two scales, macro and micro, and \bar{H} and \bar{H}^χ are scalar hardening/softening parameters, and $\bar{H}_{\bar{K}\bar{L}}^{\nabla\chi}$ is a symmetric second order hardening/softening modulus tensor, which we assume is isotropic as $\bar{H}_{\bar{K}\bar{L}}^{\nabla\chi} = (\bar{H}^{\nabla\chi})\delta_{\bar{K}\bar{L}}$. Elastic strains are defined as (Suhubi and Eringen, 1964) $2\bar{E}_{\bar{K}\bar{L}}^e = \bar{C}_{\bar{K}\bar{L}}^e - \delta_{\bar{K}\bar{L}}$ and $\bar{\mathcal{E}}_{\bar{K}\bar{L}}^e = \bar{\Psi}_{\bar{K}\bar{L}}^e - \delta_{\bar{K}\bar{L}}$. The elastic moduli are defined for isotropic linear elasticity, after manipulation of equations in Suhubi and Eringen (1964) as

$$\bar{A}_{\bar{K}\bar{L}\bar{M}\bar{N}} = \lambda\delta_{\bar{K}\bar{L}}\delta_{\bar{M}\bar{N}} + \mu(\delta_{\bar{K}\bar{M}}\delta_{\bar{L}\bar{N}} + \delta_{\bar{K}\bar{N}}\delta_{\bar{L}\bar{M}}) \quad (106)$$

$$\begin{aligned} \bar{B}_{\bar{K}\bar{L}\bar{M}\bar{N}} &= (\eta - \tau)\delta_{\bar{K}\bar{L}}\delta_{\bar{M}\bar{N}} + \kappa\delta_{\bar{K}\bar{M}}\delta_{\bar{L}\bar{N}} + \nu\delta_{\bar{K}\bar{N}}\delta_{\bar{L}\bar{M}} \\ &\quad - \sigma(\delta_{\bar{K}\bar{M}}\delta_{\bar{L}\bar{N}} + \delta_{\bar{K}\bar{N}}\delta_{\bar{L}\bar{M}}) \end{aligned} \quad (107)$$

$$\begin{aligned} \bar{C}_{\bar{K}\bar{L}\bar{M}\bar{N}\bar{P}\bar{Q}} &= \tau_1(\delta_{\bar{K}\bar{L}}\delta_{\bar{M}\bar{N}}\delta_{\bar{P}\bar{Q}} + \delta_{\bar{K}\bar{Q}}\delta_{\bar{L}\bar{M}}\delta_{\bar{N}\bar{P}}) \\ &\quad + \tau_2(\delta_{\bar{K}\bar{L}}\delta_{\bar{M}\bar{P}}\delta_{\bar{N}\bar{Q}} + \delta_{\bar{K}\bar{M}}\delta_{\bar{L}\bar{Q}}\delta_{\bar{N}\bar{P}}) \\ &\quad + \tau_3\delta_{\bar{K}\bar{L}}\delta_{\bar{M}\bar{Q}}\delta_{\bar{N}\bar{P}} + \tau_4\delta_{\bar{K}\bar{N}}\delta_{\bar{L}\bar{M}}\delta_{\bar{P}\bar{Q}} \\ &\quad + \tau_5(\delta_{\bar{K}\bar{M}}\delta_{\bar{L}\bar{N}}\delta_{\bar{P}\bar{Q}} + \delta_{\bar{K}\bar{P}}\delta_{\bar{L}\bar{M}}\delta_{\bar{N}\bar{Q}}) \\ &\quad + \tau_6\delta_{\bar{K}\bar{M}}\delta_{\bar{L}\bar{P}}\delta_{\bar{N}\bar{Q}} + \tau_7\delta_{\bar{K}\bar{N}}\delta_{\bar{L}\bar{P}}\delta_{\bar{M}\bar{Q}} \\ &\quad + \tau_8(\delta_{\bar{K}\bar{P}}\delta_{\bar{L}\bar{Q}}\delta_{\bar{M}\bar{N}} + \delta_{\bar{K}\bar{Q}}\delta_{\bar{L}\bar{N}}\delta_{\bar{M}\bar{P}}) + \tau_9\delta_{\bar{K}\bar{N}}\delta_{\bar{L}\bar{Q}}\delta_{\bar{M}\bar{P}} \\ &\quad + \tau_{10}\delta_{\bar{K}\bar{P}}\delta_{\bar{L}\bar{N}}\delta_{\bar{M}\bar{Q}} + \tau_{11}\delta_{\bar{K}\bar{Q}}\delta_{\bar{L}\bar{P}}\delta_{\bar{M}\bar{N}} \end{aligned} \quad (108)$$

$$\bar{D}_{\bar{K}\bar{L}\bar{M}\bar{N}} = \tau\delta_{\bar{K}\bar{L}}\delta_{\bar{M}\bar{N}} + \sigma(\delta_{\bar{K}\bar{M}}\delta_{\bar{L}\bar{N}} + \delta_{\bar{K}\bar{N}}\delta_{\bar{L}\bar{M}}) \quad (109)$$

where $\bar{A}_{\bar{K}\bar{L}\bar{M}\bar{N}}$ and $\bar{D}_{\bar{K}\bar{L}\bar{M}\bar{N}}$ have major and minor symmetry, while $\bar{B}_{\bar{K}\bar{L}\bar{M}\bar{N}}$ and $\bar{C}_{\bar{K}\bar{L}\bar{M}\bar{N}\bar{P}\bar{Q}}$ have only major symmetry, and the elastic parameters are $\lambda, \mu, \eta, \tau, \kappa, \nu, \sigma, \tau_1 \dots \tau_{11}$. Note that the units for $\tau_1 \dots \tau_{11}$ are stress \times length² (e.g., Pa.m²), thus there is a built-in length-scale to these elastic parameters for the higher order stress. The elastic modulus tensors $\bar{A}_{\bar{K}\bar{L}\bar{M}\bar{N}}$, $\bar{B}_{\bar{K}\bar{L}\bar{M}\bar{N}}$, and $\bar{D}_{\bar{K}\bar{L}\bar{M}\bar{N}}$ are not the same as in (Eringen, 1999) because different elastic strain measures were used, but the higher order elastic modulus tensor $\bar{C}_{\bar{K}\bar{L}\bar{M}\bar{N}\bar{P}\bar{Q}}$ is the same. Note that $\bar{\mathbf{A}}$ is the typical linear isotropic elastic tangent modulus tensor, and λ and μ are the Lamé parameters. After some algebra using equations 91–94, and 105, it can be shown that the stress constitutive relations are

$$\begin{aligned} \bar{S}_{\bar{K}\bar{L}} &= \bar{A}_{\bar{K}\bar{L}\bar{M}\bar{N}}\bar{E}_{\bar{M}\bar{N}}^e + \bar{D}_{\bar{K}\bar{B}\bar{M}\bar{N}}\bar{\mathcal{E}}_{\bar{M}\bar{N}}^e \\ &\quad + (\bar{D}_{\bar{K}\bar{B}\bar{M}\bar{N}}\bar{E}_{\bar{M}\bar{N}}^e + \bar{B}_{\bar{K}\bar{B}\bar{M}\bar{N}}\bar{\mathcal{E}}_{\bar{M}\bar{N}}^e) [\bar{C}_{\bar{L}\bar{A}}^{-1}\bar{\mathcal{E}}_{\bar{A}\bar{B}}^e + \delta_{\bar{L}\bar{B}}] \\ &\quad + \bar{C}_{\bar{K}\bar{B}\bar{C}\bar{N}\bar{P}\bar{Q}}\bar{\Gamma}_{\bar{N}\bar{P}\bar{Q}}^e\bar{C}_{\bar{L}\bar{Q}}^{e-1}\bar{\Gamma}_{\bar{Q}\bar{B}\bar{C}}^e \end{aligned} \quad (110)$$

$$\begin{aligned} \bar{\Sigma}_{\bar{K}\bar{L}} &= \bar{A}_{\bar{K}\bar{L}\bar{M}\bar{N}}\bar{E}_{\bar{M}\bar{N}}^e + \bar{D}_{\bar{K}\bar{B}\bar{M}\bar{N}}\bar{\mathcal{E}}_{\bar{M}\bar{N}}^e \\ &\quad + 2\text{sym} \{ (\bar{D}_{\bar{K}\bar{L}\bar{M}\bar{N}}\bar{E}_{\bar{M}\bar{N}}^e + \bar{B}_{\bar{K}\bar{B}\bar{M}\bar{N}}\bar{\mathcal{E}}_{\bar{M}\bar{N}}^e) [\bar{C}_{\bar{L}\bar{A}}^{e-1}\bar{\mathcal{E}}_{\bar{A}\bar{B}}^e + \delta_{\bar{L}\bar{B}}] \\ &\quad + \bar{C}_{\bar{K}\bar{B}\bar{C}\bar{N}\bar{P}\bar{Q}}\bar{\Gamma}_{\bar{N}\bar{P}\bar{Q}}^e\bar{C}_{\bar{L}\bar{Q}}^{e-1}\bar{\Gamma}_{\bar{Q}\bar{B}\bar{C}}^e \} \end{aligned} \quad (111)$$

$$\bar{M}_{\bar{K}\bar{L}\bar{M}} = \bar{C}_{\bar{K}\bar{L}\bar{M}\bar{N}\bar{P}\bar{Q}}\bar{\Gamma}_{\bar{N}\bar{P}\bar{Q}}^e \quad (112)$$

$$\bar{Q} = \bar{H}\bar{Z} \quad (113)$$

$$\bar{Q}^\chi = \bar{H}^\chi\bar{Z}^\chi \quad (114)$$

$$\bar{Q}_{\bar{L}}^\chi = \bar{H}^{\nabla\chi}\bar{Z}_{,\bar{L}}^\chi \quad (115)$$

Note that the units for $\bar{H}^{\nabla\chi}$ are stress \times length² (e.g., Pa.m²), thus there is a built-in

length-scale to this hardening/softening parameter for the higher-order stress-like ISV. Assuming elastic deformations are small, we ignore quadratic terms in equations 110 and 111 relative to the linear terms, leading to the simplified stress constitutive equations for $\bar{S}_{\bar{K}\bar{L}}$ and $\bar{\Sigma}_{\bar{K}\bar{L}}$ as

$$\begin{aligned}\bar{S}_{\bar{K}\bar{L}} &= (\bar{A}_{\bar{K}\bar{L}\bar{M}\bar{N}} + \bar{D}_{\bar{K}\bar{L}\bar{M}\bar{N}})\bar{E}_{\bar{M}\bar{N}}^e + (\bar{B}_{\bar{K}\bar{L}\bar{M}\bar{N}} + \bar{D}_{\bar{K}\bar{L}\bar{M}\bar{N}})\bar{\mathcal{E}}_{\bar{M}\bar{N}}^e \\ &= (\lambda + \tau)(\bar{E}_{\bar{M}\bar{M}}^e)\delta_{\bar{K}\bar{L}} + 2(\mu + \sigma)\bar{E}_{\bar{K}\bar{L}}^e \\ &\quad + \eta(\bar{\mathcal{E}}_{\bar{M}\bar{M}}^e)\delta_{\bar{K}\bar{L}} + \kappa\bar{\mathcal{E}}_{\bar{K}\bar{L}}^e + \nu\bar{\mathcal{E}}_{\bar{L}\bar{K}}^e\end{aligned}\tag{116}$$

$$\begin{aligned}\bar{\Sigma}_{\bar{K}\bar{L}} &= (\lambda + \tau)(\bar{E}_{\bar{M}\bar{M}}^e)\delta_{\bar{K}\bar{L}} + 2(\mu + \sigma)\bar{E}_{\bar{K}\bar{L}}^e \\ &\quad + \eta(\bar{\mathcal{E}}_{\bar{M}\bar{M}}^e)\delta_{\bar{K}\bar{L}} + 2\text{sym}[\kappa\bar{\mathcal{E}}_{\bar{K}\bar{L}}^e + \nu\bar{\mathcal{E}}_{\bar{L}\bar{K}}^e]\end{aligned}\tag{117}$$

Note that the stress difference used in equation 103 then becomes

$$\begin{aligned}\bar{\Sigma} - \bar{\mathbf{S}} &= \kappa\bar{\mathcal{E}}^{e^T} + \nu\bar{\mathcal{E}}^e \\ \bar{\Sigma}_{\bar{K}\bar{L}} - \bar{S}_{\bar{K}\bar{L}} &= \kappa\bar{\mathcal{E}}_{\bar{L}\bar{K}}^e + \nu\bar{\mathcal{E}}_{\bar{K}\bar{L}}^e\end{aligned}\tag{118}$$

Yield functions and evolution equations: In this discussion, three levels of plastic yield functions are defined based on the three conjugate stress-plastic-power terms appearing in the reduced dissipation inequality equation 98, with the intent to define the plastic deformation evolution equations such that equation 98 is satisfied. This allows separate yielding and plastic deformation at two scales (micro and macro) including the gradient deformation at the micro-scale. If only one yield function were chosen to be a function of all three stresses ($\bar{\mathbf{S}}$, $\bar{\Sigma}$, $\bar{\mathbf{M}}$), then yielding at the three scales would occur simultaneously, a representation we feel is not as physical as if the scales can yield and evolve separately (although coupled through balance equations and stress equations for $\bar{\mathbf{S}}$ and $\bar{\Sigma}$). Recall the plastic power terms in equation 98 come naturally from the kinematic assumptions $\mathbf{F} = \mathbf{F}^e\mathbf{F}^p$ and $\chi = \chi^e\chi^p$, and from the Helmholtz free energy function dependence on the invariant elastic deformation measures $\bar{\mathbf{C}}^e$, $\bar{\Psi}^e$, $\bar{\Gamma}^e$, and the plastic strain-like ISVs \bar{Z} , \bar{Z}^χ , and $\bar{\nabla}\bar{Z}^\chi$.

macroscale plasticity: For macroscale plasticity, we write the yield function \bar{F} as

$$\begin{aligned}\bar{F}(\bar{\mathbf{S}}, \bar{\alpha}) &\stackrel{\text{def}}{=} \|\text{dev}\bar{\mathbf{S}}\| - \bar{\alpha} \leq 0 \\ \|\text{dev}\bar{\mathbf{S}}\| &= \sqrt{(\text{dev}\bar{\mathbf{S}}) : (\text{dev}\bar{\mathbf{S}})} \\ (\text{dev}\bar{\mathbf{S}}) : (\text{dev}\bar{\mathbf{S}}) &= (\text{dev}\bar{S}_{\bar{I}\bar{J}})(\text{dev}\bar{S}_{\bar{I}\bar{J}}) \\ \text{dev}\bar{S}_{\bar{I}\bar{J}} &\stackrel{\text{def}}{=} \bar{S}_{\bar{I}\bar{J}} - \left(\frac{1}{3}\bar{C}_{\bar{A}\bar{B}}^e\bar{S}_{\bar{A}\bar{B}}\right)\bar{C}_{\bar{I}\bar{J}}^{e-1}\end{aligned}\tag{119}$$

where $\bar{\alpha}$ is the macro yield strength (i.e., stress-like ISV $\bar{Q} \stackrel{\text{def}}{=} \bar{\alpha}$)

The definitions of the plastic velocity gradient $\bar{\mathbf{L}}^p$ and strain-like ISV then follow as

$$\bar{C}_{\bar{L}\bar{B}}^e \bar{L}_{\bar{B}\bar{K}}^p \stackrel{\text{def}}{=} \dot{\gamma} \frac{\partial \bar{F}}{\partial \bar{S}_{\bar{K}\bar{L}}} \quad (120)$$

$$\frac{\partial \bar{F}}{\partial \bar{S}_{\bar{K}\bar{L}}} = \hat{N}_{\bar{K}\bar{L}}$$

$$\hat{N}_{\bar{K}\bar{L}} = \frac{\text{dev} \bar{S}_{\bar{K}\bar{L}}}{\|\text{dev} \bar{\mathbf{S}}\|}$$

$$\dot{\bar{Z}} \stackrel{\text{def}}{=} -\dot{\gamma} \frac{\partial \bar{F}}{\partial \bar{\alpha}} = \dot{\gamma} \quad (121)$$

$$\bar{\alpha} = \bar{H} \bar{Z} \quad (122)$$

where $\dot{\gamma}$ is the macroplastic multiplier.

Micro-scale plasticity: For micro-scale plasticity, we write the yield function \bar{F}^x as

$$\bar{F}^x(\bar{\Sigma} - \bar{\mathbf{S}}, \bar{\alpha}^x) \stackrel{\text{def}}{=} \|\text{dev}(\bar{\Sigma} - \bar{\mathbf{S}})\| - \bar{\alpha}^x \leq 0 \quad (123)$$

$$\text{dev}(\bar{\Sigma}_{\bar{I}\bar{J}} - \bar{S}_{\bar{I}\bar{J}}) \stackrel{\text{def}}{=} (\bar{\Sigma}_{\bar{I}\bar{J}} - \bar{S}_{\bar{I}\bar{J}}) - \left[\frac{1}{3} \bar{C}_{\bar{A}\bar{B}}^e (\bar{\Sigma}_{\bar{A}\bar{B}} - \bar{S}_{\bar{A}\bar{B}}) \right] \bar{C}_{\bar{I}\bar{J}}^{e-1}$$

where $\bar{\alpha}^x$ is the micro yield strength (stress-like ISV $\bar{Q}^x \stackrel{\text{def}}{=} \bar{\alpha}^x$). Note that at the microscale, the yield strength $\bar{\alpha}^x$ can be determined separately from the macroscale parameter $\bar{\alpha}$.

Remark 2. We use the same functional forms for macro and micro plasticity (\bar{F}^x with similar functional form as \bar{F} , but different ISVs and parameters), but this is only for the example model presented here. It is possible for the functional forms to be different when representing different phenomenology at the micro and macroscales. More micromechanical analysis and experimental data are necessary to determine the microplasticity functional forms in the future.

The definitions of the microscale plastic velocity gradient $\bar{\mathbf{L}}^{x,p}$ and strain-like ISV then follow as

$$\bar{\Psi}_{\bar{L}\bar{E}}^e \bar{L}_{\bar{E}\bar{F}}^{\chi,p} \bar{C}_{\bar{F}\bar{N}}^{\chi,e-1} \bar{\Psi}_{\bar{K}\bar{N}}^e \stackrel{\text{def}}{=} \dot{\gamma}^\chi \frac{\partial \bar{F}^\chi}{\partial (\bar{\Sigma}_{\bar{K}\bar{L}} - \bar{S}_{\bar{K}\bar{L}})} \quad (124)$$

$$\frac{\partial \bar{F}^\chi}{\partial (\bar{\Sigma}_{\bar{K}\bar{L}} - \bar{S}_{\bar{K}\bar{L}})} = \hat{N}_{\bar{K}\bar{L}}^\chi$$

$$\hat{N}_{\bar{K}\bar{L}}^\chi = \frac{\text{dev}(\bar{\Sigma}_{\bar{K}\bar{L}} - \bar{S}_{\bar{K}\bar{L}})}{\|\text{dev}(\bar{\Sigma} - \bar{S})\|}$$

$$\dot{\bar{Z}}^\chi \stackrel{\text{def}}{=} -\dot{\gamma}^\chi \frac{\partial \bar{F}^\chi}{\partial \bar{\alpha}^\chi} = \dot{\gamma}^\chi \quad (125)$$

$$\bar{\alpha}^\chi = \bar{H}^\chi \bar{Z}^\chi \quad (126)$$

where $\dot{\gamma}^\chi$ is the micro plastic multiplier.

Microscale gradient plasticity: For microscale gradient plasticity, we write the yield function $\bar{F}^{\nabla\chi}$ as

$$\bar{F}^{\nabla\chi}(\bar{\mathbf{M}}, \bar{\alpha}^{\nabla\chi}) \stackrel{\text{def}}{=} \|\text{dev} \bar{\mathbf{M}}\| - \|\bar{\alpha}^{\nabla\chi}\| \leq 0 \quad (127)$$

$$\text{dev} \bar{M}_{\bar{I}\bar{J}\bar{K}} \stackrel{\text{def}}{=} \bar{M}_{\bar{I}\bar{J}\bar{K}} - (\bar{C}^{e-1})_{\bar{I}\bar{J}} \left[\frac{1}{3} \bar{C}_{\bar{A}\bar{B}}^e \bar{M}_{\bar{A}\bar{B}\bar{K}} \right]$$

where $\bar{\alpha}^{\nabla\chi}$ is the microgradient yield strength (stress-like ISV $\bar{\mathbf{Q}}^{\nabla\chi} \stackrel{\text{def}}{=} \bar{\alpha}^{\nabla\chi}$) Note that at the gradient microscale, the yield strength can be determined separately from the micro and macroscale parameters, which is a constitutive assumption. The definitions of the spatial derivative of microscale plastic velocity gradient $\bar{\nabla} \bar{\mathbf{L}}^{\chi,p}$ and strain-like ISV then follow as

$$\bar{\Psi}_{\bar{L}\bar{D}}^e \bar{L}_{\bar{D}\bar{M},\bar{K}}^{\chi,p} - 2\bar{\Psi}_{\bar{L}\bar{D}}^e \text{skw} [\bar{L}_{\bar{D}\bar{C}}^{\chi,p} \bar{\Psi}_{\bar{C}\bar{F}}^{e-1} \bar{\Gamma}_{\bar{F}\bar{M}\bar{K}}^e] \stackrel{\text{def}}{=} \dot{\gamma}^{\nabla\chi} \frac{\partial \bar{F}^{\nabla\chi}}{\partial \bar{M}_{\bar{K}\bar{L}\bar{M}}} \quad (128)$$

$$\frac{\partial \bar{F}^{\nabla\chi}}{\partial \bar{M}_{\bar{K}\bar{L}\bar{M}}} = \frac{\text{dev} \bar{M}_{\bar{K}\bar{L}\bar{M}}}{\|\text{dev} \bar{\mathbf{M}}\|}$$

$$\frac{D(\bar{Z}_{,\bar{A}}^\chi)}{Dt} \stackrel{\text{def}}{=} -\dot{\gamma}^{\nabla\chi} \frac{\partial \bar{F}}{\partial \bar{\alpha}_{\bar{A}}^{\nabla\chi}} = (\dot{\gamma}^{\nabla\chi}) \frac{\bar{\alpha}_{\bar{A}}^{\nabla\chi}}{\|\bar{\alpha}^{\nabla\chi}\|} \quad (129)$$

$$\bar{\alpha}_{\bar{L}}^{\nabla\chi} = \bar{H}^{\nabla\chi} \bar{Z}_{,\bar{L}}^\chi \quad (130)$$

where $\dot{\gamma}^{\nabla\chi}$ is the microplastic gradient multiplier.

Remark 3. The main advantage to defining constitutively the evolution of the spatial derivative of the microscale plastic velocity gradient $\bar{\nabla}\bar{\mathbf{L}}^{\chi,p}$ in equation 128 separate from the microscale plastic velocity gradient $\bar{\mathbf{L}}^{\chi,p}$ in equation 124 (i.e., no PDE in $\dot{\chi}_{KK}^p$) is to avoid FE solution of an additional balance equation in weak form. One could allow $\bar{\nabla}\bar{\mathbf{L}}^{\chi,p}$ and $\bar{\nabla}\dot{\bar{\mathbf{Z}}}^\chi$ to be defined as the spatial derivatives of $\bar{\mathbf{L}}^{\chi,p}$ and $\dot{\bar{\mathbf{Z}}}^\chi$, respectively, but then the plastic evolution equations are PDEs and require coupled FE implementation (such as in Regueiro et al. (2007)). We plan to implement the model, after time integration in section 2.3.4, within a coupled finite element formulation for the coupled balance of linear and first moment of momentum, and thus avoiding another coupled equation to include in the FE equations is desired.

Remark 4. With these evolution equations in $\bar{\mathcal{B}}$, equation 120 can be integrated numerically to solve for \mathbf{F}^p and in turn \mathbf{F}^e , equation 124 can be integrated numerically to solve for χ^p and in turn χ^e , and equation 128 can be integrated numerically to solve for $\bar{\nabla}\chi^p$ and in turn $\bar{\nabla}\chi^e$. Then, the stresses $\bar{\mathbf{S}}$, $\bar{\boldsymbol{\Sigma}} - \bar{\mathbf{S}}$, and $\bar{\mathbf{M}}$ can be calculated and mapped to the current configuration to update the balance equations for FE nonlinear solution. Such numerical time integration is carried out in section 2.3.4; and FE implementation is ongoing work.

2.4.3 Drucker-Prager Pressure-Sensitive Plasticity

Following the “metric” form in equation 98, the J_2 flow plasticity model is generalized to include pressure-sensitivity of yield and volumetric plastic deformation (dilation only for now, i.e., no cap on the yield and plastic potential surfaces that allows plastic compaction, e.g., pore space collapse).

macroscale plasticity: For macroscale plasticity, we write yield \bar{F} and plastic potential \bar{G} functions as

$$\bar{F}(\bar{\mathbf{S}}, \bar{c}) \stackrel{\text{def}}{=} \|\text{dev}\bar{\mathbf{S}}\| - (A^\phi \bar{c} - B^\phi \bar{p}) \leq 0 \quad (131)$$

$$A^\phi = \beta^\phi \cos \phi, \quad B^\phi = \beta^\phi \sin \phi, \quad \beta^\phi = \frac{2\sqrt{6}}{3 + \beta \sin \phi}$$

$$\|\text{dev}\bar{\mathbf{S}}\| = \sqrt{(\text{dev}\bar{\mathbf{S}}) : (\text{dev}\bar{\mathbf{S}})}$$

$$(\text{dev}\bar{\mathbf{S}}) : (\text{dev}\bar{\mathbf{S}}) = (\text{dev}\bar{S}_{IJ})(\text{dev}\bar{S}_{IJ})$$

$$\text{dev}\bar{S}_{IJ} \stackrel{\text{def}}{=} \bar{S}_{IJ} - \left(\frac{1}{3} \bar{C}_{AB}^e \bar{S}_{AB} \right) \bar{C}_{IJ}^{e-1}$$

$$\bar{p} \stackrel{\text{def}}{=} \frac{1}{3} \bar{C}_{AB}^e \bar{S}_{AB} = \frac{1}{3} \bar{\mathbf{C}}^e : \bar{\mathbf{S}}$$

$$\bar{G}(\bar{\mathbf{S}}, \bar{c}) \stackrel{\text{def}}{=} \|\text{dev}\bar{\mathbf{S}}\| - (A^\psi \bar{c} - B^\psi \bar{p}) \quad (132)$$

where \bar{c} is the macro cohesion, ϕ is the macro friction angle, ψ is the macro dilation angle, and $-1 \leq \beta \leq 1$ ($\beta = 1$ causes the Drucker-Prager yield surface to pass through the triaxial extension vertices of the Mohr-Coulomb yield surface, and $\beta = -1$ is the triaxial compression vertices). Functional forms of A^ψ and B^ψ are similar to A^ϕ and B^ϕ , respectively, except ϕ is replaced with ψ . The yield and plastic potential functions have the usual functional form for pressure-sensitive plasticity with cohesive and frictional strength, as well as dilatancy (Desai and Siriwardane, 1984).

Remark 5. To satisfy the reduced dissipation inequality, it can be shown that $\phi \geq \psi$ (Vermeer and de Borst, 1984) which also has been verified experimentally. We note that $\phi > \psi$ leads to nonassociative plasticity, which violates the principle of maximum plastic dissipation (Lubliner 1990), but does not violate the reduced dissipation inequality. It is well known that frictional materials like concrete and rock exhibit nonassociative plastic flow, and thus such features are also included here. An associative flow rule is reached when the friction and dilation angles are equal, $\phi = \psi$.

The definitions of the plastic velocity gradient $\bar{\mathbf{L}}^p$ and strain-like ISV then follow as

$$\bar{C}_{\bar{L}\bar{B}}^e \bar{L}_{\bar{B}\bar{K}}^p \stackrel{\text{def}}{=} \dot{\gamma} \frac{\partial \bar{G}}{\partial \bar{S}_{\bar{K}\bar{L}}} \quad (133)$$

$$\frac{\partial \bar{G}}{\partial \bar{S}_{\bar{K}\bar{L}}} = \hat{N}_{\bar{K}\bar{L}} + \frac{1}{3} B^\psi \bar{C}_{\bar{K}\bar{L}}^e$$

$$\hat{N}_{\bar{K}\bar{L}} = \frac{\text{dev} \bar{S}_{\bar{K}\bar{L}}}{\|\text{dev} \bar{\mathbf{S}}\|}$$

$$\dot{\bar{Z}} \stackrel{\text{def}}{=} -\dot{\gamma} \frac{\partial \bar{G}}{\partial \bar{c}} = A^\psi \dot{\gamma} \quad (134)$$

$$\bar{c} = \bar{H} \bar{Z} \quad (135)$$

where $\dot{\gamma}$ is the macroplastic multiplier, and the stress-like ISV is $\bar{Q} \stackrel{\text{def}}{=} \bar{c}$.

Remark 6. Note that the functional forms of the plastic evolution equations are similar to those dictated by the principle of maximum plastic dissipation [Lubliner, 1990], except that a plastic potential function \bar{G} is used in place of the yield function \bar{F} (i.e., nonassociative). For purposes of discussion, we show the evolution equations for small strain plasticity:

$$\epsilon^p \stackrel{\text{def}}{=} \dot{\gamma} \frac{\partial g}{\partial \sigma}, \quad \zeta \stackrel{\text{def}}{=} -\dot{\gamma} \frac{\partial g}{\partial c} \quad (136)$$

where ϵ^p is the plastic strain, and ζ the strain-like ISV. nonassociative plasticity violates the principle of maximum plastic dissipation, but we use similar functional forms that satisfies

the reduced dissipation inequality (i.e., the second law of thermodynamics is satisfied).

Microscale plasticity: For microscale plasticity, we write the yield \bar{F}^χ and plastic potential \bar{G}^χ functions as

$$\bar{F}^\chi(\bar{\Sigma} - \bar{\mathbf{S}}, \bar{c}^\chi) \stackrel{\text{def}}{=} \|\text{dev}(\bar{\Sigma} - \bar{\mathbf{S}})\| - (A^{\chi,\phi} \bar{c}^\chi - B^{\chi,\phi} \bar{p}^\chi) \leq 0 \quad (137)$$

$$A^{\chi,\phi} = \beta^{\chi,\phi} \cos \phi^\chi, \quad B^{\chi,\phi} = \beta^{\chi,\phi} \sin \phi^\chi, \quad \beta^{\chi,\phi} = \frac{2\sqrt{6}}{3 + \beta^\chi \sin \phi^\chi}$$

$$\text{dev}(\bar{\Sigma}_{\bar{I}\bar{J}} - \bar{S}_{\bar{I}\bar{J}}) \stackrel{\text{def}}{=} (\bar{\Sigma}_{\bar{I}\bar{J}} - \bar{S}_{\bar{I}\bar{J}}) - \bar{p}^\chi \bar{C}_{\bar{I}\bar{J}}^{e-1}$$

$$\bar{p}^\chi \stackrel{\text{def}}{=} \frac{1}{3} \bar{C}_{\bar{A}\bar{B}}^e (\bar{\Sigma}_{\bar{A}\bar{B}} - \bar{S}_{\bar{A}\bar{B}})$$

$$\bar{G}^\chi(\bar{\Sigma} - \bar{\mathbf{S}}, \bar{c}^\chi) \stackrel{\text{def}}{=} \|\text{dev}(\bar{\Sigma} - \bar{\mathbf{S}})\| - (A^{\chi,\psi} \bar{c}^\chi - B^{\chi,\psi} \bar{p}^\chi) \quad (138)$$

where \bar{c}^χ is the microcohesion, ϕ^χ is the microfriction angle, ψ^χ is the micro dilation angle, and $-1 \leq \beta^\chi \leq 1$, which are material parameters for the microscale. Functional forms of $A^{\chi,\psi}$ and $B^{\chi,\psi}$ are similar to $A^{\chi,\phi}$ and $B^{\chi,\phi}$, respectively, except ϕ^χ is replaced with ψ^χ . Note that at the microscale, the cohesion, friction, and dilation angles can be determined separately from the macroscale parameters, and likewise the yielding and plastic deformation.

Remark 7. We use the same functional forms for macro and microplasticity (\bar{F}^χ and \bar{G}^χ with similar functional form as \bar{F} and \bar{G}), but this is only for the example model presented here. It is possible for the functional forms to be different when representing different phenomenology at the micro and macroscales. More micromechanical analysis and experimental data are necessary to determine the pressure-sensitive microplasticity functional forms in the future.

The definitions of the microscale plastic velocity gradient $\bar{\mathbf{L}}^{\chi,p}$ and strain-like ISV then follow as

$$\bar{\Psi}_{\bar{L}\bar{E}}^e \bar{L}_{\bar{E}\bar{F}}^{\chi,p} \bar{C}_{\bar{F}\bar{N}}^{\chi,e-1} \bar{\Psi}_{\bar{K}\bar{N}}^e \stackrel{\text{def}}{=} \dot{\gamma}^\chi \frac{\partial \bar{G}^\chi}{\partial (\bar{\Sigma}_{\bar{K}\bar{L}} - \bar{S}_{\bar{K}\bar{L}})} \quad (139)$$

$$\frac{\partial \bar{G}^\chi}{\partial (\bar{\Sigma}_{\bar{K}\bar{L}} - \bar{S}_{\bar{K}\bar{L}})} = \hat{N}_{\bar{K}\bar{L}}^\chi + \frac{1}{3} B^{\chi,\psi} \bar{C}_{\bar{K}\bar{L}}^e$$

$$\hat{N}_{\bar{K}\bar{L}}^\chi = \frac{\text{dev}(\bar{\Sigma}_{\bar{K}\bar{L}} - \bar{S}_{\bar{K}\bar{L}})}{\|\text{dev}(\bar{\Sigma} - \bar{\mathbf{S}})\|}$$

$$\dot{\bar{Z}}^\chi \stackrel{\text{def}}{=} -\dot{\gamma}^\chi \frac{\partial \bar{G}^\chi}{\partial \bar{c}^\chi} = A^{\chi,\psi} \dot{\gamma}^\chi \quad (140)$$

$$\bar{c}^\chi = \bar{H}^\chi \bar{Z}^\chi \quad (141)$$

where $\dot{\gamma}^\chi$ is the microplastic multiplier, and $\bar{Q}^\chi \stackrel{\text{def}}{=} \bar{c}^\chi$.

Microscale gradient plasticity: For microscale gradient plasticity, we write the yield $\bar{F}^{\nabla\chi}$ and plastic potential $\bar{G}^{\nabla\chi}$ functions as

$$\bar{F}^{\nabla\chi}(\bar{\mathbf{M}}, \bar{\mathbf{c}}^{\nabla\chi}) \stackrel{\text{def}}{=} \|\text{dev}\bar{\mathbf{M}}\| - (A^{\nabla\chi,\phi} \|\bar{\mathbf{c}}^{\nabla\chi}\| - B^{\nabla\chi,\phi} \|\bar{\mathbf{p}}^{\nabla\chi}\|) \leq 0 \quad (142)$$

$$A^{\nabla\chi,\phi} = \beta^{\nabla\chi,\phi} \cos \phi^{\nabla\chi}, \quad B^{\nabla\chi,\phi} = \beta^{\nabla\chi,\phi} \sin \phi^{\nabla\chi}, \quad \beta^{\nabla\chi,\phi} = \frac{2\sqrt{6}}{3 + \beta^{\nabla\chi} \sin \phi^{\nabla\chi}}$$

$$\text{dev}\bar{M}_{\bar{I}\bar{J}\bar{K}} \stackrel{\text{def}}{=} \bar{M}_{\bar{I}\bar{J}\bar{K}} - \bar{C}_{\bar{I}\bar{J}}^{e-1} \bar{p}_{\bar{K}}^{\nabla\chi}$$

$$\bar{p}_{\bar{K}}^{\nabla\chi} \stackrel{\text{def}}{=} \frac{1}{3} \bar{C}_{\bar{A}\bar{B}}^e \bar{M}_{\bar{A}\bar{B}\bar{K}}$$

$$\bar{G}^{\nabla\chi}(\bar{\mathbf{M}}, \bar{\mathbf{c}}^{\nabla\chi}) \stackrel{\text{def}}{=} \|\text{dev}\bar{\mathbf{M}}\| - (A^{\nabla\chi,\psi} \|\bar{\mathbf{c}}^{\nabla\chi}\| - B^{\nabla\chi,\psi} \|\bar{\mathbf{p}}^{\nabla\chi}\|) \quad (143)$$

where $\bar{\mathbf{c}}^{\nabla\chi}$ is the microgradient cohesion, $\phi^{\nabla\chi}$ the microgradient friction angle, $\psi^{\nabla\chi}$ the microgradient dilation angle, and $-1 \leq \beta^{\nabla\chi} \leq 1$, which are material parameters for the gradient microscale. Functional forms of $A^{\nabla\chi,\psi}$ and $B^{\nabla\chi,\psi}$ are similar to $A^{\nabla\chi,\phi}$ and $B^{\nabla\chi,\phi}$, respectively, except $\phi^{\nabla\chi}$ is replaced with $\psi^{\nabla\chi}$. Note that at the gradient microscale, the cohesion, friction, and dilation angles can be determined separately from the micro and macroscale parameters, which is a constitutive assumption. The definitions of the gradient of microscale plastic velocity gradient $\bar{\nabla}\bar{\mathbf{L}}^{\chi,p}$ and strain-like ISV then follow as

$$\bar{\Psi}_{\bar{L}\bar{D}}^e \bar{L}_{\bar{D}\bar{M},\bar{K}}^{\chi,p} - 2\bar{\Psi}_{\bar{L}\bar{D}}^e \text{skw} [\bar{L}_{\bar{D}\bar{C}}^{\chi,p} \bar{\Psi}_{\bar{C}\bar{F}}^{e-1} \bar{\Gamma}_{\bar{F}\bar{M}\bar{K}}^e] \stackrel{\text{def}}{=} \dot{\gamma}^{\nabla\chi} \frac{\partial \bar{G}^{\nabla\chi}}{\partial \bar{M}_{\bar{K}\bar{L}\bar{M}}} \quad (144)$$

$$\frac{\partial \bar{G}^{\nabla\chi}}{\partial \bar{M}_{\bar{K}\bar{L}\bar{M}}} = \frac{\text{dev}\bar{M}_{\bar{K}\bar{L}\bar{M}}}{\|\text{dev}\bar{\mathbf{M}}\|} + \frac{1}{3} B^{\nabla\chi,\psi} \bar{C}_{\bar{K}\bar{L}}^e \frac{\bar{p}_{\bar{M}}^{\nabla\chi}}{\|\bar{\mathbf{p}}^{\nabla\chi}\|}$$

$$\dot{\bar{Z}}_{,\bar{A}}^\chi \stackrel{\text{def}}{=} -\dot{\gamma}^{\nabla\chi} \frac{\partial \bar{G}^{\nabla\chi}}{\partial \bar{c}_{\bar{A}}^{\nabla\chi}} = A^{\nabla\chi,\psi} (\dot{\gamma}^{\nabla\chi}) \frac{\bar{c}_{\bar{A}}^{\nabla\chi}}{\|\bar{\mathbf{c}}^{\nabla\chi}\|} \quad (145)$$

$$\bar{c}_{\bar{L}}^{\nabla\chi} = \bar{H}^{\nabla\chi} \bar{Z}_{,\bar{L}}^\chi \quad (146)$$

where $\dot{\gamma}^{\nabla\chi}$ is the micro plastic gradient multiplier.

Remark 8. With these evolution equations in $\bar{\mathcal{B}}$, equation 133 can be integrated numerically to solve for \mathbf{F}^p and in turn \mathbf{F}^e , equation 139 can be integrated numerically to solve for χ^p and in turn χ^e , and equation 144 can be integrated numerically to solve for $\bar{\nabla}\chi^p$ and in turn $\bar{\nabla}\chi^e$. Then, the stresses $\bar{\mathbf{S}}$, $\bar{\Sigma} - \bar{\mathbf{S}}$, and $\bar{\mathbf{M}}$ can be calculated and mapped

to the current configuration to update the balance equations for finite element nonlinear solution. Such numerical time integration are carried out in section 2.3.4 for the form of the constitutive equations after mapping to the current configuration.

Mapping constitutive equations to current configuration \mathcal{B} : often, the constitutive equations in the intermediate configuration are mapped to the current configuration Eringen and Suhubi [1964], and the material time derivative is taken to obtain an objective stress rate and corresponding stress evolution equation in \mathcal{B} (cf. Moran et al. (1990); Simo (1998b)). Recall the stress mappings in equations 86–88, which when we take the material time derivative, leads to the following equations

$$\dot{\sigma}_{kl} = -\frac{j^e}{J^e}\sigma_{kl} + \ell_{ki}^e\sigma_{il} + \sigma_{ki}\ell_{li}^e + \frac{1}{J^e}F_{k\bar{K}}^e\dot{\bar{S}}_{\bar{K}\bar{L}}F_{l\bar{L}}^e \quad (147)$$

$$\dot{s}_{kl} = -\frac{j^e}{J^e}s_{kl} + \ell_{ki}^es_{il} + s_{ki}\ell_{li}^e + \frac{1}{J^e}F_{k\bar{K}}^e\dot{\bar{\Sigma}}_{\bar{K}\bar{L}}F_{l\bar{L}}^e \quad (148)$$

$$\dot{m}_{klm} = -\frac{j^e}{J^e}m_{klm} + \ell_{ki}^em_{ilm} + m_{kim}\ell_{li}^e + m_{kli}\nu_{mi}^e + \frac{1}{J^e}F_{k\bar{K}}^eF_{l\bar{L}}^e\chi_{m\bar{M}}^e\dot{\bar{M}}_{\bar{K}\bar{L}\bar{M}} \quad (149)$$

To complete these equations, we need the material time derivative of the stresses in the intermediate configuration, $\dot{\bar{S}}_{\bar{K}\bar{L}}$, $\dot{\bar{\Sigma}}_{\bar{K}\bar{L}}$, and $\dot{\bar{M}}_{\bar{K}\bar{L}\bar{M}}$, as well as the mapping of the plastic evolutions equations to the current configuration. Given the constitutive equation for $\bar{S}_{\bar{K}\bar{L}}$ in equation 116, we can write

$$\begin{aligned} \dot{\bar{S}}_{\bar{K}\bar{L}} = & (\lambda + \tau)(\dot{\bar{E}}_{\bar{M}\bar{M}}^e)\delta_{\bar{K}\bar{L}} + 2(\mu + \sigma)\dot{\bar{E}}_{\bar{K}\bar{L}}^e + \eta(\dot{\bar{\mathcal{E}}}_{\bar{M}\bar{M}}^e)\delta_{\bar{K}\bar{L}} \\ & + \kappa\dot{\bar{\mathcal{E}}}_{\bar{K}\bar{L}}^e + \nu\dot{\bar{\mathcal{E}}}_{\bar{L}\bar{K}}^e \end{aligned} \quad (150)$$

where $\dot{\bar{E}}_{\bar{M}\bar{N}}^e = \dot{\bar{C}}_{\bar{M}\bar{N}}^e/2$ and $\dot{\bar{\mathcal{E}}}_{\bar{M}\bar{N}}^e = \dot{\bar{\Psi}}_{\bar{M}\bar{N}}^e$. We can show that

$$\dot{\bar{C}}_{\bar{M}\bar{N}}^e = 2F_{i\bar{M}}^ed_{ij}^eF_{j\bar{N}}^e, \quad d_{ij}^e = (\ell_{ij}^e + \ell_{ji}^e)/2, \quad \ell_{ij}^e = \dot{F}_{i\bar{I}}^eF_{\bar{I}j}^{e-1} \quad (151)$$

$$\dot{\bar{\Psi}}_{\bar{M}\bar{N}}^e = F_{i\bar{M}}^e\varepsilon_{ij}^e\chi_{j\bar{N}}^e, \quad \varepsilon_{ij}^e = \nu_{ij}^e + \ell_{ji}^e, \quad \nu_{ij}^e = \dot{\chi}_{i\bar{I}}^e\chi_{\bar{I}j}^{e-1} \quad (152)$$

where \mathbf{d}^e is the symmetric elastic deformation rate in \mathcal{B} , and ε^e a mixed micro-macro elastic velocity gradient in \mathcal{B} . Then we can write

$$\begin{aligned}
F_{k\bar{K}}^e \dot{\bar{S}}_{\bar{K}\bar{L}} F_{l\bar{L}}^e &= (\lambda + \tau)(b_{ij}^e d_{ij}^e) b_{kl}^e + 2(\mu + \sigma) b_{ki}^e d_{ij}^e b_{jl}^e + \eta(\psi_{ij}^e \varepsilon_{ij}^e) b_{kl}^e \\
&\quad + \kappa b_{ki}^e \varepsilon_{ij}^e \psi_{jl}^e + \nu b_{li}^e \varepsilon_{ij}^e \psi_{jk}^e
\end{aligned} \tag{153}$$

where the left elastic Cauchy-Green tensor is $b_{ij}^e = F_{i\bar{N}}^e F_{j\bar{N}}^e$ and a mixed elastic deformation tensor $\psi_{ij}^e = F_{i\bar{N}}^e \chi_{j\bar{N}}^e$. It is then possible to write the material time derivative of the stress difference map as

$$F_{k\bar{K}}^e (\dot{\bar{S}}_{\bar{K}\bar{L}} - \dot{\bar{S}}_{\bar{K}\bar{L}}) F_{l\bar{L}}^e = \kappa b_{li}^e \varepsilon_{ij}^e \psi_{jk}^e + \nu b_{ki}^e \varepsilon_{ij}^e \psi_{jl}^e \tag{154}$$

For the couple stress, the material time derivative is written as

$$\dot{M}_{\bar{K}\bar{L}\bar{M}} = \bar{C}_{\bar{K}\bar{L}\bar{M}\bar{N}\bar{P}\bar{Q}} \dot{\bar{\Gamma}}_{\bar{N}\bar{P}\bar{Q}}^e \tag{155}$$

We can rewrite the gradient of elastic microdeformation as

$$\bar{\Gamma}_{\bar{N}\bar{P}\bar{Q}}^e = F_{n\bar{N}}^e \gamma_{npq}^e \chi_{p\bar{P}}^e F_{q\bar{Q}}^e, \quad \gamma_{npq}^e \stackrel{\text{def}}{=} \chi_{\bar{A}p}^{e-1} \chi_{n\bar{A},q}^e \tag{156}$$

such that

$$\dot{\bar{\Gamma}}_{\bar{N}\bar{P}\bar{Q}}^e = F_{n\bar{N}}^e \overset{\circ}{\gamma}_{npq}^e \chi_{p\bar{P}}^e F_{q\bar{Q}}^e \tag{157}$$

$$\overset{\circ}{\gamma}_{npq}^e \stackrel{\text{def}}{=} \dot{\gamma}_{npq}^e + \ell_{an}^e \gamma_{apq}^e + \gamma_{npa}^e \ell_{aq}^e + \gamma_{naq}^e \nu_{ap}^e \tag{158}$$

Then, the couple stress material time derivative map becomes

$$\begin{aligned}
F_{k\bar{K}}^e F_{l\bar{L}}^e \chi_{m\bar{M}}^e \dot{M}_{\bar{K}\bar{L}\bar{M}} &= [\tau_1 (b_{kl}^e \psi_{nm}^e \psi_{qp}^e + \psi_{lm}^e \psi_{np}^e b_{kq}^e) \\
&\quad + \tau_2 (b_{kl}^e b^{\chi,e}_{mp} b_{nq}^e + \psi_{km}^e b_{lq}^e \psi_{np}^e) \\
&\quad + \tau_3 b_{kl}^e \psi_{qm}^e \psi_{np}^e + \tau_4 \psi_{lm}^e b_{kn}^e \psi_{qp}^e \\
&\quad + \tau_5 (\psi_{km}^e b_{ln}^e \psi_{qp}^e + \psi_{lm}^e \psi_{kp}^e b_{nq}^e) \\
&\quad + \tau_6 \psi_{km}^e \psi_{lp}^e b_{nq}^e + \tau_7 b_{kn}^e \psi_{lp}^e \psi_{qm}^e \\
&\quad + \tau_8 (\psi_{kp}^e b_{lq}^e \psi_{nm}^e + b_{kq}^e b_{ln}^e b^{\chi,e}_{mp}) \\
&\quad + \tau_9 b_{kn}^e b_{lq}^e b^{\chi,e}_{mp} + \tau_{10} \psi_{kp}^e b_{ln}^e \psi_{qm}^e \\
&\quad + \tau_{11} b_{kq}^e \psi_{lp}^e \psi_{nm}^e] \overset{\circ}{\gamma}_{npq}^e
\end{aligned} \tag{159}$$

where $b^{\chi,e}_{mp} = \chi^e_{m\bar{M}} \chi^e_{p\bar{M}}$. In summary, we have the stress evolution equations in \mathcal{B} as

$$\begin{aligned} \dot{\sigma}_{kl} &= -\frac{\dot{J}^e}{J^e} \sigma_{kl} + \ell^e_{ki} \sigma_{il} + \sigma_{ki} \ell^e_{li} + \\ &\quad \frac{1}{J^e} [(\lambda + \tau)(b^e_{ij} d^e_{ij}) b^e_{kl} + 2(\mu + \sigma) b^e_{ki} d^e_{ij} b^e_{jl} + \eta(\psi^e_{ij} \varepsilon^e_{ij}) b^e_{kl} \\ &\quad + \kappa b^e_{ki} \varepsilon^e_{ij} \psi^e_{jl} + \nu b^e_{li} \varepsilon^e_{ij} \psi^e_{jk}] \end{aligned} \quad (160)$$

$$\begin{aligned} \dot{s}_{kl} - \dot{\sigma}_{kl} &= -\frac{\dot{J}^e}{J^e} (s_{kl} - \sigma_{kl}) + \ell^e_{ki} (s_{il} - \sigma_{il}) + (s_{ki} - \sigma_{ki}) \ell^e_{li} + \\ &\quad \frac{1}{J^e} (\kappa b^e_{li} \varepsilon^e_{ij} \psi^e_{jk} + \nu b^e_{ki} \varepsilon^e_{ij} \psi^e_{jl}) \end{aligned} \quad (161)$$

$$\begin{aligned} \dot{m}_{klm} &= -\frac{\dot{J}^e}{J^e} m_{klm} + \ell^e_{ki} m_{ilm} + m_{kim} \ell^e_{li} + m_{kli} \nu^e_{mi} + \\ &\quad \frac{1}{J^e} [\tau_1 (b^e_{kl} \psi^e_{nm} \psi^e_{qp} + \psi^e_{lm} \psi^e_{np} b^e_{kq}) + \tau_2 (b^e_{kl} b^{\chi,e}_{mp} b^e_{nq} + \psi^e_{km} b^e_{lq} \psi^e_{np}) \\ &\quad + \tau_3 b^e_{kl} \psi^e_{qm} \psi^e_{np} + \tau_4 \psi^e_{lm} b^e_{kn} \psi^e_{qp} + \tau_5 (\psi^e_{km} b^e_{ln} \psi^e_{qp} + \psi^e_{lm} \psi^e_{kp} b^e_{nq}) \\ &\quad + \tau_6 \psi^e_{km} \psi^e_{lp} b^e_{nq} + \tau_7 b^e_{kn} \psi^e_{lp} \psi^e_{qm} + \tau_8 (\psi^e_{kp} b^e_{lq} \psi^e_{nm} + b^e_{kq} b^e_{ln} b^{\chi,e}_{mp}) \\ &\quad + \tau_9 b^e_{kn} b^e_{lq} b^{\chi,e}_{mp} + \tau_{10} \psi^e_{kp} b^e_{ln} \psi^e_{qm} + \tau_{11} b^e_{kq} \psi^e_{lp} \psi^e_{nm}] \overset{\circ}{\gamma}_{npq} \end{aligned} \quad (162)$$

where objective elastic stress rates are defined as

$$\overset{\square}{\sigma}_{kl} \stackrel{\text{def}}{=} \dot{\sigma}_{kl} - \ell^e_{ki} \sigma_{il} - \sigma_{ki} \ell^e_{li} + d^e_{ii} \sigma_{kl} \quad (163)$$

$$\frac{\overset{\square}{s}_{kl}}{(s_{kl} - \sigma_{kl})} \stackrel{\text{def}}{=} (\dot{s}_{kl} - \dot{\sigma}_{kl}) - \ell^e_{ki} (s_{il} - \sigma_{il}) - (s_{ki} - \sigma_{ki}) \ell^e_{li} + d^e_{ii} (s_{kl} - \sigma_{kl}) \quad (164)$$

$$\overset{\square}{m}_{klm} \stackrel{\text{def}}{=} \dot{m}_{klm} - \ell^e_{ki} m_{ilm} - m_{kim} \ell^e_{li} - m_{kli} \nu^e_{mi} + d^e_{ii} m_{klm} \quad (165)$$

where $\dot{J}^e/J^e = d^e_{ii}$. The stress rates on σ and $(\mathbf{s} - \sigma)$ are recognized as the elastic Truesdell stress rates (Holzapfel, 2000), whereas the stress rate on the higher order stress is new, and can similarly be defined as an elastic Truesdell higher order stress rate. To show $\overset{\square}{\mathbf{m}}$ is objective, consider a rigid body motion (Holzapfel, 2000), with translation \mathbf{c} and rotation \mathbf{Q} (orthogonal: $\mathbf{Q}\mathbf{Q}^T = 1$) on the current configuration \mathcal{B} , resulting in \mathcal{B}^+ , such that

$$\mathbf{x}'^+ = \mathbf{c} + \mathbf{Q}(\mathbf{x} + \xi) = \mathbf{c} + \mathbf{Q}\mathbf{x}' \quad (166)$$

Recall the definition of the higher order stress through the area-averaging, but now on the translated and rotated configuration \mathcal{B}^+ as

$$\begin{aligned}
m_{klm}^+ n_k^+ da &\stackrel{\text{def}}{=} \int_{da} \sigma_{kl}^+ \xi_m^+ n_k^+ da' \\
&\quad \text{where } \sigma_{kl}^+ = Q_{ka} \sigma'_{ab} Q_{lb}, \quad \xi_m^+ = Q_{mc} \xi_c, \quad n_k^+ = Q_{kd} n'_d \\
&= \int_{da} Q_{ka} \sigma'_{ab} Q_{lb} Q_{mc} \xi_c Q_{kd} n'_d da' \\
&= Q_{ka} \underbrace{\left(\int_{da} \sigma'_{ab} \xi_c n'_d da' \right)}_{\stackrel{\text{def}}{=} m_{abc} n_d da} Q_{lb} Q_{mc} Q_{kd} \\
&= \underbrace{Q_{ka} m_{abc} Q_{lb} Q_{mc}}_{=m_{klm}^+} n_k^+ da
\end{aligned} \tag{167}$$

We employ the standard results (Holzapfel, 2000)

$$\ell_{kl}^{e+} = \Omega_{kl} + Q_{ki} \ell_{ij}^e Q_{lj} \tag{168}$$

$$\nu_{kl}^{e+} = \Omega_{kl} + Q_{ki} \nu_{ij}^e Q_{lj} \tag{169}$$

$$d_{ii}^{e+} = d_{ii}^e \tag{170}$$

where $\Omega_{kl} = \dot{Q}_{ka} Q_{la}$. We substitute into the expression for $\mathbf{m}^{\square+}$, with after some tensor algebra, we can show that \mathbf{m}^{\square} is objective:

$$\begin{aligned}
\mathbf{m}_{klm}^{\square+} &\stackrel{\text{def}}{=} \dot{m}_{klm}^+ - \ell_{ki}^{e+} m_{ilm}^+ - m_{kim}^+ \ell_{li}^{e+} - m_{kli}^+ \nu_{mi}^{e+} + d_{ii}^{e+} m_{klm}^+ \\
&= Q_{ka} (\dot{m}_{klm} - \ell_{ki}^e m_{ilm} - m_{kim} \ell_{li}^e - m_{kli} \nu_{mi}^e + d_{ii}^e m_{klm}) Q_{lb} Q_{mc} \\
&= Q_{ka} \mathbf{m}_{klm}^{\square} Q_{lb} Q_{mc} \\
&\quad q.e.d.
\end{aligned} \tag{171}$$

Now, to map the plastic evolution equations, we start with the macroscale plasticity. The yield and plastic potential functions in \mathcal{B} become

$$F(\sigma, c) = J^e \|\text{dev} \sigma\|^e - J^e (A^\phi c - B^\phi p) \leq 0 \tag{172}$$

$$\begin{aligned}
\|\text{dev} \sigma\|^e &\stackrel{\text{def}}{=} \sqrt{(\text{dev} \sigma_{ij}) b_{im}^{e-1} b_{jn}^{e-1} (\text{dev} \sigma_{mn})} \\
\text{dev} \sigma_{ij} &= \sigma_{ij} - \left(\frac{1}{3} \sigma_{kk} \right) \delta_{ij}, \quad p = \frac{1}{3} \sigma_{kk}
\end{aligned}$$

$$G(\sigma, c) = J^e \|\text{dev} \sigma\|^e - J^e (A^\psi c - B^\psi p) \tag{173}$$

where $b_{ij}^{e-1} = F_{\bar{M}i}^{e-1} F_{\bar{M}j}^{e-1}$. The map of the plastic velocity gradient and strain-like ISV become

$$\ell_{lk}^p = \dot{\gamma} \frac{\partial G}{\partial \sigma_{kl}} \quad (174)$$

$$\frac{\partial G}{\partial \sigma_{kl}} = J^e \left(b_{ka}^{e-1} \frac{\text{dev} \sigma_{ab}}{\|\text{dev} \sigma\|^e} b_{bl}^{e-1} + \frac{1}{3} B^\psi \delta_{kl} \right)$$

$$\dot{Z} = -\dot{\gamma} \frac{\partial G}{\partial c} = A^\psi \dot{\gamma} J^e \quad (175)$$

$$c = HZ \quad (176)$$

Next, for microscale plasticity, the yield and plastic potential functions in \mathcal{B} become

$$F^x(\mathbf{s} - \sigma, c^x) = J^e \|\text{dev}(\mathbf{s} - \sigma)\|^e - J^e (A^{x,\phi} c^x - B^{x,\phi} p^x) \leq 0 \quad (177)$$

$$p^x = \frac{1}{3} (s_{kl} - \sigma_{kl}) \delta_{kl}$$

$$G^x(\mathbf{s} - \sigma, c^x) = J^e \|\text{dev}(\mathbf{s} - \sigma)\|^e - J^e (A^{x,\psi} c^x - B^{x,\psi} p^x) \quad (178)$$

The map of the plastic microgyration tensor and strain-like ISV become

$$\nu_{lk}^p = \dot{\gamma}^x \frac{\partial G^x}{\partial (s_{kl} - \sigma_{kl})} \quad (179)$$

$$\frac{\partial G^x}{\partial (s_{kl} - \sigma_{kl})} = J^e \left(b_{ka}^{e-1} \frac{\text{dev}(s_{ab} - \sigma_{ab})}{\|\text{dev}(\mathbf{s} - \sigma)\|^e} b_{bl}^{e-1} + \frac{1}{3} B^{x,\psi} \delta_{kl} \right)$$

$$\dot{Z}^x = -\dot{\gamma}^x \frac{\partial G^x}{\partial c^x} = A^{x,\psi} \dot{\gamma} J^e \quad (180)$$

$$c^x = H^x Z^x \quad (181)$$

For microscale gradient plasticity, the yield and plastic potential functions in \mathcal{B} become

$$F^{\nabla x}(\mathbf{m}, \mathbf{c}^{\nabla x}) = J^e \|\text{dev} \mathbf{m}\|^x - J^e (A^{\nabla x, \phi} \|\mathbf{c}^{\nabla x}\|^x - B^{\nabla x, \phi} \|\mathbf{p}^{\nabla x}\|^x) \leq 0 \quad (182)$$

$$\|\mathbf{c}^{\nabla x}\|^x \stackrel{\text{def}}{=} \sqrt{c_m^{\nabla x} b_{mn, e-1}^{\nabla x} c_n^{\nabla x}}$$

$$\|\text{dev} \mathbf{m}\|^x \stackrel{\text{def}}{=} \sqrt{(\text{dev} m_{ijk}) b_{im}^{-1} b_{jn}^{-1} b_{kp}^{-1} (\text{dev} m_{mnp})}$$

$$\|\mathbf{p}^{\nabla x}\|^x \stackrel{\text{def}}{=} \sqrt{p_m^{\nabla x} b_{mn, e-1}^{\nabla x} p_n^{\nabla x}}, \quad p_m^{\nabla x} = \frac{1}{3} m_{kk m}$$

$$G^{\nabla x}(\mathbf{m}, \mathbf{c}^{\nabla x}) = J^e \|\text{dev} \mathbf{m}\|^x - J^e (A^{\nabla x, \psi} \|\mathbf{c}^{\nabla x}\|^x - B^{\nabla x, \psi} \|\mathbf{p}^{\nabla x}\|^x) \quad (183)$$

The map of the gradient plastic microgyration tensor and strain-like ISV become

$$\nu_{lm,k}^p = (\dot{\gamma}^{\nabla\chi}) \frac{\partial G^{\nabla\chi}}{\partial m_{klm}} \quad (184)$$

$$\frac{\partial G^{\nabla\chi}}{\partial m_{klm}} = J^e \left(\frac{\text{dev} m_{abc}}{\|\text{dev} \mathbf{m}\|^\chi} b^{e-1}_{ka} b^{e-1}_{lb} b^{\chi,e-1}_{mc} + \frac{1}{3} B^{\nabla\chi,\psi} \delta_{kl} \frac{p_a^{\nabla\chi}}{\|\mathbf{p}^{\nabla\chi}\|^\chi} b^{\chi,e-1}_{am} \right)$$

$$\dot{Z}_{,a}^\chi = -(\dot{\gamma}^{\nabla\chi}) \frac{\partial G^{\nabla\chi}}{\partial c_a^{\nabla\chi}} = A^{\nabla\chi,\psi} (\dot{\gamma}^{\nabla\chi}) J^e \frac{c_b^{\nabla\chi}}{\|\mathbf{c}^{\nabla\chi}\|^\chi} b^{\chi,e-1}_{ba} \quad (185)$$

$$c_l^{\nabla\chi} = H^{\nabla\chi} Z_{,a}^\chi b_{al}^{\chi,e} \quad (186)$$

Remark 9. It is reassuring to see that the left hand sides of the plastic deformation evolution equations 174, 179, 184 simplify considerably in the current configuration from the forms in the intermediate configuration 133, 139, 144. They are further simplified when assuming small elastic deformations.

Remark 10. Solving numerically for the increment of $\nu_{lm,k}^p$ leads to the solution of the increment of $\nu_{lm,k}^e$, and, in turn, the evolution of the couple stress m_{klm} over time. We see this by taking the spatial derivative of the microgyration tensor as

$$\nu_{lm,k} = \nu_{lm,k}^e + \nu_{lm,k}^p \quad (187)$$

$$\begin{aligned} \nu_{lm,k} &= [\dot{\chi}_{lK} \chi_{Km}^{-1}]_{,k} \\ \nu_{lm,k}^e &= \dot{\gamma}_{lmk}^e - \nu_{la}^e \gamma_{amk}^e + \nu_{am}^e \gamma_{lak}^e \end{aligned} \quad (188)$$

Remark 11. With the definition of the plastic evolution equations, plastic deformation can be calculated, and elastic deformation updated to calculate the stresses. A FE implementations solve these equations. We take advantage of the small deformation elasticity, such that elastic deformation in the current configuration, b_{ij}^{e-1} , b_{ij}^e , etc., can be approximated by the second-order unit tensor δ_{ij} .

To illustrate the implementation, we apply assumptions for small elastic deformation in the next section.

Small elastic deformation and Cartesian coordinates for current configuration

\mathcal{B} : Assuming small elastic deformation, the tensors b_{ij}^{e-1} , b_{ij}^e , ψ_{ij}^e , $b^{\chi,e-1}_{ij} \approx \delta_{ij}$ and $J^e \approx 1$, when multiplied by another variable that is not δ_{ij} or 1, such as $b_{ka}^{e-1} \text{dev} \sigma_{ab} b_{bl}^{e-1} \approx \text{dev} \sigma_{kl}$. Also, the rate of elastic volumetric deformation is $\dot{J}^e / J^e = d_{ii}^e$. With these approximations, in summary, we have the stress evolution equations in \mathcal{B} as

$$\begin{aligned}\dot{\sigma}_{kl} &= -(d_{ii}^e)\sigma_{kl} + \ell_{ki}^e\sigma_{il} + \sigma_{ki}\ell_{li}^e + (\lambda + \tau)(d_{ii}^e)\delta_{kl} + 2(\mu + \sigma)d_{kl}^e \\ &\quad + \eta(\varepsilon_{ii}^e)\delta_{kl} + \kappa\varepsilon_{kl}^e + \nu\varepsilon_{lk}^e\end{aligned}\quad (189)$$

$$\dot{s}_{kl} - \dot{\sigma}_{kl} = -(d_{ii}^e)(s_{kl} - \sigma_{kl}) + \ell_{ki}^e(s_{il} - \sigma_{il}) + (s_{ki} - \sigma_{ki})\ell_{li}^e + \kappa\varepsilon_{lk}^e + \nu\varepsilon_{kl}^e \quad (190)$$

$$\begin{aligned}\dot{m}_{klm} &= -(d_{ii}^e)m_{klm} + \ell_{ki}^e m_{ilm} + m_{kim}\ell_{li}^e + m_{kli}\nu_{mi}^e + c_{klmnpq}\overset{\circ}{\gamma}_{npq}^e \\ c_{klmnpq} &= \tau_1(\delta_{kl}\delta_{nm}\delta_{qp} + \delta_{lm}\delta_{np}\delta_{kq}) + \tau_2(\delta_{kl}\delta_{mp}\delta_{nq} + \delta_{km}\delta_{lp}\delta_{nq}) \\ &\quad + \tau_3\delta_{kl}\delta_{qm}\delta_{np} + \tau_4\delta_{lm}\delta_{kn}\delta_{qp} + \tau_5(\delta_{km}\delta_{ln}\delta_{qp} + \delta_{lm}\delta_{kp}\delta_{nq}) \\ &\quad + \tau_6\delta_{km}\delta_{lp}\delta_{nq} + \tau_7\delta_{kn}\delta_{lp}\delta_{qm} + \tau_8(\delta_{kp}\delta_{lq}\delta_{nm} + \delta_{kq}\delta_{ln}\delta_{mp}) \\ &\quad + \tau_9\delta_{kn}\delta_{lq}\delta_{mp} + \tau_{10}\delta_{kp}\delta_{ln}\delta_{qm} + \tau_{11}\delta_{kq}\delta_{lp}\delta_{nm}\end{aligned}\quad (191)$$

The yield and plastic potential functions in \mathcal{B} become

$$F(\sigma, c) = \|\text{dev}\sigma\| - (A^\phi c - B^\phi p) \leq 0 \quad (192)$$

$$\|\text{dev}\sigma\| = \sqrt{(\text{dev}\sigma_{ij})(\text{dev}\sigma_{ij})}$$

$$\text{dev}\sigma_{ij} = \sigma_{ij} - \left(\frac{1}{3}\sigma_{kk}\right)\delta_{ij}, \quad p = \frac{1}{3}\sigma_{kk}$$

$$G(\sigma, c) = \|\text{dev}\sigma\| - (A^\psi c - B^\psi p) \quad (193)$$

The map of the plastic velocity gradient and strain-like ISV become

$$\ell_{lk}^p = \dot{\gamma} \frac{\partial G}{\partial \sigma_{kl}} \quad (194)$$

$$\frac{\partial G}{\partial \sigma_{kl}} = \frac{\text{dev}\sigma_{kl}}{\|\text{dev}\sigma\|} + \frac{1}{3}B^\psi \delta_{kl}$$

$$\dot{Z} = -\dot{\gamma} \frac{\partial G}{\partial c} = A^\psi \dot{\gamma} \quad (195)$$

$$c = HZ \quad (196)$$

Notice that $\ell^p = \dot{\gamma}(\partial G/\partial \sigma)^T$. Next, for microscale plasticity, the yield and plastic potential functions in \mathcal{B} become

$$F^\chi(\mathbf{s} - \sigma, c^\chi) = \|\text{dev}(\mathbf{s} - \sigma)\| - (A^{\chi,\phi}c^\chi - B^{\chi,\phi}p^\chi) \leq 0 \quad (197)$$

$$p^\chi = \frac{1}{3}(s_{kk} - \sigma_{kk})$$

$$G^\chi(\mathbf{s} - \sigma, c^\chi) = \|\text{dev}(\mathbf{s} - \sigma)\| - (A^{\chi,\psi}c^\chi - B^{\chi,\psi}p^\chi) \quad (198)$$

The map of the plastic microgyration tensor and strain-like ISV become

$$\nu_{lk}^p = \dot{\gamma}^\chi \frac{\partial G^\chi}{\partial (s_{kl} - \sigma_{kl})} \quad (199)$$

$$\frac{\partial G^\chi}{\partial (s_{kl} - \sigma_{kl})} = \frac{\text{dev}(s_{kl} - \sigma_{kl})}{\|\text{dev}(\mathbf{s} - \boldsymbol{\sigma})\|} + \frac{1}{3} B^{\chi, \psi} \delta_{kl}$$

$$\dot{Z}^\chi = -\dot{\gamma}^\chi \frac{\partial G^\chi}{\partial c^\chi} = A^{\chi, \psi} \dot{\gamma}^\chi \quad (200)$$

$$c^\chi = H^\chi Z^\chi \quad (201)$$

For microscale gradient plasticity, the yield and plastic potential functions in \mathcal{B} become

$$F^{\nabla\chi}(\mathbf{m}, \mathbf{c}^{\nabla\chi}) = \|\text{dev}\mathbf{m}\| - (A^{\nabla\chi, \phi} \|\mathbf{c}^{\nabla\chi}\| - B^{\nabla\chi, \phi} \|\mathbf{p}^{\nabla\chi}\|) \leq 0 \quad (202)$$

$$\|\mathbf{c}^{\nabla\chi}\| = \sqrt{c_m^{\nabla\chi} c_m^{\nabla\chi}}$$

$$\|\text{dev}\mathbf{m}\| = \sqrt{(\text{dev}m_{ijk})(\text{dev}m_{ijk})}$$

$$\text{dev}m_{ijk} = m_{ijk} - \frac{1}{3} \delta_{ij} m_{aak} \quad (203)$$

$$\|\mathbf{p}^{\nabla\chi}\| = \sqrt{p_m^{\nabla\chi} p_m^{\nabla\chi}}, \quad p_m^{\nabla\chi} = \frac{1}{3} m_{kkk}$$

$$G^{\nabla\chi}(\mathbf{m}, \mathbf{c}^{\nabla\chi}) = \|\text{dev}\mathbf{m}\| - (A^{\nabla\chi, \psi} \|\mathbf{c}^{\nabla\chi}\| - B^{\nabla\chi, \psi} \|\mathbf{p}^{\nabla\chi}\|) \quad (204)$$

The map of the gradient plastic microgyration tensor and strain-like ISV become

$$\nu_{lm,k}^p = (\dot{\gamma}^{\nabla\chi}) \frac{\partial G^{\nabla\chi}}{\partial m_{klm}}, \quad \frac{\partial G^{\nabla\chi}}{\partial m_{klm}} = \frac{\text{dev}m_{klm}}{\|\text{dev}\mathbf{m}\|} + \frac{1}{3} B^{\nabla\chi, \psi} \delta_{kl} \frac{p_m^{\nabla\chi}}{\|\mathbf{p}^{\nabla\chi}\|} \quad (205)$$

$$\dot{Z}_{,a}^\chi = -(\dot{\gamma}^{\nabla\chi}) \frac{\partial G^{\nabla\chi}}{\partial c_a^{\nabla\chi}} = A^{\nabla\chi, \psi} (\dot{\gamma}^{\nabla\chi}) \frac{c_a^{\nabla\chi}}{\|\mathbf{c}^{\nabla\chi}\|} \quad (206)$$

$$c_l^{\nabla\chi} = H^{\nabla\chi} Z_{,l}^\chi \quad (207)$$

Solving numerically for the increment of $\nu_{lm,k}^p$ leads to the solution of the increment of $\nu_{lm,k}^e$, and, in turn, the evolution of the couple stress m_{klm} over time. We see this by taking the spatial derivative of the microgyration tensor as

$$\begin{aligned}
\nu_{lm,k} &= \nu_{lm,k}^e + \nu_{lm,k}^p \\
\nu_{lm,k} &= [\dot{\chi}_{lK} \chi_{Km}^{-1}]_{,k} \\
\nu_{lm,k}^e &= \dot{\gamma}_{lmk}^e - \nu_{la}^e \gamma_{amk}^e + \nu_{am}^e \gamma_{lak}^e
\end{aligned} \tag{208}$$

Boxes 1 and 2 provide summaries of the stress and plastic evolution equations, respectively, in symbolic form to solve numerically in time. The details of the symbolic equations have been provided in index notation in this section. The numerical time integration scheme is presented in section 2.3.4.

Box 1. Summary of stress evolution equations in the current configuration in symbolic notation.

$$\begin{aligned}\dot{\sigma} &= -(\text{tr} \mathbf{d}^e) \sigma + \ell^e \sigma + \sigma \ell^{eT} + (\lambda + \tau)(\text{tr} \mathbf{d}^e) \mathbf{1} + 2(\mu + \sigma) \mathbf{d}^e \\ &\quad + \eta(\text{tr} \varepsilon^e) \mathbf{1} + \kappa \varepsilon^e + \nu \varepsilon^{eT}\end{aligned}\quad (209)$$

$$\dot{\mathbf{s}} - \dot{\sigma} = -(\text{tr} \mathbf{d}^e)(\mathbf{s} - \sigma) + \ell^e(\mathbf{s} - \sigma) + (\mathbf{s} - \sigma) \ell^{eT} + \kappa \varepsilon^{eT} + \nu \varepsilon^e \quad (210)$$

$$\dot{\mathbf{m}} = -(\text{tr} \mathbf{d}^e) \mathbf{m} + \ell^e \mathbf{m} + \mathbf{m} \odot \ell^{eT} + \mathbf{m} \nu^{eT} + \mathbf{c} \dot{\gamma}^e \quad (211)$$

Box 2. Summary of plastic evolution equations in the current configuration in symbolic notation.

$$\ell^p = \dot{\gamma} \left(\frac{\partial G}{\partial \sigma} \right)^T \quad (212)$$

$$\frac{\partial G}{\partial \sigma} = \frac{\text{dev} \sigma}{\|\text{dev} \sigma\|} + \frac{1}{3} B^\psi \mathbf{1} = \hat{\mathbf{r}}$$

$$\dot{Z} = A^\psi \dot{\gamma} \quad (213)$$

$$\nu^p = \dot{\gamma}^\chi \left(\frac{\partial G^\chi}{\partial (\mathbf{s} - \sigma)} \right)^T \quad (214)$$

$$\frac{\partial G^\chi}{\partial (\mathbf{s} - \sigma)} = \frac{\text{dev}(\mathbf{s} - \sigma)}{\|\text{dev}(\mathbf{s} - \sigma)\|} + \frac{1}{3} B^{\chi, \psi} \mathbf{1} = \hat{\mathbf{r}}^\chi$$

$$\dot{Z}^\chi = A^{\chi, \psi} \dot{\gamma} \quad (215)$$

$$\nabla \nu^p = (\dot{\gamma}^{\nabla \chi}) \left(\frac{\partial G^{\nabla \chi}}{\partial \mathbf{m}} \right)^T \quad (216)$$

$$\frac{\partial G^{\nabla \chi}}{\partial \mathbf{m}} = \frac{\text{dev} \mathbf{m}}{\|\text{dev} \mathbf{m}\|} + \frac{1}{3} B^{\nabla \chi, \psi} \mathbf{1} \otimes \frac{\mathbf{p}^{\nabla \chi}}{\|\mathbf{p}^{\nabla \chi}\|} = \hat{\mathbf{r}}^{\nabla \chi}$$

$$\nabla \dot{Z}^\chi = A^{\nabla \chi, \psi} (\dot{\gamma}^{\nabla \chi}) \frac{\mathbf{c}^{\nabla \chi}}{\|\mathbf{c}^{\nabla \chi}\|} \quad (217)$$

2.5 Numerical Time Integration

The constitutive equations in section 2.3.3 are integrated numerically in time following a semi-implicit scheme (Moran et al., 1990). We will solve for plastic multiplier increments $\Delta\gamma$ and $\Delta\gamma^\chi$ in a coupled fashion (if yielding is detected at both scales; see Box 9), and multiplier $\Delta\gamma^{\nabla\chi}$ afterward because it is uncoupled. It is uncoupled because of the assumption that quadratic terms in equations 110 and 111 were ignored, leading to uncoupling of the higher order stress \mathbf{m} from Cauchy stress σ and microstress \mathbf{s} , whereas σ and \mathbf{s} remain coupled (thus coupling $\dot{\gamma}$ and $\dot{\gamma}^\chi$).

We assume a deformation-driven time integration scheme within a FE program solving the isothermal coupled balance of linear momentum and first moment of momentum equations 57₃ and 57₄, respectively, such that deformation gradient \mathbf{F}_{n+1} and microdeformation tensor χ_{n+1} are given at time t_{n+1} , as well as their increments $\Delta\mathbf{F}_{n+1} = \mathbf{F}_{n+1} - \mathbf{F}_n$ and $\Delta\chi_{n+1} = \chi_{n+1} - \chi_n$. We assume a time step $\Delta t = t_{n+1} - t_n$. Boxes 3-8 provide summaries of the semi-implicit time integration of the stress and plastic evolution equations, respectively, in symbolic form.

To obtain $\dot{\gamma}^e$ in Box 1 through $\overset{\circ}{\gamma}^e$, we use equation 208 such that

$$\begin{aligned} \nabla\nu &= \nabla\nu^e + \nabla\nu^p \\ \nabla\nu &= \nabla[\dot{\chi}\chi^{-1}] \\ \nabla\nu^e &= \dot{\gamma}^e - \nu^e\gamma^e + \nu^{eT} \odot \gamma^e \\ \implies \dot{\gamma}^e &= \nu^e\gamma^e - \nu^{eT} \odot \gamma^e + \nabla\nu - \nabla\nu^p \end{aligned} \tag{218}$$

Recall equation 158 which gives the equation for the objective rate of γ^e as

$$\overset{\circ}{\gamma}^e \stackrel{\text{def}}{=} \dot{\gamma}^e + \ell^{eT}\gamma^e + \gamma^e\ell^e + \gamma^e \odot \nu^e \tag{219}$$

which appears in equation 211 in Box 1, and in Box 4 for the numerical integration. For $\nabla(\chi_{n+1} - \chi_n)$ and $\nabla\chi_{n+1}$ in Box 4, because χ is a nodal DOF in a FE solution and thus interpolated in a standard fashion, its spatial gradient can be calculated.

Box 9 summarizes the algorithm for solving the plastic multipliers from evaluating the yield functions at time t_{n+1} . It involves multiple plastic yield checks, such that macro and/or micro plasticity could be enabled, and/or microgradient plasticity. Because the macro and micro plasticity yield functions F and F^χ , respectively, are decoupled from the microgradient plastic multiplier $\dot{\gamma}^{\nabla\chi}$, we solve first for the micro and macroplastic

multipliers, as indicated by (I) in Box 9, and then for the microgradient plastic multiplier in (II) afterward. Once the plastic multipliers are calculated, the stresses and ISVs can be updated as indicated in Boxes 5-8.

This micromorphic plasticity model numerical integration scheme fit nicely into a coupled Lagrangian FE formulation and implementation of the balance of linear momentum and first moment of momentum. Such work is ongoing.

Box 3. Summary of semi-implicit time integration of Cauchy stress σ and microstress-Cauchy-stress difference $(\mathbf{s} - \sigma)$ evolution equations. $(\bullet)^{\text{tr}}$ implies the trial value, in this case the trial stress. Results of the semi-implicit time integration of the plastic evolution equations in Box 5 are included here.

$$\begin{aligned}\sigma_{n+1} = & (1 - \text{tr}(\Delta t \mathbf{d}_{n+1}^e))\sigma_n + (\Delta t \ell_{n+1}^e)\sigma_n + \sigma_n(\Delta t \ell_{n+1}^e)^T + \\ & (\lambda + \tau)\text{tr}(\Delta t \mathbf{d}_{n+1}^e)\mathbf{1} + 2(\mu + \sigma)(\Delta t \mathbf{d}_{n+1}^e) + \eta\text{tr}(\Delta t \varepsilon_{n+1}^e)\mathbf{1} \\ & + \kappa(\Delta t \varepsilon_{n+1}^e) + \nu(\Delta t \varepsilon_{n+1}^e)^T\end{aligned}\quad (220)$$

$$\begin{aligned}(\mathbf{s} - \sigma)_{n+1} = & (1 - \text{tr}(\Delta t \mathbf{d}_{n+1}^e))(\mathbf{s} - \sigma)_n + (\Delta t \ell_{n+1}^e)(\mathbf{s} - \sigma)_n + (\mathbf{s} - \sigma)_n(\Delta t \ell_{n+1}^e)^T + \\ & \kappa(\Delta t \varepsilon_{n+1}^e)^T + \nu(\Delta t \varepsilon_{n+1}^e)\end{aligned}\quad (221)$$

$$\Delta t \ell_{n+1}^e = \Delta t \ell_{n+1} - \Delta t \ell_{n+1}^p \quad (222)$$

$$\Delta t \ell_{n+1} = (\Delta \mathbf{F}_{n+1})\mathbf{F}_{n+1}^{-1}$$

$$\Delta t \ell_{n+1}^p = (\Delta \gamma_{n+1})(\hat{\mathbf{r}}^{\text{tr}})^T, \quad \hat{\mathbf{r}}^{\text{tr}} = \frac{\text{dev} \sigma^{\text{tr}}}{\|\text{dev} \sigma^{\text{tr}}\|} + \frac{1}{3}B^\psi \mathbf{1}$$

$$\text{tr}(\Delta t \mathbf{d}_{n+1}^e) = \text{tr}(\Delta t \ell_{n+1}) - \text{tr}(\Delta t \ell_{n+1}^p) = \text{tr}(\Delta t \ell_{n+1}) - B^\psi(\Delta \gamma_{n+1})$$

$$\Delta t \varepsilon_{n+1}^e = \Delta t \nu_{n+1}^e + \Delta t \ell_{n+1}^{eT} \quad (223)$$

$$\Delta t \nu_{n+1}^e = \Delta t \nu_{n+1} - \Delta t \nu_{n+1}^p$$

$$\Delta t \nu_{n+1} = (\Delta \chi_{n+1})\chi_{n+1}^{-1}$$

$$\Delta t \nu_{n+1}^p = (\Delta \gamma_{n+1}^\chi)(\hat{\mathbf{r}}^{\chi, \text{tr}})^T, \quad \hat{\mathbf{r}}^{\chi, \text{tr}} = \frac{\text{dev}(\mathbf{s} - \sigma)^{\text{tr}}}{\|\text{dev}(\mathbf{s} - \sigma)^{\text{tr}}\|} + \frac{1}{3}B^{\chi, \psi} \mathbf{1}$$

$$\text{tr}(\Delta t \varepsilon_{n+1}^e) = \text{tr}(\Delta t \varepsilon_{n+1}) - \text{tr}(\Delta t \varepsilon_{n+1}^p) = \text{tr}(\Delta t \varepsilon_{n+1}) - B^{\chi, \psi}(\Delta \gamma_{n+1}^\chi)$$

$$\text{tr}(\Delta t \varepsilon_{n+1}) = \text{tr}(\Delta t \nu_{n+1}) + \text{tr}(\Delta t \ell_{n+1})$$

Box 4. Summary of semi-implicit time integration of higher-order stress \mathbf{m} evolution equation.

Results of the semi-implicit time integration of the plastic evolution equations in Box 5 are included here.

$$\begin{aligned} \mathbf{m}_{n+1} = & (1 - \text{tr}(\Delta t \mathbf{d}_{n+1}^e)) \mathbf{m}_n + (\Delta t \ell_{n+1}^e) \mathbf{m}_n + \mathbf{m}_n \odot (\Delta t \ell_{n+1}^e)^T + \mathbf{m}_n (\Delta t \nu_{n+1}^e)^T + \\ & \mathbf{c} : (\Delta t \overset{\circ}{\gamma}_{n+1}^e) \end{aligned} \quad (224)$$

$$\Delta t \overset{\circ}{\gamma}_{n+1}^e = \Delta t \dot{\gamma}_{n+1}^e + (\Delta t \ell_{n+1}^e)^T \gamma_n^e + \gamma_n^e (\Delta t \ell_{n+1}^e) + \gamma_n^e \odot (\Delta t \nu_{n+1}^e) \quad (225)$$

$$\Delta t \dot{\gamma}_{n+1}^e = (\Delta t \nu_{n+1}^e) \gamma_n^e - (\Delta t \nu_{n+1}^e)^T \odot \gamma_n^e + \Delta t \nabla \nu_{n+1} - \Delta t \nabla \nu_{n+1}^p \quad (226)$$

$$\Delta t \nabla \nu_{n+1} = \nabla (\chi_{n+1} - \chi_n) \chi_{n+1}^{-1} - (\chi_{n+1} - \chi_n) \chi_{n+1}^{-1} (\nabla \chi_{n+1}) \chi_{n+1}^{-1} \quad (227)$$

$$\Delta t \nabla \nu_{n+1}^p = (\Delta \gamma_{n+1}^{\nabla \chi}) (\hat{\mathbf{r}}^{\nabla \chi, \text{tr}})^T \quad (228)$$

$$\hat{\mathbf{r}}^{\nabla \chi, \text{tr}} = \frac{\text{dev} \mathbf{m}^{\text{tr}}}{\|\text{dev} \mathbf{m}^{\text{tr}}\|} + \frac{1}{3} B^{\nabla \chi, \psi} \mathbf{1} \otimes \frac{\mathbf{p}^{\nabla \chi, \text{tr}}}{\|\mathbf{p}^{\nabla \chi, \text{tr}}\|}$$

$$\Delta t \ell_{n+1}^p = \Delta \gamma_{n+1} \left(\frac{\partial G}{\partial \sigma^{\text{tr}}} \right)^T \quad (229)$$

$$\frac{\partial G}{\partial \sigma^{\text{tr}}} = \frac{\text{dev} \sigma^{\text{tr}}}{\|\text{dev} \sigma^{\text{tr}}\|} + \frac{1}{3} B^\psi \mathbf{1} = \hat{\mathbf{r}}^{\text{tr}}$$

$$Z_{n+1} = Z_n + A^\psi \Delta \gamma_{n+1} \quad (230)$$

$$c_{n+1} = H Z_{n+1} \quad (231)$$

$$\Delta t \nu_{n+1}^p = \Delta \gamma_{n+1}^\chi \left(\frac{\partial G^\chi}{\partial (\mathbf{s} - \sigma)^{\text{tr}}} \right)^T \quad (232)$$

$$\frac{\partial G^\chi}{\partial (\mathbf{s} - \sigma)^{\text{tr}}} = \frac{\text{dev}(\mathbf{s} - \sigma)^{\text{tr}}}{\|\text{dev}(\mathbf{s} - \sigma)^{\text{tr}}\|} + \frac{1}{3} B^{\chi, \psi} \mathbf{1} = \hat{\mathbf{r}}^{\chi, \text{tr}}$$

$$Z_{n+1}^\chi = Z_n^\chi + A^{\chi, \psi} \Delta \gamma_{n+1}^\chi \quad (233)$$

$$c_{n+1}^\chi = H^\chi Z_{n+1}^\chi \quad (234)$$

$$\Delta t \nabla \nu_{n+1}^p = (\Delta \gamma_{n+1}^{\nabla \chi}) \left(\frac{\partial G^{\nabla \chi}}{\partial \mathbf{m}^{\text{tr}}} \right)^T \quad (235)$$

$$\frac{\partial G^{\nabla \chi}}{\partial \mathbf{m}^{\text{tr}}} = \frac{\text{dev} \mathbf{m}^{\text{tr}}}{\|\text{dev} \mathbf{m}^{\text{tr}}\|} + \frac{1}{3} B^{\nabla \chi, \psi} \mathbf{1} \otimes \frac{\mathbf{p}^{\nabla \chi, \text{tr}}}{\|\mathbf{p}^{\nabla \chi, \text{tr}}\|} = \hat{\mathbf{r}}^{\nabla \chi, \text{tr}}$$

$$\nabla Z_{n+1}^\chi = \nabla Z_n^\chi + A^{\nabla \chi, \psi} (\Delta \gamma_{n+1}^{\nabla \chi}) \frac{\mathbf{c}_n^{\nabla \chi}}{\|\mathbf{c}_n^{\nabla \chi}\|} \quad (236)$$

$$\mathbf{c}_{n+1}^{\nabla \chi} = H^{\nabla \chi} \nabla Z_{n+1}^\chi \quad (237)$$

Box 6. Elastic-predictor-plastic-corrector form of semi-implicit time integration of stress σ evolution equation in the current configuration.

$$\sigma_{n+1} = \sigma^{\text{tr}} - (\Delta\gamma_{n+1})\mathbf{D}^{p,\text{tr}} - (\Delta\gamma_{n+1}^\chi)\mathbf{D}^{\chi,p,\text{tr}} \quad (238)$$

$$\begin{aligned} \sigma^{\text{tr}} = & (1 - \text{tr}(\Delta t\ell_{n+1}))\sigma_n + (\Delta t\ell_{n+1})\sigma_n + \sigma_n(\Delta t\ell_{n+1})^T + (\lambda + \tau)\text{tr}(\Delta t\ell_{n+1})\mathbf{1} + \\ & 2(\mu + \sigma)\text{sym}(\Delta t\ell_{n+1}) + \eta[\text{tr}(\Delta t\nu_{n+1}) + \text{tr}(\Delta t\ell_{n+1})]\mathbf{1} \\ & + \kappa[\Delta t\nu_{n+1} + (\Delta t\ell_{n+1})^T] + \nu[(\Delta t\nu_{n+1})^T + \Delta t\ell_{n+1}] \end{aligned} \quad (239)$$

$$\begin{aligned} \mathbf{D}^{p,\text{tr}} = & -B^\psi\sigma_n + (\hat{\mathbf{r}}^{\text{tr}})^T\sigma_n + \sigma_n\hat{\mathbf{r}}^{\text{tr}} + (\lambda + \tau)B^\psi\mathbf{1} + 2(\mu + \sigma)\text{sym}(\hat{\mathbf{r}}^{\text{tr}}) + \eta B^\psi\mathbf{1} \\ & + \kappa\hat{\mathbf{r}}^{\text{tr}} + \nu(\hat{\mathbf{r}}^{\text{tr}})^T \end{aligned} \quad (240)$$

$$\mathbf{D}^{\chi,p,\text{tr}} = \eta B^{\chi,\psi}\mathbf{1} + \kappa(\hat{\mathbf{r}}^{\chi,\text{tr}})^T + \nu\hat{\mathbf{r}}^{\chi,\text{tr}} \quad (241)$$

Box 7. Elastic-predictor-plastic-corrector form of semi-implicit time integration of microstress-Cauchy-stress difference $(\mathbf{s} - \sigma)$ evolution equation in the current configuration.

$$(\mathbf{s} - \sigma)_{n+1} = (\mathbf{s} - \sigma)^{\text{tr}} - (\Delta\gamma_{n+1})\mathbf{E}^{p,\text{tr}} - (\Delta\gamma_{n+1}^\chi)\mathbf{E}^{\chi,p,\text{tr}} \quad (242)$$

$$\begin{aligned} (\mathbf{s} - \sigma)^{\text{tr}} = & (1 - \text{tr}(\Delta t\ell_{n+1}))(\mathbf{s} - \sigma)_n + (\Delta t\ell_{n+1})(\mathbf{s} - \sigma)_n + (\mathbf{s} - \sigma)_n(\Delta t\ell_{n+1})^T \\ & + \kappa[(\Delta t\nu_{n+1})^T + \Delta t\ell_{n+1}] + \nu[\Delta t\nu_{n+1} + (\Delta t\ell_{n+1})^T] \end{aligned} \quad (243)$$

$$\mathbf{E}^{p,\text{tr}} = -B^\psi(\mathbf{s} - \sigma)_n + (\hat{\mathbf{r}}^{\text{tr}})^T(\mathbf{s} - \sigma)_n + (\mathbf{s} - \sigma)_n\hat{\mathbf{r}}^{\text{tr}} + \kappa(\hat{\mathbf{r}}^{\text{tr}})^T + \nu\hat{\mathbf{r}}^{\text{tr}} \quad (244)$$

$$\mathbf{E}^{\chi,p,\text{tr}} = \kappa\hat{\mathbf{r}}^{\chi,\text{tr}} + \nu(\hat{\mathbf{r}}^{\chi,\text{tr}})^T \quad (245)$$

Box 8. Elastic-predictor-plastic-corrector form of semi-implicit time integration of higher-order couple stress \mathbf{m} evolution equation in the current configuration.

$$\mathbf{m}_{n+1} = \mathbf{m}^{\text{tr}} - (\Delta\gamma_{n+1})\mathbf{K}^{p,\text{tr}} - (\Delta\gamma_{n+1}^\chi)\mathbf{K}^{\chi,p,\text{tr}} - (\Delta\gamma_{n+1}^{\nabla\chi})\mathbf{K}^{\nabla\chi,p,\text{tr}} \quad (246)$$

$$\begin{aligned} \mathbf{m}^{\text{tr}} = & (1 - \text{tr}(\Delta t\ell_{n+1}))\mathbf{m}_n + (\Delta t\ell_{n+1})\mathbf{m}_n + \mathbf{m}_n \odot (\Delta t\ell_{n+1})^T + \mathbf{m}_n(\Delta t\nu_{n+1})^T \\ & + \mathbf{c}:[(\Delta t\nu_{n+1})\gamma_n^e - (\Delta t\nu_{n+1})^T \odot \gamma_n^e + \gamma_n^e \odot (\Delta t\nu_{n+1}) + \Delta t\nabla\nu_{n+1} \\ & + (\Delta t\ell_{n+1})^T\gamma_n^e + \gamma_n^e(\Delta t\ell_{n+1})] \end{aligned} \quad (247)$$

$$\mathbf{K}^{p,\text{tr}} = B^\psi\mathbf{m}_n + (\hat{\mathbf{r}}^{\text{tr}})^T\mathbf{m}_n + \mathbf{m}_n \odot \hat{\mathbf{r}}^{\text{tr}} + \mathbf{c}:[\hat{\mathbf{r}}^{\text{tr}}\gamma_n^e + \gamma_n^e(\hat{\mathbf{r}}^{\text{tr}})^T] \quad (248)$$

$$\mathbf{K}^{\chi,p,\text{tr}} = \mathbf{m}_n\hat{\mathbf{r}}^{\chi,\text{tr}} + \mathbf{c}:[(\hat{\mathbf{r}}^{\chi,\text{tr}})^T\gamma_n^e - \hat{\mathbf{r}}^{\chi,\text{tr}} \odot \gamma_n^e + \gamma_n^e \odot (\hat{\mathbf{r}}^{\chi,\text{tr}})^T] \quad (249)$$

$$\mathbf{K}^{\nabla\chi,p,\text{tr}} = \mathbf{c}:(\hat{\mathbf{r}}^{\nabla\chi,\text{tr}})^T \quad (250)$$

(I) solve for macro and micro plastic multipliers $\Delta\gamma$ and $\Delta\gamma^\chi$:

Step 1. Compute trial stresses σ^{tr} , $(\mathbf{s} - \sigma)^{\text{tr}}$, and trial yield functions F^{tr} , $F^{\chi,\text{tr}}$

Step 2. Consider 3 cases:

(i) If $F^{\text{tr}} > 0$ and $F^{\chi,\text{tr}} > 0$, solve for $\Delta\gamma_{n+1}$ and $\Delta\gamma_{n+1}^\chi$ using Newton-Raphson for coupled equations:

$$F(\sigma_{n+1}, c_{n+1}) = F(\Delta\gamma_{n+1}, \Delta\gamma_{n+1}^\chi) = 0 \quad (251)$$

$$F^\chi((\mathbf{s} - \sigma)_{n+1}, c_{n+1}^\chi) = F^\chi(\Delta\gamma_{n+1}, \Delta\gamma_{n+1}^\chi) = 0 \quad (252)$$

(ii) If $F^{\text{tr}} > 0$ and $F^{\chi,\text{tr}} < 0$, solve for $\Delta\gamma_{n+1}$ with $\Delta\gamma_{n+1}^\chi = 0$ using Newton-Raphson:

$$F(\sigma_{n+1}, c_{n+1}) = F(\Delta\gamma_{n+1}, \Delta\gamma_{n+1}^\chi = 0) = 0 \quad (253)$$

(iii) If $F^{\text{tr}} < 0$ and $F^{\chi,\text{tr}} > 0$, solve for $\Delta\gamma_{n+1}^\chi$ with $\Delta\gamma_{n+1} = 0$ using Newton-Raphson:

$$F^\chi((\mathbf{s} - \sigma)_{n+1}, c_{n+1}^\chi) = F^\chi(\Delta\gamma_{n+1} = 0, \Delta\gamma_{n+1}^\chi) = 0 \quad (254)$$

(II) solve for microgradient plastic multiplier $\Delta\gamma^{\nabla\chi}$, given $\Delta\gamma$ and $\Delta\gamma^\chi$:

Step 1. Compute trial stress \mathbf{m}^{tr} and trial yield function $F^{\nabla\chi,\text{tr}}$

Step 2. If $F^{\nabla\chi,\text{tr}} > 0$, solve for $\Delta\gamma_{n+1}^{\nabla\chi}$ using Newton-Raphson:

$$F^{\nabla\chi}(\mathbf{m}_{n+1}, \mathbf{c}_{n+1}^{\nabla\chi}) = F^{\nabla\chi}(\Delta\gamma_{n+1}^{\nabla\chi}) = 0 \quad (255)$$

3. Upscaling from Grain-Scale to Micromorphic Elastoplasticity

In the overlapping domain, the continuum-scale micromorphic solution can be calculated as a partly homogenized representation of the grain-scale solution (figure 6)[¶]. This is useful for fitting micromorphic material parameters, and also in estimating DNS material parameters when converting from micromorphic continuum FE mesh to DNS in a future adaptive scheme. Thus, a micromorphic continuum-scale field $\square^{\text{micromorphic}}$ is defined as a weighted average (over volume and area) of the corresponding field \square^{grain} at the grain-scale, which is written as follows:

$$\square^{\text{micromorphic,vol}} \stackrel{\text{def}}{=} \langle \square^{\text{grain}} \rangle_v \stackrel{\text{def}}{=} \frac{1}{v^{\omega,\text{avg}}} \int_{\Omega^{\text{avg}}} \omega(r, \theta, \vartheta) \square^{\text{grain}} dv \quad (256)$$

$$\square^{\text{micromorphic,area}} \mathbf{n} \stackrel{\text{def}}{=} \langle \square^{\text{grain}} \mathbf{n}^{\text{grain}} \rangle_a \stackrel{\text{def}}{=} \frac{1}{\Gamma^{\text{avg}}} \int_{\Gamma^{\text{avg}}} \square^{\text{grain}} \mathbf{n}^{\text{grain}} da \quad (257)$$

where $\langle \bullet \rangle_v$ denotes the volume-averaging operator, $v^{\omega,\text{avg}} \stackrel{\text{def}}{=} \int_{\Omega^{\text{avg}}} \omega(r, \theta, \vartheta) dv$ the weighted average current volume, $\omega(r, \theta, \vartheta)$ denotes the kernel function (if using spherical coordinates in 3-D averaging), Ω^{avg} is the grain-scale volume averaging domain, $\langle \bullet \rangle_a$ denotes the area-averaging operator, and Γ^{avg} is the grain-scale area averaging domain. These averaging operators are mapped back to the reference configuration, such that the domains Ω_0^{avg} and Γ_0^{avg} are fixed. A length ℓ (approximate diameter of Ω^{avg} and Γ^{avg}) is a material property and is directly related to the length scale used in the micromorphic constitutive model.

A macroelement material point (figures 5 and 6) can be characterized as fully overlapping, non-overlapping, or partly overlapping according to the level of overlapping between the averaging domain Ω^{avg} and the full grain-scale DNS region Ω^{grain} . Within the fully-overlapping averaging domain, the Cauchy stress tensor $\sigma_{kl}^{\text{grain}}$ and vector of ISVs q_a^{grain} at the grain-scale are projected to the micromorphic continuum-scale using the averaging operators $\langle \square^{\text{grain}} \rangle_v$ and $\langle \square^{\text{grain}} \rangle_a$ to define the unsymmetric Cauchy stress σ_{kl} , the symmetric microstress s_{kl} , and the higher order stress m_{klm} :

$$\sigma_{kl} n_k \stackrel{\text{def}}{=} \left\langle \sigma_{kl}^{\text{grain}} n_k^{\text{grain}} \right\rangle_a \quad (258)$$

$$s_{kl} \stackrel{\text{def}}{=} \left\langle \sigma_{kl}^{\text{grain}} \right\rangle_v \quad (259)$$

$$m_{klm} n_k \stackrel{\text{def}}{=} \left\langle \sigma_{kl}^{\text{grain}} \xi_m n_k^{\text{grain}} \right\rangle_a \quad (260)$$

$$q_a \stackrel{\text{def}}{=} \left\langle q_a^{\text{grain}} \right\rangle_v \quad (261)$$

[¶]Wewould like to acknowledge discussions with his colleague at University of Colorado Boulder (UCB), Prof. F. Vernerey, regarding the natural built-in homogenization in micromorphic continuum theories of Eringen (1999); Eringen and Suhubi (1964).

where it is assumed the variables on the left-hand sides are micromorphic. Kinematic coupling and energy partitioning determine the percent contribution of grain-scale DNS and micromorphic continuum FE to the balance equations in the overlapping domain.

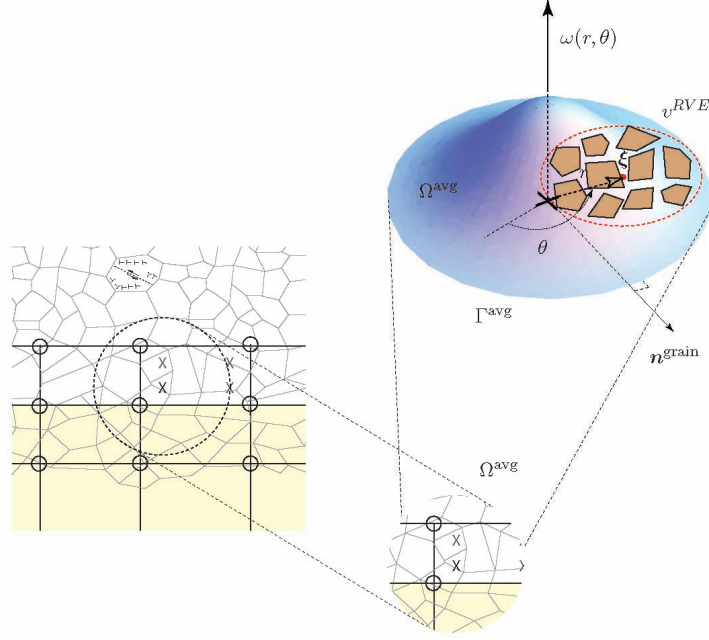


Figure 6. Two-dimensional illustration of micromorphic continuum homogenization of grain-scale response at a FE Gauss integration point X in the overlap region. v^{RVE} implies a RVE if needed to approximate stress from a DE simulation at a particular point of integration in Ω^{avg} , for example in Christoffersen et al. (1981); Rothenburg and Selvadurai (1981).

4. Coupled Formulation

We consider here the bridging-scale decomposition (Kadowaki and Liu, 2004, Klein and Zimmerman, 2006, Wagner and Liu, 2003) to provide proper BC constraints on a DNS region to remove fictitious boundary forces and wave reflections.

4.1 Kinematics

The kinematics of the coupled regions are given, following the illustration shown in figure 2. It is assumed that the micromorphic continuum-FE mesh covers the domain of the problem in which the bound particulate mechanics not significantly dominant, whereas in regions of significant grain-matrix debonding or intra-granular cracking leading to a macro-crack, a grain-scale mechanics representation is used (grain-FE or grain-DE-FE). Following some of the same notation presented in Kadowaki and Liu (2004), Wagner and Liu (2003), grain-FE displacements in the system in the current configuration \mathcal{B} are defined as

$$\check{\mathbf{Q}} = [\mathbf{q}_\alpha, \mathbf{q}_\beta, \dots, \mathbf{q}_\gamma]^T, \quad \alpha, \beta, \dots, \gamma \in \check{\mathcal{A}} \quad (262)$$

where \mathbf{q}_α is the displacement vector of grain-FE node α , and $\check{\mathcal{A}}$ is the set of all grain-FE nodes. The micromorphic continuum-FE nodal displacements \mathbf{d}_a and microdisplacement-gradients ϕ_d (see below for $\chi^h = \mathbf{1} + \Phi^h$ (Eringen 1968)) are written as

$$\check{\mathbf{D}} = [\mathbf{d}_a, \mathbf{d}_b, \dots, \mathbf{d}_c, \phi_d, \phi_e, \dots, \phi_f]^T \quad (263)$$

$$a, b, \dots, c \in \check{\mathcal{N}}, \quad d, e, \dots, f \in \check{\mathcal{M}}$$

where \mathbf{d}_a is the displacement vector at node a , ϕ_d is the microdisplacement-gradient matrix at node d , $\check{\mathcal{N}}$ is the set of all nodes, and $\check{\mathcal{M}}$ is the set of FE nodes with microdisplacement-gradient DOFs, where typically $\check{\mathcal{M}} \subset \check{\mathcal{N}}$. In order to satisfy the BCs for both regions, the motion of the grain-FE nodes in the overlap region (referred to as “ghost” grain-FE nodes, figure 2) is prescribed by the micromorphic continuum displacement and microdisplacement-gradient fields, and written as $\hat{\mathbf{Q}} \in \hat{\mathcal{A}}$, while the unprescribed (or free) grain-FE nodal displacements are $\mathbf{Q} \in \mathcal{A}$, where $\hat{\mathcal{A}} \cup \mathcal{A} = \check{\mathcal{A}}$ and $\hat{\mathcal{A}} \cap \mathcal{A} = \emptyset$. The displacements and microdisplacement-gradients of continuum-FE nodes overlaying the grain-FE are driven by the grain-FE motion (also through the averaging shown in figure 6) and written as $\hat{\mathbf{D}} \in \hat{\mathcal{N}}, \hat{\mathcal{M}}$, while the unprescribed (or free) nodal displacements and microdisplacement-gradients are $\mathbf{D} \in \mathcal{N}, \mathcal{M}$, where

In general, the displacement vector of a grain-FE node α can be represented by the FE interpolation of the continuum macro-displacement field \mathbf{u}^h and microdisplacement-gradient field Φ^h (where $\chi^h = \mathbf{1} + \Phi^h$ (Eringen, 1968)) evaluated at the grain-FE node in the reference configuration \mathbf{X}_α , such that

$$\mathbf{u}^h(\mathbf{X}_\alpha, t) = \sum_{a \in \check{\mathcal{N}}} N_a^u(\mathbf{X}_\alpha) \mathbf{d}_a(t), \quad \Phi^h(\mathbf{X}_\alpha, t) = \sum_{b \in \check{\mathcal{M}}} N_b^\Phi(\mathbf{X}_\alpha) \phi_b(t) \quad \alpha \in \check{\mathcal{A}} \quad (264)$$

where N_a^u are the shape functions associated with the continuum displacement field \mathbf{u}^h , and N_b^Φ the shape functions associated with the continuum microdisplacement-gradient field Φ^h . Recall that N_a^u and N_b^Φ have compact support and thus are evaluated only for grain-FE nodes that lie within a micromorphic continuum element containing nodes a and b in its domain. The displacement of a microelement (figure 3) can be written as

$$\begin{aligned} \mathbf{u}'(\mathbf{X}, \Xi, t) &= \mathbf{x}'(\mathbf{X}, \Xi, t) - \mathbf{X}'(\mathbf{X}, \Xi) \\ &= \mathbf{x}(\mathbf{X}, t) + \xi(\mathbf{X}, \Xi, t) - \mathbf{X} - \Xi \\ &= \underbrace{\mathbf{x}(\mathbf{X}, t) - \mathbf{X}}_{\mathbf{u}(\mathbf{X}, t)} + \underbrace{\xi(\mathbf{X}, \Xi, t) - \Xi}_{\chi(\mathbf{X}, t)\Xi} \\ &= \mathbf{u}(\mathbf{X}, t) + \underbrace{[\chi(\mathbf{X}, t) - \mathbf{1}] \Xi}_{\Phi(\mathbf{X}, t)} \\ &= \mathbf{u}(\mathbf{X}, t) + \Phi(\mathbf{X}, t)\Xi \end{aligned} \quad (265)$$

where we used the definition $\chi = \mathbf{1} + \Phi$ (Eringen, 1968) to put the form of microdeformation tensor χ similar to the deformation gradient $\mathbf{F} = \mathbf{1} + \partial \mathbf{u} / \partial \mathbf{X}$. The prescribed displacement of ghost grain-FE node α can then be written as

$$\mathbf{q}_\alpha(t) = (\mathbf{u}')^h(\mathbf{X}_\alpha, \Xi_\alpha, t) = \mathbf{u}^h(\mathbf{X}_\alpha, t) + \Phi^h(\mathbf{X}_\alpha, t)\Xi_\alpha \quad \alpha \in \hat{\mathcal{A}} \quad (266)$$

where Ξ_α is the relative position of grain-FE node α from a micromorphic continuum point. The choice of this continuum point could be either a continuum-FE node or Gauss integration point. This will be investigated in the multiscale implementation. The influence of the microdisplacement-gradient tensor Φ^h in the overlap region on the ghost grain-FE nodal displacement could, through specific micromorphic viscoelastic constitutive relations for χ^e , act to “damp out” high-frequency waves propagating through the fine mesh grain-FE region to the overlap/coupling region. The partitioning of potential and kinetic energies between grain-FE and micromorphic-continuum-FE systems within the overlap region will be dependent on the grain-FE equations of the bound particulate system and the micromorphic continuum-FE equations of the continuum system.

For all ghost grain-FE nodes, the interpolations can be written as

$$\hat{\mathbf{Q}} = \mathbf{N}_{\hat{Q}D} \cdot \mathbf{D} + \mathbf{N}_{\hat{Q}\hat{D}} \cdot \hat{\mathbf{D}} \quad (267)$$

where $\mathbf{N}_{\hat{Q}D}$ and $\mathbf{N}_{\hat{Q}\hat{D}}$ are shape function matrices containing individual nodal shape functions N_a^u and N_b^Φ , but for now these matrices are left general to increase our flexibility in choosing interpolation/projection functions (such as those used in meshfree methods). Overall, the grain-FE displacements may be written as

$$\begin{bmatrix} \mathbf{Q} \\ \hat{\mathbf{Q}} \end{bmatrix} = \begin{bmatrix} \mathbf{N}_{QD} & \mathbf{N}_{Q\hat{D}} \\ \mathbf{N}_{\hat{Q}D} & \mathbf{N}_{\hat{Q}\hat{D}} \end{bmatrix} \cdot \begin{bmatrix} \mathbf{D} \\ \hat{\mathbf{D}} \end{bmatrix} + \begin{bmatrix} \mathbf{Q}' \\ \mathbf{0} \end{bmatrix} \quad (268)$$

where \mathbf{Q}' is introduced (Klein and Zimmerman, 2006) as the error (or “fine-scale” (Wagner and Liu, 2003)) in the interpolation of the free grain-FE displacements \mathbf{Q} , whose function space is not rich enough to represent the true free grain-FE nodal motion. The shape function matrices \mathbf{N} are, in general, not square because the number of free grain-FE nodes are not the same as free micromorphic-FE nodes and prescribed nodes, and number of ghost grain-FE nodes not the same as prescribed and free micromorphic-FE nodes. A scalar measure of error in grain-FE nodal displacements is defined as (Klein and Zimmerman, 2006)

$$e = \mathbf{Q}' \cdot \mathbf{Q}' \quad (269)$$

which may be minimized with respect to prescribed continuum micromorphic-FE nodal DOFs $\hat{\mathbf{D}}$ to solve for $\hat{\mathbf{D}}$ in terms of free grain-FE nodal DOFs and micromorphic continuum FE nodal DOFs as

$$\hat{\mathbf{D}} = \mathbf{M}_{\hat{D}\hat{D}}^{-1} \mathbf{N}_{Q\hat{D}}^T (\mathbf{Q} - \mathbf{N}_{QD} \mathbf{D}), \quad \mathbf{M}_{\hat{D}\hat{D}} = \mathbf{N}_{Q\hat{D}}^T \mathbf{N}_{Q\hat{D}} \quad (270)$$

This is known as the “discretized L_2 projection” (Klein and Zimmerman, 2006) of the free grain-FE nodal motion \mathbf{Q} and free micromorphic-FE nodal DOFs \mathbf{D} onto the prescribed micromorphic-FE nodals DOFs $\hat{\mathbf{D}}$. Upon substituting equation 270 into equation 267, we may write the prescribed grain-FE nodal DOFs $\hat{\mathbf{Q}}$ in terms of free grain-FE nodal \mathbf{Q} and micromorphic-FE nodal \mathbf{D} DOFs. In summary, these relations are written as

$$\hat{\mathbf{Q}} = \mathbf{B}_{\hat{Q}Q} \mathbf{Q} + \mathbf{B}_{\hat{Q}D} \mathbf{D} \quad (271)$$

$$\hat{\mathbf{D}} = \mathbf{B}_{\hat{D}Q} \mathbf{Q} + \mathbf{B}_{\hat{D}D} \mathbf{D} \quad (272)$$

where

$$\mathbf{B}_{\hat{Q}Q} = \mathbf{N}_{\hat{Q}\hat{D}}\mathbf{B}_{\hat{D}Q} \quad (273)$$

$$\mathbf{B}_{\hat{Q}D} = \mathbf{N}_{\hat{Q}D} + \mathbf{N}_{\hat{Q}\hat{D}}\mathbf{B}_{\hat{D}D} \quad (274)$$

$$\mathbf{B}_{\hat{D}Q} = \mathbf{M}_{\hat{D}\hat{D}}^{-1}\mathbf{N}_{Q\hat{D}}^T \quad (275)$$

$$\mathbf{B}_{\hat{D}D} = -\mathbf{M}_{\hat{D}\hat{D}}^{-1}\mathbf{N}_{Q\hat{D}}^T\mathbf{N}_{QD} \quad (276)$$

As shown in figure 2, for a FE implementation of this DOF coupling, we expect that free grain-FE nodal DOFs \mathbf{Q} will not fall within the support of free micromorphic continuum FE nodal DOFs \mathbf{D} , such that it can be assumed that $\mathbf{N}_{QD} = \mathbf{0}$ and

$$\hat{\mathbf{Q}} = \mathbf{B}_{\hat{Q}Q}\mathbf{Q} + \mathbf{B}_{\hat{Q}D}\mathbf{D} \quad (277)$$

$$\hat{\mathbf{D}} = \mathbf{B}_{\hat{D}Q}\mathbf{Q} \quad (278)$$

where

$$\mathbf{B}_{\hat{Q}Q} = \mathbf{N}_{\hat{Q}\hat{D}}\mathbf{B}_{\hat{D}Q} \quad (279)$$

$$\mathbf{B}_{\hat{Q}D} = \mathbf{N}_{\hat{Q}D} \quad (280)$$

$$\mathbf{B}_{\hat{D}Q} = \mathbf{M}_{\hat{D}\hat{D}}^{-1}\mathbf{N}_{Q\hat{D}}^T \quad (281)$$

$$\mathbf{B}_{\hat{D}D} = \mathbf{0} \quad (282)$$

The assumption $\mathbf{N}_{QD} \neq \mathbf{0}$ would be valid for a meshfree projection of the grain-FE nodal motions to the micromorphic-FE nodal DOFs, as in Klein and Zimmerman (2006), where we could imagine that the domain of influence of the meshfree projection could encompass a free grain-FE node; the degree of encompassment would be controlled by the chosen support size of the meshfree kernel function. The choice of meshfree projection in Klein and Zimmerman (2006) was not necessarily to allow \mathbf{Q} be projected to \mathbf{D} (and vice versa), but to remove the computationally costly calculation of the inverse $\mathbf{M}_{\hat{D}\hat{D}}^{-1}$ in equations 271 and 272. Since we will also be using the TAHOE code for the coupled multiscale grain-FE-micromorphic-FE implementation, where the meshfree projection has been implemented for atomistic-continuum coupling (Klein and Zimmerman, 2006), we will also consider the meshfree projection in the future.

FE Balance Equations:

Following standard FE methods to formulate the nonlinear dynamic matrix FE equations, using the DOFs defined in the previous section, the balance of linear momentum for the grain-scale FE is

$$\mathbf{M}^Q \ddot{\mathbf{Q}} + \mathbf{F}^{INT,Q}(\mathbf{Q}) = \mathbf{F}^{EXT,Q} \quad (283)$$

where \mathbf{M}^Q is the mass matrix (lumped or consistent (Hughes, 1987)), $\mathbf{F}^{INT,Q}(\mathbf{Q})$ is the nonlinear internal force vector, and $\mathbf{F}^{EXT,Q}$ is the external force vector (which could be a function of \mathbf{Q} , but here such dependence is not shown).

For the balance of linear momentum and balance of first moment of momentum in equation 57, the weak form can be derived following the method of weighted residuals in Hughes (1987) (details not shown), the Galerkin form expressed, and then the FE matrix equations written in coupled form as

$$\mathbf{M}^D \ddot{\mathbf{D}} + \mathbf{F}^{INT,D}(\mathbf{D}) = \mathbf{F}^{EXT,D} \quad (284)$$

where \mathbf{M}^D is the mass and microinertia matrix, $\mathbf{F}^{INT,D}(\mathbf{D})$ the nonlinear internal force vector, $\mathbf{F}^{EXT,D}$ the external force vector, and $\mathbf{D} = [\mathbf{d} \phi]^T$ is the generalized DOF vector for the coupled micromorphic FE formulation.

These FE equations can be written in energy form to make the partitioning of energy in the next section more straightforward. For the FE matrix form of balance of linear momentum at the grain-scale, we have

$$\frac{d}{dt} \left(\frac{\partial T^Q}{\partial \dot{\mathbf{Q}}} \right) - \frac{\partial T^Q}{\partial \mathbf{Q}} + \frac{\partial U^Q}{\partial \mathbf{Q}} = \mathbf{F}^{EXT,Q} \quad (285)$$

where T^Q is the kinetic energy and U^Q the potential energy, such that

$$\begin{aligned} T^Q &= \frac{1}{2} \dot{\mathbf{Q}} \mathbf{M}^Q \dot{\mathbf{Q}} \\ U^Q(\mathbf{Q}) &= \int_0^{\mathbf{Q}} \mathbf{F}^{INT,Q}(\mathbf{S}) d\mathbf{S} \end{aligned}$$

Carrying out the derivatives in equation 285, and using the Second Fundamental Theorem of Calculus for $\partial U^Q / \partial \mathbf{Q}$, leads to equation 283. Likewise, for the coupled micromorphic balance equations, we have the energy form

$$\frac{d}{dt} \left(\frac{\partial T^D}{\partial \dot{\mathbf{D}}} \right) - \frac{\partial T^D}{\partial \mathbf{D}} + \frac{\partial U^D}{\partial \mathbf{D}} = \mathbf{F}^{EXT,D} \quad (286)$$

where T^D is the kinetic energy and U^D is the potential energy, such that

$$\begin{aligned} T^D &= \frac{1}{2} \dot{\mathbf{D}} \mathbf{M}^D \dot{\mathbf{D}} \\ U^D(\mathbf{D}) &= \int_0^{\mathbf{D}} \mathbf{F}^{INT,D}(\mathbf{S}) d\mathbf{S} \end{aligned}$$

4.2 Partitioning of Energy

We assume the total kinetic and potential energy of the coupled grain-FE-micromorphic-FE system may be written as the sum of the energies

$$T(\dot{\mathbf{Q}}, \dot{\mathbf{D}}) = T^Q(\dot{\mathbf{Q}}, \hat{\dot{\mathbf{Q}}}(\dot{\mathbf{Q}}, \dot{\mathbf{D}})) + T^D(\dot{\mathbf{D}}, \hat{\dot{\mathbf{D}}}(\dot{\mathbf{Q}})) \quad (287)$$

$$U(\mathbf{Q}, \mathbf{D}) = U^Q(\mathbf{Q}, \hat{\mathbf{Q}}(\mathbf{Q}, \mathbf{D})) + U^D(\mathbf{D}, \hat{\mathbf{D}}(\mathbf{Q})) \quad (288)$$

where we have indicated the functional dependence of the prescribed grain-FE nodal DOFs and micromorphic-FE nodal DOFs solely upon the free grain-FE nodal DOFs and micromorphic-FE nodal DOFs \mathbf{Q} and \mathbf{D} , respectively. Lagrange's equations may then be stated as

$$\begin{aligned} \frac{d}{dt} \left(\frac{\partial T}{\partial \dot{\mathbf{Q}}} \right) - \frac{\partial T}{\partial \mathbf{Q}} + \frac{\partial U}{\partial \mathbf{Q}} &= \mathbf{F}^{EXT,Q} \\ \frac{d}{dt} \left(\frac{\partial T}{\partial \dot{\mathbf{D}}} \right) - \frac{\partial T}{\partial \mathbf{D}} + \frac{\partial U}{\partial \mathbf{D}} &= \mathbf{F}^{EXT,D} \end{aligned} \quad (289)$$

which lead to a coupled system of governing equations (linear and first moment of momentum) for the coupled grain-FE-micromorphic-FE mechanics. Details of the derivatives, partitioning coefficients, and numerical examples will follow in a future report and journal articles.

5. Conclusion

5.1 Results

The schematic for a concurrent multiscale computational modeling approach for simulating dynamic fracture in bound particulate materials was presented that accounts for grain-scale micro-cracking influences on macroscale fracture. Details of a finite strain micromorphic pressure-sensitive Drucker-Prager elastoplastic constitutive model were presented, as well as its semi-implicit numerical integration. The approach for coupling grain-scale FE equations to the macroscale micromorphic FE equations was presented.

5.2 Conclusions

A three-level (macro, micro, and microgradient) micromorphic pressure-sensitive plasticity model provides additional flexibility in coupling with grain-scale mechanics in an overlapping region (figure 1.2) for attempting to account for influences of grain-scale micro-cracking on macroscale fracture nucleation and propagation under dynamic loading of bound particulate materials. The thorough formulation of the finite strain micromorphic elastoplastic constitutive equations in the context of nonlinear micromorphic continuum mechanics has been established, allowing the multiscale framework to stand on a firm footing, which heretofore was not presented in the literature.

5.3 Future Work

Future work will involve completing the FE implementation of the finite strain micromorphic pressure-sensitive Drucker-Prager plasticity model, and coupling it via an overlapping region to the grain-scale FE mesh where a projectile may impact a bound particulate materials target (figure 2).

6. References

- Baer, M.R.; Hall, C.A.; Gustavsen, R.L.; Hooks, D.E.; Sheffield, S.A. Sheffield. Isentropic Loading Experiments of a Plastic Bonded Explosive and Constituents. *J. Appl. Phys.* **2007**, *101* (3), 34906–1.
- Belytschko, T.; Loehnert, S.; Song, J.-H. Multiscale Aggregating Discontinuities: A Method for Circumventing Loss of Material Stability. *Int. J. Numer. Methods Eng.* **2008**, *73*, 869–894.
- Bilby, B.A.; Bullough, R.; Smith, E. Continuous Distributions of Dislocations: A New Application of the Methods of Non-Riemannian Geometry. *Proc. R. Soc. Lond. A, Math. Phys. Eng. Sci.* **1955**, *231*, 263–273.
- Caballero, A.; Carol, I.; Lopez, C.M. A Meso-level Approach to the 3d Numerical Analysis of Cracking and Fracture of Concrete Materials. *Fatigue Fract. Eng. Mater. Struct.* **2006**, *29* (12), 979–991. ISSN 8756-758X.
- Chawla, N.; Ganesh, V.V.; Wunsch, B. Three-dimensional (3d) Microstructure Visualization and Finite Element Modeling of the Mechanical Behavior of sic Particle Reinforced Aluminum Composites. *Scripta Mater.* **2004**, *51* (2), 161–165.
- Chen, W.; Ravichandran, G. Dynamic Compressive Failure of a Glass Ceramic Under Lateral Confinement. *J. Mech. Phys. Solids* **1997**, *45*, 1303–1328.
- Christoffersen, J.; Mehrabadi, M.M.; Nemat-Nasser, S. A Micromechanical Description of Granular Material Behavior. *J. App. Mech.* **1981**, *48*, 339–344.
- Clayton, J.D.; Bammann, D.J.; McDowell, D.L. Anholonomic Configuration Spaces and Metric Tensors in Finite Elastoplasticity. *Int. J. Non. Linear Mech.* **2004**, *39* (6), 1039–1049.
- Clayton, J.D.; Bammann, D.J.; McDowell, D.L. A geometric Framework for the Kinematics of Crystals with Defects. *Philos. Mag.* **2005**, *85* (33–35), 3983–4010.
- Clayton, J.D.; McDowell, D.L.; Bammann, D.J. Modeling Dislocations and Disclinations with Finite Micropolar Elastoplasticity. *Int. J. Plast.* **2006**, *22* (2), 210–256.

Coleman, B. D.; Noll, W. The Thermodynamics of Elastic Materials with Heat Conduction and Viscosity. *Arch. Ration. Mech. Anal.* **1963**, *13*, 167-178.

Desai, C.S.; Siriwardane, H.J. Constitutive Laws for Engineering Materials: With Emphasis on Geologic Materials. Prentice-Hall, 1984.

Dienes, J.K.; Zuo, Q.H.; Kershner, and J.D. Impact Initiation of Explosives and Propellants via Statistical Crack Mechanics. *J. Mech. Phys. Solids* **2006**, *54* (6), 1237-1275.

Eringen, A.C. Nonlinear Theory of Continuous Media. McGraw-Hill, 1 edition, 1962.

Eringen, A.C. Theory of Micropolar Elasticity. In H. Liebowitz, editor, Fracture, An Advanced Treatise, volume 2, pages 622-729. Academic Press, 1968.

Eringen, A.C. Eringen. Microcontinuum Field Theories I: Foundations and Solids. Springer-Verlag, 1999.

Eringen, A.C.; Suhubi, E.S. Nonlinear Theory of Simple Micro-elastic Solids. *Int. J. Engr. Sci.* **1964**, *2* (2), 189-203.

Feyel, F. A Multilevel Finite Element Method (FE2) to Describe the Response of Highly Nonlinear Structures Using Generalized Continua. *Comp. Meth. App. Mech. Engr.* **2003**, *192*, 3233-3244.

Feyel, F.; Chaboche, J.L. FE2 Multiscale Approach for Modelling the Elastoviscoplastic Behaviour of Long Fibre SiC/Ti Composite Materials. *Comp. Meth. App. Mech. Engr.* **2000**, *183*, 309-330.

Forest, S.; Sievert, R. Elastoviscoplastic Constitutive Frameworks for Generalized Continua. *Acta Mech.* **2003**, *160* (1-2), 71-111.

Forest, S.; Sievert, R. Nonlinear Microstrain Theories. *Int. J. Solids Struct.* **2006**, *43* (24), 7224-7245.

Fredrich, J.T.; DiGiovanni, A.A.; Noble, D.R. Predicting Macroscopic Transport Properties Using Microscopic Image Data. *J. Geophy. Res., B, Solid Earth (USA)* **2006**, *111* (B3), 14.

Germain, P. The Method of Virtual Power in the Mechanics of Continuous Media. ii. Microstructure. *SIAM J. Appl. Math.* **1973**, *25* (3), 556-575.

- Guduru, P.R.; Rosakis, A.J.; Ravichandran, G. Dynamic Shear Bands: An Investigation Using High Speed Optical and Infrared Diagnostics. *Mech. Mater.* **2001**, *33*, 371-402.
- Holzappel, G. A. Nonlinear Solid Mechanics: A Continuum Approach for Engineering. John Wiley and Sons, 2000.
- Hughes, T.J.R. The Finite Element Method. Prentice-Hall: New Jersey, 1987.
- Johnson, G.R.; Holmquist T.J. Response of Boron Carbide Subjected to Large Strains, High Strain Rates, and High Pressures. *J. App. Phys.*, **1999** *85* (12), 8060-8073.
- Kadowaki, H.; Liu, W.K. Bridging multiscale Method for Localization Problems. *Comp. Meth. App. Mech. Engr.* **2004**, *193* (30–32), 3267-3302.
- Kipp, M.E.; Grady, D.E.; Swegle, J.W. Numerical and Experimental Studies of Highvelocity Impact Fragmentation. *Int. J. Impact Eng.* **1003**, *14*, 427-438.
- Klein, P.A.; Zimmerman, J.A. Coupled Atomistic-continuum Simulations Using Arbitrary Overlapping Domains. *J. Comput. Phys.* **2006**, *213* (1), 86-116.
- Kondo, K. On the Geometrical and Physical Foundations of the Theory of Yielding. In Proceedings of the 2nd Japan National Congress for Appl. Mech., pages 41-47, 1952.
- Kraft, R.H.; Molinari, J.F. A Statistical Investigation of the Effects of Grain Boundary Properties on Transgranular Fracture. *Acta Mater.* **2008**, *56* (17), 4739-4749.
- Kraft, R.H.; Molinari, J.F.; Ramesh, K.T.; Warner, D.H. Computational Micromechanics of Dynamic Compressive Loading of a Brittle Polycrystalline Material Using a Distribution of Grain Boundary Properties. *J. Mech. Phys. Solids* **2008**, *56*, 2618-2641.
- Kroner, E. Allgemeine kontinuumstheorie der versetzungen and eigenspannungen. *Arch. Ration. Mech. Anal.* **1960**, *4*, 273-334.
- Lee, E.H. Elastic-plastic Deformation at Finite Strains. *J. App. Mech.* **1969**, *36*, 1-6.
- Lee, E.H.; Liu, D.T. Finite-strain Elastic-plastic Theory With Application to Plane-wave Analysis. *J. App. Phys.* **1967**, *38*, 19-27.
- Lee, J.D.; Chen, Y. Constitutive Relations of Micromorphic Thermoplasticity. *Int. J. Engr. Sci.* **2003**, *41* (3–5), 387-399. ISSN 0020-7225.

Lubliner, J. Plasticity Theory. Macmillan Pub., NY, 1990.

Mandel, J. Thermodynamics and plasticity. In J.J. Delgado et al., editor, Foundations of Continuum Thermodynamics, pages 283-304. Macmillan, New York, 1974.

Mindlin, R.D. Microstructure in Linear Elasticity. *Arch. Ration. Mech. Anal.* **1964**, *16*, 51-78.

Moran, B.; Ortiz, M.; Shih, C.F. Formulation of Implicit Finite-element Methods for Multiplicative Finite Deformation Plasticity. *Int. J. Numer. Methods Eng.* **1990**, *29* (3), 483-514.

Rajendran, A.M.; Grove, D.J. Modeling the Shock Response of Silicon Carbide, Boron Carbide and Titanium Diboride. *Int. J. Impact Eng.* **1996**, *18* (6), 611-631.

Regueiro, R.A. Finite Strain Micromorphic Pressure-sensitive Plasticity. *J. Eng. Mech.* **2009**, *135*, 178-191.

Regueiro, R.A. On Finite Strain Micromorphic Elastoplasticity. *Int. J. Solids Struct.* **2010**, *47*, 786-800.

Regueiro, R.A.; Dixit, P.A.; Garikipati, K. On Standard and Vector Finite Element Analysis of a Strict Anti-plane Shear Plasticity Model with Elastic Curvature. *Comp. Meth. App. Mech. Engr.* **2007**, *196*, 2692-2712.

Rothenburg, L.; Selvadurai, A.P.S. Micromechanical definition of the Cauchy stress tensor for particulate media. In A.P.S. Selvadurai, editor, Mechanics of Structured Media, pages 469-486. Elsevier Scientific, 1981.

Sansour, C. Unified Concept of Elastic-viscoplastic Cosserat and Micromorphic Continua. *Journal De Physique. IV* **1998**, *8* (8) 341-348.

Simo, J.C. Numerical Analysis and Simulation of Plasticity. In P.G. Ciarlet and J.L. Lions, editors, Handbook of Numerical Analysis. Elsevier Science, 1998.

Suhubi, E.S.; Eringen, A.C. Nonlinear Theory of Simple Micro-elastic Solidsii. *Int. J. Engr. Sci.* **1964**, *2* (2), 389-404.

TAHOE. Tahoe Development Server. <http://tahoe.ca.sandia.gov>.

Vermeest, P. A.; de Borst, R. Non-associated Plasticity for Soils, Concrete, and Rock. *Heron* **1984**, *29* (3), 3-64.

Vernerey, F.; Liu, W.K.; Moran, B. multiscale Micromorphic Theory for Hierarchical Materials. *J. Mech. Phys. Solids* **2007**, *55* (12), 2603-2651.

Wagner, G.J.; Liu, W.K. Coupling of Atomistic and Continuum Simulations Using a Bridging Scale Decomposition. *J. Comput. Phys.* **2003**, *190* (1), 249-274.

INTENTIONALLY LEFT BLANK.

Appendix A. Derivation of \mathbf{F}'

The formulation of equation 5 is presented in this appendix, using direct notation. To start, we recognize that

$$\mathbf{F}' = \frac{\partial \mathbf{x}'}{\partial \mathbf{X}'} = \frac{\partial \mathbf{x}'}{\partial \mathbf{X}} \frac{\partial \mathbf{X}}{\partial \mathbf{X}'} \quad (\text{A-1})$$

$$\frac{\partial \mathbf{x}'}{\partial \mathbf{X}} = \mathbf{F} + \frac{\partial \chi}{\partial \mathbf{X}} \boldsymbol{\Xi} + \chi \frac{\partial \boldsymbol{\Xi}}{\partial \mathbf{X}} \quad (\text{A-2})$$

and

$$\frac{\partial \mathbf{X}}{\partial \mathbf{X}'} = 1 - \frac{\partial \boldsymbol{\Xi}}{\partial \mathbf{X}'} \quad (\text{A-3})$$

It is possible to show that $\partial \boldsymbol{\Xi} / \partial \mathbf{X}' \approx \partial \boldsymbol{\Xi} / \partial \mathbf{X}$, starting with

$$\frac{\partial \boldsymbol{\Xi}}{\partial \mathbf{X}'} = \frac{\partial \boldsymbol{\Xi}}{\partial \mathbf{X}} \frac{\partial \mathbf{X}}{\partial \mathbf{X}'} \quad (\text{A-4})$$

which using equation A-3 leads to

$$\frac{\partial \boldsymbol{\Xi}}{\partial \mathbf{X}'} = \left(1 + \frac{\partial \boldsymbol{\Xi}}{\partial \mathbf{X}} \right)^{-1} \frac{\partial \boldsymbol{\Xi}}{\partial \mathbf{X}} \quad (\text{A-5})$$

Assuming the gradient of microstructural internal length is small, $\|\partial \boldsymbol{\Xi} / \partial \mathbf{X}\| \ll 1$ for the region of interest where the micromorphic continuum model is used, then

$$\left(1 + \frac{\partial \boldsymbol{\Xi}}{\partial \mathbf{X}} \right)^{-1} \approx 1 - \frac{\partial \boldsymbol{\Xi}}{\partial \mathbf{X}} \quad (\text{A-6})$$

where then

$$\frac{\partial \boldsymbol{\Xi}}{\partial \mathbf{X}'} = \left(1 - \frac{\partial \boldsymbol{\Xi}}{\partial \mathbf{X}} \right) \frac{\partial \boldsymbol{\Xi}}{\partial \mathbf{X}} \approx \frac{\partial \boldsymbol{\Xi}}{\partial \mathbf{X}} \quad (\text{A-7})$$

The expression for \mathbf{F}' then results as in equation 5.

INTENTIONALLY LEFT BLANK.

Appendix B. Another Set of Elastic Deformation Measures

Here, another set of elastic deformation measures, from equation 1.5.11 in (Eringen, 1999), are considered as

$$\bar{C}_{\bar{K}\bar{L}}^{\chi,e} = \chi_{k\bar{K}}^e \chi_{k\bar{L}}^e, \quad \bar{\Upsilon}_{\bar{K}\bar{L}}^e = \chi_{\bar{L}a}^{e-1} F_{a\bar{K}}^e, \quad \bar{\Pi}_{\bar{K}\bar{L}\bar{M}}^e = \chi_{\bar{K}a}^{e-1} \chi_{a\bar{L},\bar{M}}^e \quad (\text{B-1})$$

Thus, the Helmholtz free energy function is written as

$$\bar{\rho}\bar{\psi}(\bar{C}_{\bar{K}\bar{L}}^{\chi,e}, \bar{\Upsilon}_{\bar{K}\bar{L}}^e, \bar{\Pi}_{\bar{K}\bar{L}\bar{M}}^e, \bar{Z}_{\bar{K}}, \bar{Z}_{\bar{K}}^{\chi}, \bar{Z}_{\bar{K},\bar{L}}^{\chi}, \theta) \quad (\text{B-2})$$

and the constitutive equations for stress result from equations 82 - 84 as

$$\bar{S}_{\bar{K}\bar{L}} = \frac{\partial(\bar{\rho}\bar{\psi})}{\partial\bar{\Upsilon}_{\bar{K}\bar{B}}^e} \chi_{\bar{B}k}^{e-1} F_{\bar{L}k}^{e-1} \quad (\text{B-3})$$

$$\bar{\Sigma}_{\bar{K}\bar{L}} = 2\bar{\Upsilon}_{\bar{A}\bar{K}}^{e-1} \frac{\partial(\bar{\rho}\bar{\psi})}{\partial\bar{C}_{\bar{A}\bar{B}}^{\chi,e}} \bar{\Upsilon}_{\bar{B}\bar{L}}^{e-1} \quad (\text{B-4})$$

$$\bar{M}_{\bar{K}\bar{L}\bar{M}} = \frac{\partial(\bar{\rho}\bar{\psi})}{\partial\bar{\Pi}_{\bar{I}\bar{M}\bar{K}}^e} \chi_{\bar{I}k}^{e-1} F_{\bar{L}k}^{e-1} \quad (\text{B-5})$$

where $\bar{\Upsilon}_{\bar{A}\bar{K}}^{e-1} = F_{\bar{K}k}^{e-1} \chi_{k\bar{A}}^e$. These stress equations take a somewhat simpler form than in equations 91 - 93. Thus, it becomes a choice of the modeler how the specific constitutive form of the elastic part of the Helmholtz free energy function is written, i.e. in terms of equation 90 or equation B-2. Eringen (1999) advocated the use of equation B-2 for micromorphic elasticity, whereas Suhubi and Eringen (1964) used equation 90. We use equation 90.

INTENTIONALLY LEFT BLANK.

Appendix C. Deformation Measures

It was mentioned that the change in the square of microelement arc-lengths $(ds')^2 - (d\bar{S}')^2$ should include only three unique elastic deformation measures (the two sets proposed by Eringen (1999) and considered in this report for finite strain elastoplasticity). Here, we write directly

$$(ds')^2 = d\mathbf{x}'d\mathbf{x}' = dx'_k dx'_k \quad (\text{C-1})$$

where

$$dx'_k = F_{k\bar{K}}^e d\bar{X}_{\bar{K}} + \chi_{k\bar{K},\bar{L}}^e \bar{\Xi}_{\bar{K}} d\bar{X}_{\bar{L}} + \chi_{k\bar{K}}^e \chi_{\bar{K}\bar{K},\bar{L}}^p \Xi_{\bar{K}} d\bar{X}_{\bar{L}} + \chi_{k\bar{K}}^e d\bar{\Xi}_{\bar{K}} \quad (\text{C-2})$$

Then

$$\begin{aligned} (ds')^2 = & \left[\bar{C}_{\bar{K}\bar{L}}^e + 2\text{sym}(\bar{\Gamma}_{\bar{K}\bar{B}\bar{L}}^e) \bar{\Xi}_{\bar{B}} + \bar{\Gamma}_{\bar{D}\bar{A}\bar{K}}^e \bar{C}_{\bar{D}\bar{M}}^{e-1} \bar{\Gamma}_{\bar{M}\bar{B}\bar{L}}^e \bar{\Xi}_{\bar{A}} \bar{\Xi}_{\bar{B}} \right. \\ & + 2\text{sym}(\bar{\Psi}_{\bar{B}\bar{E}}^e \bar{C}_{\bar{B}\bar{C}}^{e-1} \bar{\Gamma}_{\bar{C}\bar{A}\bar{K}}^e \chi_{\bar{E}\bar{E},\bar{L}}^p) \bar{\Xi}_{\bar{A}} \Xi_{\bar{E}} \\ & + \bar{\Psi}_{\bar{A}\bar{D}}^e \bar{C}_{\bar{A}\bar{B}}^{e-1} \bar{\Psi}_{\bar{B}\bar{E}}^e \chi_{\bar{D}\bar{D},\bar{K}}^p \chi_{\bar{E}\bar{E},\bar{L}}^p \Xi_{\bar{D}} \Xi_{\bar{E}} \\ & \left. + 2\text{sym}(\bar{\Psi}_{\bar{K}\bar{E}}^e \chi_{\bar{E}\bar{E},\bar{L}}^p) \Xi_{\bar{E}} \right] d\bar{X}_{\bar{K}} d\bar{X}_{\bar{L}} \\ & + 2 \left[\bar{\Psi}_{\bar{K}\bar{L}}^e + \bar{\Psi}_{\bar{B}\bar{L}}^e \bar{C}_{\bar{B}\bar{C}}^{e-1} \bar{\Gamma}_{\bar{C}\bar{A}\bar{K}}^e \bar{\Xi}_{\bar{A}} \right. \\ & \left. + \bar{\Psi}_{\bar{A}\bar{L}}^e \bar{C}_{\bar{A}\bar{B}}^{e-1} \bar{\Psi}_{\bar{B}\bar{D}}^e \chi_{\bar{D}\bar{D},\bar{K}}^p \Xi_{\bar{D}} \right] d\bar{X}_{\bar{K}} d\bar{\Xi}_{\bar{L}} \\ & + \left[\bar{\Psi}_{\bar{A}\bar{K}}^e \bar{C}_{\bar{A}\bar{B}}^{e-1} \bar{\Psi}_{\bar{B}\bar{L}}^e \right] d\bar{\Xi}_{\bar{K}} d\bar{\Xi}_{\bar{L}} \end{aligned} \quad (\text{C-3})$$

and

$$(d\bar{S}')^2 = d\bar{X}_{\bar{K}} d\bar{X}_{\bar{K}} + 2d\bar{X}_{\bar{K}} d\bar{\Xi}_{\bar{K}} + d\bar{\Xi}_{\bar{K}} d\bar{\Xi}_{\bar{K}} \quad (\text{C-4})$$

It can be seen that the first set in equation 89 appears exclusively as elastic deformation in equation C-3; there are also some plastic terms, which do not appear in equation 1.5.8 in Eringen (1999). Equation C-3 could likewise be expressed in terms of the elastic set in equation B-1. But one or the other set is unique, as outlined by Eringen (1999) for micromorphic elasticity, here put into context for finite strain micromorphic elastoplasticity.

INTENTIONALLY LEFT BLANK.

NO. OF COPIES	ORGANIZATION	NO. OF COPIES	ORGANIZATION
1 PDF	DEFENSE TECH INFO CTR ATTN DTIC OCA 8725 JOHN J KINGMAN RD STE 0944 FT BELVOIR VA 22060-6218	7	US ARMY RSRCH LAB ATTN RDRL WMP B C WILLIAMS ATTN RDRL WMP B J CLAYTON (5 COPIES) ATTN RDRL WMP B M GREENFIELD ABERDEEN PROVING GROUND MD 21005
1	SANDIA NATIONAL LAB ATTN J ZIMMERMANN PO BOX 969 MS 9404 LIVERMORE CA 94551		
1	GEORGE WASHINGTON UNIVERSITY ATTN J LEE PHILLIPS HALL STE 739 801 22ND ST NW WASHINGTON DC 20052	1	US ARMY RSRCH LAB ATTN RDRL WMP B M RAFTENBERG BLDG 4600 ABERDEEN PROVING GROUND MD 21005
1	MISSISSIPPI STATE UNIVERSITY ATTN D BAMMANN PO BOX 5405 MISSISSIPPI STATE MS 39762-5405	2	US ARMY RSRCH LAB ATTN RDRL WMP B M SCHEIDLER ATTN RDRL WMP B R BECKER BLDG 390 ABERDEEN PROVING GROUND MD 21005
10	UNIVERSITY OF COLORADO AT BOULDER ATTN 428 UCB, ECOT 441 R REGUEIRO (10 COPIES) 1111 ENGINEERING DR BOULDER CO 80309-0428	1	US ARMY RSRCH LAB ATTN RDRL WMP B R KRAFT ABERDEEN PROVING GROUND MD 21005
1	US ARMY RSRCH LAB ATTN RDRL WMP B Y HUANG ABERDEEN PROVING GROUND MD 21005	2	US ARMY RSRCH LAB ATTN RDRL WMP B S BILYK ATTN RDRL WMP C T W BJERKE BLDG 4600 ABERDEEN PROVING GROUND MD 21005
1	US ARMY RSRCH LAB ATTN RDRL WMP B B LEAVY BLDG 393 ABERDEEN PROVING GROUND MD 21005	1	US ARMY RSRCH LAB ATTN RDRL WMP F N GNIAZDOWSKI BLDG 390 ABERDEEN PROVING GROUND MD 21005
1	US ARMY RSRCH LAB ATTN RDRL WMP B B LOVE BLDG 4600 ABERDEEN PROVING GROUND MD 21005	1	US ARMY RSRCH LAB ATTN RDRL CIM G T LANDFRIED BLDG 4600 ABERDEEN PROVING GROUND MD 21005-5066
1	US ARMY RSRCH LAB ATTN RDRL WMP B C HOPPEL BLDG 393 ABERDEEN PROVING GROUND MD 21005	1	US ARMY RSRCH LAB ATTN RDRL WMP B D DANDEKAR ABERDEEN PROVING GROUND MD 21005-5069

NO. OF COPIES	ORGANIZATION
3	US ARMY RSRCH LAB ATTN IMNE ALC HRR MAIL & RECORDS MGMT ATTN RDRL CIM L TECHL LIB ATTN RDRL CIM P TECHL PUB ADELPHI MD 20783-1197